AFATL-TR-80-118

The Influence Of Sting And Strut Supports On The Aerodynamic Loads On An Ogive Cylinder At High Angles Of Attack At Transonic Speeds

Tom N Canning
Jack N Nielsen

NIELSEN ENGINEERING & RESEARCH, INC
510 CLYDE AVENUE
MOUNTAIN VIEW, CALIFORNIA 94043

OCTOBER 1980

FINAL REPORT FOR PERIOD MARCH 1979-SEPTEMBER 1980

Approved for public release; distribution unlimited

Air Force Armament Laboratory
AIR FORCE SYSTEMS COMMAND★UNITED STATES AIR FORCE★EGLIN AIR FORCE BASE, FLORIDA

NOTICE

Please do not request copies of this report from the Air Force Armament Laboratory. Additional copies may be purchased from:

National Technical Information Service
5285 Port Royal Road
Springfield, Virginia 22161

Federal Government agencies and their contractors registered with Defense Technical Information Center should direct requests for copies of this report to:

Defense Technical Information Center
Cameron Station
Alexandria, Virginia 22314

UNCLASSIFIED

SECURITY CLASSIFICATION OF THIS PAGE (When Data Entered)

REPORT DOCUMENTATION PAGE	READ INSTRUCTIONS BEFORE COMPLETING FORM
1. REPORT NUMBER: AFATL-TR-80-118	2. GOVT ACCESSION NO.: AD-A109 394
	3. RECIPIENT'S CATALOG NUMBER:
4. TITLE (and Subtitle): THE INFLUENCE OF STING AND STRUT SUPPORTS ON THE AERODYNAMIC LOADS ON AN OGIVE CYLINDER AT HIGH ANGLES OF ATTACK AT TRANSONIC SPEEDS	5. TYPE OF REPORT & PERIOD COVERED: Final Report: March 1979-September 1980
	6. PERFORMING ORG. REPORT NUMBER: NEAR-TR-229
7. AUTHOR(s): Tom N. Canning and Jack N. Nielsen	8. CONTRACT OR GRANT NUMBER(s): F08635-79-C-0119
9. PERFORMING ORGANIZATION NAME AND ADDRESS: Nielsen Engineering & Research, Inc. 510 Clyde Avenue Mountain View, California 94043	10. PROGRAM ELEMENT, PROJECT, TASK AREA & WORK UNIT NUMBERS: PE:61102F Jon:2307-E1-09
11. CONTROLLING OFFICE NAME AND ADDRESS: Air Force Armament Laboratory Armament Division Eglin Air Force Base, Florida 32542	12. REPORT DATE: October 1980
	13. NUMBER OF PAGES: 85
14. MONITORING AGENCY NAME & ADDRESS(if different from Controlling Office)	15. SECURITY CLASS. (of this report): UNCLASSIFIED
	15a. DECLASSIFICATION/DOWNGRADING SCHEDULE

16. DISTRIBUTION STATEMENT (of this Report)

This document has been approved for public release and sale; its distribution is unlimited.

17. DISTRIBUTION STATEMENT (of the abstract entered in Block 20, if different from Report)

18. SUPPLEMENTARY NOTES

Availability of this report is specified on verso of front cover.

19. KEY WORDS (Continue on reverse side if necessary and identify by block number)

Support Interference

20. ABSTRACT (Continue on reverse side if necessary and identify by block number)

The influence of the model support system on an ogive cylinder at high angles of attack has been determined in transonic tests. Stings of varying diameter and struts in various orientations were studied. The stings did not alter the development of large side loads resulting from asymmetric vortex separation and had only moderate progressive effects on in-plane forces and moments. Struts supporting the model through its leeward meridian seriously

DD FORM 1 JAN 73 1473

UNCLASSIFIED 389783

SECURITY CLASSIFICATION OF THIS PAGE (When Data Entered)

20. ABSTRACT (Concluded)

altered normal and side forces and sharply reduced base drag at several combinations of Mach number and angle of attack. A strut supporting the model at its windward meridian (near the base) yielded results like those for the stings.

PREFACE

This report was prepared by Nielsen Engineering & Research, Inc., 510 Clyde Avenue, Mountain View, California 94043, under Contract No. F08635-79-C-0119 with the Air Force Armament Laboratory, Armament Division, Eglin Air Force Base, Florida 32542. This work was performed during the period from March 1979 to September 1980.

The assistance of the Program Manager, Dr. D. C. Daniel (DLJ), is gratefully acknowledged.

Professor Robert C. Nelson of the University of Notre Dame acted as consultant on the program and contributed several helpful suggestions.

This report has been reviewed by the Public Affairs Office (PA) and is releasable to the National Technical Information Service (NTIS). At NTIS it will be available to the general public, including foreign nationals.

This technical report has been reviewed and is approved for publication.

FOR THE COMMANDER

BARNES E. HOLDER, JR., Colonel, USAF
Chief, Munitions Division

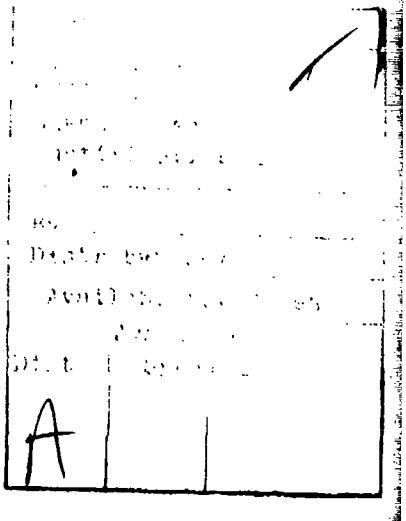

(The reverse of this page is blank)

TABLE OF CONTENTS

TABLE OF CONTENTS (Concluded)

LIST OF FIGURES

LIST OF FIGURES (Concluded)

LIST OF TABLES

(The reverse of this page is blank)

SECTION I

INTRODUCTION

The need for guided missiles and aircraft to undergo high accelerations results in the requirement for flight at high angles of attack. In order to design the vehicles and their control systems, it is necessary to know what aerodynamic forces and moments act on the body. Tests in wind tunnels to provide the needed information usually involve conventional supports (sting or strut); the effects of these supports on the measurements must be known in order to interpret the test results. The support interference at small model incidence has been the subject of many experiments conducted in a wide range of environments for many configurations. Very little data exist, however, for even simple bodies at very high incidence, and some of the tests indicate that rather large effects are introduced by supporting struts, particularly at subsonic and transonic speeds (References 1 and 2).

The present test program investigates support interference for a body of revolution supported by stings and struts. Measurements were made to determine how support position, size, and shape affect the forces, moments, and base pressure acting on a fineness-ratio 7.5 ogive cylinder. In particular, the asymmetry of the flow and the corresponding side force and yawing moment acting on the body as affected by stings of various size and struts having different positions and sweep angles were studied.

SECTION II

BACKGROUND

At high angles of attack the flow around a body exhibits important separated vortex patterns whose effects dominate the induced forces and moments. The flow around a body of revolution will now be described to provide physical insight.

In recent years the flow patterns around a slender body at high angle of attack have become very well-known, as has the remarkable extent to which the analogy between two- and three-dimensional flow fields holds. The elucidation of three-dimensional flow fields has been pursued by several authors (References 1, 2, and 3). They have shown that the separated vortical patterns on the lee sides of bodies exhibit fairly well-defined phenomena, depending on angle of attack, approximately as follows for reasonably high Reynolds numbers.

$25 \leq \alpha^\circ \leq 60$ Vortices form a steady asymmetric street which has two major configurations. Whether one or the other occurs depends on two Mach number-related quantities, M_∞ and M_C, the free-stream and cross-flow Mach numbers, respectively.

(a) At some combinations of M_C and M_∞, the asymmetry begins very close to the body. In this case, M_∞ and M_C are usually low as in region I of Figure 1.

(b) When M_∞ is high (≥ 0.9 say), then at values of $M_C > 0.5$ (i.e. region II of Figure 1), the pattern near the body shows a diffuse, symmetric cloud and the asymmetry develops well away from the body. The presence of this pattern is often inferred from the disappearance of the steady side forces produced by the asymmetric pattern of (a).

These phenomena are discussed in more detail in Reference 4.

$60 \leq \alpha^\circ \leq 90$ The vortices are unsteady. For $\alpha \to 90^\circ$ the Karman vortex street can develop.

The phenomena discussed above occur in the approximate regions summarized in Figure 1. Here, the regions of vortex asymmetry beginning at the body are shown to be a relatively

small portion of tl overall chart. However, it is in this area that many aircraft and some missiles perform their very high angle maneuvers.

It is likely that if the vortex patterns above are artificially disturbed, the effect will be felt in the forces and moments induced on the body. It is this postulated phenomenon, thought to underly recent results from three-dimensional body tests (Figure 2), whic! showed differences in body aerodynamic characteristics between a base-mounted sting and a lee side strut support. The angles of attack shown (60° to 90°) fall in the range for unsteady wakes. The model, when supported by a conventional round sting inserted at the model base experienced different aerodynamic forces and moments from those felt when it was supported by the strut mounted in the wake. The effect is apparently most pronounced at lower free-stream Mach numbers. Using the analogy between steady three-dimensional flow and unsteady two-dimensional flow, an interpretation will now be made of the force and moment differences exhibited in Figure 2, beginning with a discussion of recent investigations involving wake-altering devices in two-dimensional flow.

A three-dimensional strut support has the two-dimensional analogy in crossflow planes of a thin plate positioned in the wake at various distances downstream. Nelson and Mouch (Reference 2) have investigated the effects of such plates in two dimensions at very low crossflow Mach and Reynolds numbers and have discovered that the plates induce considerable differences in wake pattern and crossflow drag. A short, thin plate near the cylinder will cause the asymmetric, oscillating wake to lose its oscillating character and will reduce crossflow drag from its high, subcritical Re_c value (about 1.2) to a value of about 0.8. At some separation distance between the plate and cylinder the oscillatory flow becomes reestablished and Cd_c rises rapidly to 1.2 again. By using these crossflow drag coefficients, Nelson was able to correct three-dimensional, wind-tunnel, normal-force data, obtained with a blade sting (i.e. strut) to approximately that which would be expected with a base sting. It is not clear, however, if a base sting is the optimum support device for minimizing interference.

Based on the previous discussions and Nelson's results, it is possible to interpret the data of Figure 2 as follows. It appears that in the unsteady wake region shown ($60 \leq \alpha° \leq 90$) the truly oscillatory (unsteady) three-dimensional wake responds to the wake plate in very much the same way as in two dimensions. For $M_\infty = 0.6$, the asymmetry begins immediately behind the body and a strut placed in this wake seems to act like a two-dimensional thin plate. For $M_\infty = 0.9$, the wake will exhibit the

near-body, symmetric, distributed-vorticity clouds discussed earlier. It is less likely that a plate in this flow will induce large pattern or force changes.

SECTION III

WIND TUNNEL AND TEST CONFIGURATIONS

1. WIND TUNNEL

The Ames 14-Foot Transonic Wind Tunnel is a closed-return continuous flow wind tunnel. Its test section is enclosed in a plenum and has slotted walls to reduce interference with the model flow at transonic speeds. The stagnation pressure is atmospheric because temperature control is effected by passive air exchange with the exterior atmosphere. For this reason, only the slightest control over Reynolds number at constant Mach number is possible. Therefore, no effort was made to control Reynolds number.

2. MODEL

The model for the present study was a 7-inch-diameter tangent-ogive cylinder of fineness ratio 7.5. The ogive was sharp and had a fineness ratio of 2 [see Figure 3(a)].

The model was mounted on the internal force and moment strain-gage balance in such a fashion as to permit remote adjustment of the roll position at any time during the test without consideration for Mach number or angle of attack. Roll position was sensed by a ten-turn precision potentiometer mounted on the pinion-gear shaft. The resolution of the model-position indication was about 0.4 degree, but backlash in the drive system degraded the achievable accuracy to ±1 degree.

Model surface finish, which has been found to be critical in earlier basic investigations of the phenomena of asymmetric vortex separation, was not controllable during this investigation. The interior of the Ames 14-Foot Transonic Wind Tunnel is dirty and is subject to continuing flaking of paint. Furthermore, dust from outside the tunnel may gain access through the air exchanger in the return path. The resulting sandblasting is so rapid that a short operating sequence started with a perfect surface would end with a large number of craters, some with burrs as high as several thousandths of an inch. It was therefore decided that only the most severe burrs would be removed between tests so as to have a quite rough surface to start the test of each configuration and to minimize the change in overall roughness during the tests of that configuration. In an effort to provide a single feature which would predominate over the sandblasting burrs in controlling the flow asymmetries, the model was equipped with a trigger near the apex. This trigger was a ridge of epoxy glue approximately 0.015 inch thick by

0.060 inch wide which extended about 0.70 inch along one generator of the ogive starting at 0.30 inch from the tip. The trigger was much larger than any of the burrs and was placed near the nose in order to achieve high effectiveness.

3. STING AND HIGH-ALPHA STRUT

The model was mounted, by way of the balance, on a tapered steel sting which extended 5 model diameters from the model base to its mounting socket, as shown in Figure 4. Where the sting exited the model base its diameter was 3 inches, to yield a diameter ratio of 0.43. The socket was, in turn, installed on the end of a massive strut mounted at a 45 degree angle from the wind tunnel main model support body of revolution. The full range of angle of attack provided by this mounting arrangement extended from approximately 34 degrees to slightly over 73 degrees.

4. DUMMY SUPPORTS

In all tests the model was mounted on the sting support system described above. The simulation of other support arrangements was provided by adding thick sleeves around the support sting or by a strut simulator mounted as indicated in Figure 3.

a. Dummy Stings

To investigate the influence of stings on the forces and moments experienced by the model, dummy stings of various diameters were mounted on the real sting [Figure 3(a)]. Extrapolating any observed influence of sting size to zero sting diameter would then give the best baseline data free of interference from the supports. The baseline used herein, however, is that obtained with the sting having $d/D = 0.43$. The dummy stings were machined from wooden blocks to provide diameters of 4.5, 5.5, and 6.5 inches. The tapered holes were bored eccentric to the axis of the exterior surface in order to offset a slight asymmetry in manufacturing of the steel sting. Each dummy sting was a right circular cylinder 14 inches long, and all dummies were sharply boattailed at the downstream end. All were mounted so as to provide a 0.25-inch (0.04 D) gap between the forward end and the model base-closure plate. The sting-mounted base-pressure tubes, four in all, projected about 0.06 inch into the gap between the dummy stings and the aft closure plate of the model, as indicated in the inset of Figure 3(a).

b. Dummy Strut

The dummy strut [Figure 3(b)] was fabricated by laying up a glass-reinforced plastic structure around a thin plate of oak. The resulting structure had a chord of 7 inches (normal to the long axis) and was slightly over 1 inch thick with semi-cylindrical leading and trailing edges.

Because it was necessary to maneuver the dummy strut during the tests to align its chord plane with the axis of the model, a compliant, rubber-cushioned mount was provided at the support end of the strut and two controllable guy wires were fastened to a fitting which passed through the dummy strut near its tip. Two tip extensions were provided for the dummy strut: one for a sweep-back of 15 degrees and one for 45 degrees; the latter is visible in Figure 4.

c. Dummy-Strut Support and Control

The base end of the dummy strut was fastened as appropriate to either of two support blades, one windward and one leeward [Figures 3(b) and (c)], by multiple-bolt joints which allowed the dummy blade to move through a flapping angle of about 5 degrees with relatively little restraint.

The outer part of the strut was provided, as noted above, with a through fitting and adjustable cables, 0.125 diameter, which extended through the tunnel side walls to electrically driven actuators. The guy wires are visible in Figure 4(a), slack, and Figure 4(b), taut. Load cells were provided so that the tension in each cable could be monitored and maintained within safe limits. These cables prevented aeroelastic divergence of the dummy strut and allowed it to be positioned as noted above. The alignment was monitored by means of a closed-circuit television camera mounted in the air plenum above the test section.

The support blades were mounted to the most convenient portions of the basic model-support system. Vibrations of the model-support boom are damped by means of the three-cable tether seen in the background in Figure 4(a).

SECTION IV

TESTS

The effects of supports on the observed aerodynamic characteristics were determined from comparison of data obtained using the various dummy supports with data obtained with the most slender sting without the dummy support systems or with the leeward support blade installed, as appropriate. The three types of tests described below were conducted to permit the required comparisons.

1. TEST CONFIGURATIONS

Three types of test configurations were tested in order to assess the effect of introducing the enlarged (i.e. dummy) stings and the strut. For the sting-diameter case tests included the model supported by the most slender sting and the same configuration with dummy stings enclosing the slender sting. For the leeward-strut results the slender-sting installation was augmented by the leeward support blade to provide a basis for comparison with tests in which the strut was mounted on the leeward blade. For the case of the windward strut tests, the slender-sting results were used as a baseline; no tests were conducted with the windward blade in the absence of the dummy strut.

a. Test Sequence

In order to obtain a comprehensive sample of the aerodynamic behavior of the model, a compromise was struck among increments in angle of attack, roll angle, and free-stream Mach number. The Mach numbers selected were 0.5 (the lowest at which the wind tunnel could operate satisfactorily), 0.7, and 0.9 (a Mach number at which earlier studies indicated greatly reduced effects of flow asymmetry). The free-stream Reynolds numbers based on model diameter were 1.8×10^6 at M = 0.5, 2.2×10^6 at M = 0.7, and 2.4×10^6 at M = 0.9. The angles of attack selected covered the full range possible; the angle of attack increments were either 5 or 10 degrees depending on the need for a fine data mesh. Nine roll positions (the last repeated the first) were set at each test condition (Mach number and angle of attack).

b. Configurations Without Dummy Struts

Five configurations were tested in which no dummy struts were used. These were the baseline configuration with the sting wrapped with a single layer of glass-reinforced plastic to secure the base-pressure tubes and the sting-fouling wire;

the baseline configuration with three dummy stings enclosing the bare sting; and the baseline configuration with the leeward support blade mounted in place. This last configuration was tested to detect any effect of the blade on the airflow over the model.

c. Test Procedures

With the desired configuration in place and at the lowest angle of attack, the wind tunnel airspeed was established at a Mach number of 0.5. With these conditions, a complete data readout was recorded at each of eight roll orientations (at 45 degree intervals) and repeating the first by completing the revolution. Following each set of roll-position settings at constant Mach number and angle of attack, the model was returned at roughly constant roll rate of about 6 degrees per second to the starting point. During this roll-back the outputs of the main balance normal- and side-force gauges were recorded continuously along with the model roll position so as to record in detail the complete variation of the applied forces as they varied with roll position.

Angle of attack was then increased to the next value and the roll sequence repeated. Data were obtained at all Mach numbers without stopping the airflow unless, as occasionally occurred, either steady or unsteady loads threatened the structural integrity of the configuration. Those instances are implied by gaps in the matrix of data. After completion of the angle-of-attack sequence, the model was returned to the minimum angle of attack before increasing the Mach number. During this return to minimum angle of attack, the normal and side forces were recorded continuously on the oscillograph as they were for the roll-back. These two records provided, then, a roll sweep at constant angle of attack and an angle-of-attack sweep at one roll position.

d. Dummy Strut Configuration

Five configurations employing the dummy strut were tested: four with the strut mounted leeward of the model and one mounted windward. In all dummy-strut tests a gap as great as 1.0 inch separated the strut tip from the model in order to prevent mechanical interference. It was necessary to estimate the deflections to be expected and to install the dummy strut so as to remain clear of the model but with minimum safe gap. In all three installations with the dummy strut near the model base, an effort was made to place the strut trailing edge such that its forward extension would pass through the edge of the model base in the position corresponding to the maximum expected normal force. For the tests of the strut mounted at mid-cylinder

alignment of the strut mid-chord line to intercept the model surface at mid-cylinder was also sought for the same maximum-deflection case. Two tests were terminated before the complete test matrix was recorded because of fouling.

e. Dummy Strut Test Sequence

For the tests of the five dummy-strut configurations fewer angles of attack were employed than for the other configurations. More importantly, however, asymmetric air loads sometimes deflected the model to the side by more than one inch. In order to simulate an aligned strut, it was therefore necessary to force the dummy strut (against its own spring resistance and the side force resulting from the sidewash acting on the model) into alignment with the model. This alignment was reset by the test technician every time a significant change in model lateral position occurred. The strut position was observed by the technician by means of a closed circuit television. The accuracy of positioning was judged by the project engineer to be better than ±0.25 inch; i.e., about 4 percent of the body diameter. The maximum side load, estimated from the load cell outputs, was about 300 pounds, which used the full safe load for the cable employed.

Following collection of data at each of the nine roll settings at each angle of attack, the model was rolled slowly to its initial position before setting the next angle of attack. No adjustments of strut position were made during these roll-backs because of the irregularity of the side forces and the danger of overloading the guy-wire system by erroneous control movements. Therefore, the roll-back records for the strut tests are to some degree less representative of the desired results than are those for the tests without the dummy strut.

As noted in the discussion of model surface finish, this wind tunnel, by nature, is destructive of polished model surfaces because of dust and paint chips blown at high speed. Also this tunnel has a high turbulence level.

SECTION V

RESULTS AND DISCUSSION

Table 1 lists the configurations tested. The nomenclature for the printout is provided therein. Most of the results are presented in graphical form in Figures 5 through 25 to illustrate the findings. Some portions of the data which show no systematic effects of flow asymmetry or of support interference are not presented graphically.

1. AERODYNAMICS OF BASELINE CONFIGURATION AND EFFECTS OF STING DIAMETER

The test model mounted on the sting of minimum diameter (baseline) is naturally a member of the sting-diameter test series. Therefore, the baseline data are described in this section. The same data will be repeated in the discussion of the leeward support blade and windward dummy strut.

a. Normal Force

At each test condition--angle of attack and Mach number--the balance and base-pressure data were recorded at eight different roll positions (twice at one roll position). The smallest of the observed values of normal-force coefficient for the thinnest sting is plotted as a function of angle of attack for the three Mach numbers in Figure 5. As the sting diameter was increased, the observed minimum normal force increased slowly at low angles of attack at the lower Mach numbers and more rapidly at the higher angles of attack. These variations are plotted in Figure 6. At M = 0.9, only the largest sting caused a large increase at angles of attack below 59 degrees.

As will be described later, the model was subjected to large side loads despite its ostensibly symmetric geometry. The normal force was frequently observed to change systematically with observed side force. Examples of this variation are illustrated in Figure 7 for several tests at M = 0.50. The corresponding data for the higher Mach numbers are in Figures 8 and 9. It is to be expected that the systematic behavior should be symmetrical about a side force of zero. The data indicate an asymmetry which remained essentially unchanged with increasing angle of attack. This suggests that the wind-tunnel airstream has a side-flow component.

At a fixed small angle of attack and with no real aerodynamic asymmetries, a side force can result from mounting the model with a yaw angle in a straight airstream. Similarly, a

side force can be developed on a model mounted straight if there is sidewash in the airstream. In the former case, the side load will approach zero as the angle of attack is increased to 90 degrees since the balance axis is perpendicular to the straight airstream (only normal force would be experienced). If, on the other hand, the side-force experienced at low incidence results from sidewash in the airflow, the model will continue to experience a side force even at 90 degrees angle of attack relative to the wind tunnel axis. The near constancy of the side-force bias from 31 to 72 degrees angle of attack suggests that sidewash is responsible.

Much more important than the apparent bias towards positive side force is the sensitivity of normal force to asymmetric flow about the model; increments in normal force as great as 30 percent or more of the minimum were observed when the model was simply rolled to eight different positions while holding a constant angle of attack. Since this wide range of normal force results solely from changes in roll position of an apparently axially symmetric model, it is important to recognize the effects of model-flow asymmetry. In designing a support system it is important to avoid altering this apparently natural asymmetry and its effects on the aerodynamic loads.

The data of Figures 7, 8, and 9 show a weak tendency towards increasing incremental normal force with increasing sting diameter at a given side force. This tendency is in addition to the stronger tendency towards increasing the minimum normal force illustrated in Figure 6 and listed in Figures 7, 8, and 9. At the highest angles of attack, large variations of normal force were observed, again resulting solely from changes in roll position, even though the side force remained fairly small (see Figure 9). This comparatively large variation (total range over 6 percent for $d/D = 0.78$) is believed, for the reason outlined below, to have resulted from accumulated damage to the model surface during the many tests which preceded this series. Much earlier in the test program, the baseline configuration with the leeward support blade (but no strut) added was tested at the same Mach number and angle of attack. The leeward blade appears not to have altered the average normal force felt by the model, and it is considered even more unlikely that it would alter the range of normal force observed in a revolution in roll. These data (in increments of C_N form) are compared in Figure 10 with the normal-force increments for all but the largest dummy sting. If there were no incremental damage between the leeward blade test (flagged circles) and the baseline test (plain circles), the total variation would have remained at 1.7 percent of the normal force at $\phi = 0$ degrees. The protracted test period, during which the model was fouled twice by the dummy strut, is believed to be responsible for the change. It is felt that

interruption of the test program for a thorough refinishing would have reduced the increments noted in C_N for the sting-diameter series at the higher angles of attack.

A brief scan of the normal force data for moderate angles of attack revealed no such smooth cyclic variation of normal force with roll angle. The model asymmetry which yields the one cycle of ΔC_N in one roll cycle at $\alpha = 73$ degrees probably does not control the flow asymmetry at lower angles. Instead, the normal-force variations correlate with the irregular changes in side-force discussed below.

b. Side Force

The effect of asymmetric flow on side force are well illustrated in the continuous records of side force as a function of roll position for one combination of Mach number and angle of attack (Figure 11). These records were made by an oscillograph after measurements at the eight roll positions were completed and while the model was being rolled at about 5 degrees per second back to its initial position. The irregular variations proved to be fairly repeatable in overall form but changed in detail from run to run as evidenced by the data in Figure 11. There is no discernible trend in side-force signature with increasing sting diameter. The rollback records were compared with the force-readout records of Table 2 to verify that the eight positions tested gave a good representation of the complete record.

The flow asymmetries which can yield large side forces are known to be controlled by minor irregularities or asymmetries in model or airstream. Just which model asymmetries affect the results of a particular test is difficult to determine; in the present test, a fixed asymmetry was provided in the form of the trigger applied to the model nose. This trigger was easily the largest asymmetry on the model. Had it been the only irregular feature capable of affecting the flow, the side force data at those roll positions where the trigger was effective would be precisely antisymmetric about the roll positions at which the trigger passes through the windward or leeward meridian. To visualize this test of antisymmetry, consider one of the line plots in Figure 11. If one cuts the plot in two at the roll angle for antisymmetry (e.g., where the trigger passes through the leeward meridian) and then swings one piece of the plot through an angle of 180 degrees about the point where the horizontal axis crosses the cut, the rotated plot will have a reversal in sign conventions for both roll position and side-force. As previously noted, a systematic positive side-force is believed to exist in the data because of tunnel sidewash. The curves of Figure 12 were constructed by folding the data of Figure 11 about various roll positions until the best fit was

obtained. The cut-and-rotate point to give the best overall overlay was at a roll position of about ϕ = -117 degrees; the roll angle at which the trigger passed through the leeward meridian was measured to be about -118 degrees. The good match suggests that the trigger was the principal irregularity influencing the flow asymmetries in the vicinity of that roll position. In contrast to this suggestion of antisymmetry at $\phi \approx$ -117 degrees, the data in the region of ϕ = 63 degrees, when treated in the same way, show no evidence of antisymmetry. It is concluded that the trigger was quite ineffective when oriented within 30 degrees of the windward meridian at α = 50 degrees.

Turning from the variation of side force with changing roll position to variation with angle of attack, Figure 13 shows that fairly orderly, nonrandom, changes in C_Y from side to side occur as the angle of attack increases. The angle-of-attack increment between reversals appears to vary with roll position, and the effects of Mach number at fixed angle of attack are different for each roll position. That is to say, side force reversals may result from changing Mach number, angle of attack, or roll position.

c. Normal-Force Center of Pressure

As sting diameter is progressively increased, the center of pressure of the normal force acting on the model moves aft. This effect is greatest at the lower Mach numbers and highest angle of attack, as seen in Figures 14(a) and (b). At Mach 0.7 and 72.2 degree angle of attack, the center of pressure moves aft on the average of about 24 percent of the body diameter when the largest dummy sting is installed over the baseline sting. This effect is greatly reduced for the highest Mach number, smaller stings, and smaller angles of attack.

To put these trends into perspective, however, it is noted that the change in center-of-pressure position at a given value of d/D (depending on roll position, i.e., side force) can be as much as 0.5D, about three times that resulting from increasing sting diameter from d/D = 0.43 to 0.93. The large rearward shift of the center of pressure as angle of attack is increased from 63 to 70 degrees at M = 0.9 is not seriously altered by interference of even the largest sting.

d. Side-Force Center-of-Pressure Position

The movements of the center-of-pressure position of the side force were studied by comparing, systematically, plots of side-force center of pressure and side-force amplitude versus roll position for the four sting diameters. A few general

observations can be drawn from the study of those test pairs where the side force itself was fairly large, $|C_Y| > 0.75$, and did not change greatly. (In general, the side force did remain roughly constant, but there were notable exceptions as well.) At the lower angles of attack, i.e., <55 degrees, the center-of-pressure position of side force typically remained stationary (±0.15D) for all sting diameters tested. At an angle of attack of 55 degrees the side-force center of pressure appeared to move gradually forward by about 0.4 diameter as the sting size was changed from 0.43 to 0.93.

e. Forebody Axial Force

Unlike all other aerodynamic properties of the model, the axial force, exclusive of base drag, varied only slightly as the model roll position was varied for the tests with the smallest sting diameter; a tendency towards reduced axial force with increased side force was seen. While all of the drag measurements are reported in the tabulated data, no analysis of the influence (if any) of the sting diameter on forebody axial force is included. High-speed flow between the dummy stings and the base-closure plate [see inset in Figure 3(a)] probably produced complicated pressure distributions which were poorly represented by averaging the measurements at the four pressure taps.

f. Base Pressure

As mentioned above, the base pressure determinations for all cases where the dummy stings were employed are of doubtful utility. Therefore, the discussion here is limited to pointing out the systematic increase of base drag with increasing side force, shown in Figure 15, for the thinnest sting and for the test with the leeward support blade in place. The narrow passages between dummy-sting sleeves and the model closure plate were not a factor in the tests with dummy struts, because only the baseline sting was used. While even the most slender sting doubtless altered the base pressure from its support-free value, it is assumed without justification that any increments resulting from inserting the strut were unaffected by the presence of the sting.

g. Repeatability of Data

The rather unusual and occasionally unsystematic nature of the data presented thus far raises the issue of repeatability of test conditions and balance operation. The degree of both short-term and long-term repeatability can be drawn from the sting-diameter series when augmented by data to be used presently for the dummy-strut analysis. The shortest-term repeatability is indicated by comparison of data for ±180 degree roll positions.

These dozens of data pairs, which are nominally identical, gave the best direct checks, because the accumulated damage to the model surface between the pairs of readings was minimal. An additional comparison can be drawn from two tests separated by less than two hours of running time by examining the plots of data for eight roll positions in nominally identical or closely similar tests (see Figure 16). The small changes are apparent. For tests run many hours apart, one configuration with the leeward support blade and one without, refer to Figure 17. The comparison indicates only a moderately degraded repetition resulting from increased opportunity for surface damage on the model. It is concluded that major systematic changes in aerodynamic loads resulted from changes in sting diameter and not from progressive surface damage. This same conclusion is assumed to apply to the results for dummy struts, as indicated in Figure 16.

2. INFLUENCE OF DUMMY-STRUT SUPPORT BLADE

The possibility that the support blade, on which the dummy strut was mounted for the leeward configurations, would interfere seriously enough with the model's vortex wake to mask the effect of the strut itself was investigated in a test using the leeward blade but no strut. The data obtained with this installation are plotted along with those for the various leeward-strut tests as appropriate. The principal influence of the support blade is a modest reduction of the forces acting on the model, probably by virtue of a reduction in dynamic pressure; the results in Figure 15 show that, except at the highest two angles of attack at M = 0.5, no tendency to reduce or increase the inherent asymmetry of the model flow field (i.e., side force) is indicated. The apparent suppression of side force at these two test conditions does not persist when the leeward strut is installed, as is noted later.

3. EFFECT OF LEEWARD STRUT AT MODEL BASE

In general, the influence of the strut on the aerodynamic loads was very small for those cases where it intercepted the model near the base. It must be emphasized, however, that at high angles of attack the strut was immersed in the wake of the sting so that its true influence if used in the absence of the sting may not have been adequately determined.

a. Normal Force

The frequently systematic variation of normal force with side force at several angles of attack and three Mach numbers is illustrated in Figure 18. The results for model with support blade and for model with support blade and dummy strut (two sweep

angles) are presented in comprehensive plots. For the cases showing small maximum side force, there appears to be a small reduction in normal force resulting from adding the dummy strut and its fairly bulky mount and guy wires. At 72 degrees angle of attack at M = 0.7, introducing the dummy strut reduces the normal force by about 5 percent, or slightly more than it was increased when the leeward support blade was added. There appears to be only a slightly more serious effect on the normal force for the highly asymmetric cases (large side force). At α = 50.7 degrees and M = 0.5, a 10-percent change is evident. No effect of strut sweepback angle is noted at $\alpha \leq 50.7$ degrees, but at angles of attack above 60 degrees, where the correlation seen at low incidence between normal force and side force no longer holds, the 15-degree sweep strut frequently yields a 20-percent increment in normal force. Except in these latter cases, the progressive, slow reduction of normal force as more hardware is added remains clear.

b. Side Force

There appears to be little or no evidence in the data of Figure 18 that the leeward, aft-mounted strut affected the development of flow asymmetries, because the side-force magnitude remained similar except at the highest incidence. Here there appears to be a suppression of side force by the support blade at M = 0.5.

c. Normal-Force Center-of-Pressure Location

The introduction of the leeward aft-mounted strut (15-degree and 45-degree sweep angles) caused only small changes in normal-force center-of-pressure position at all angles of attack except 50.7 degrees at M = 0.5 [Figure 19(a)]. Here the shift was typically 0.1 to 0.2 of the body diameter throughout the side-load range. A 10-percent forward shift was observed at M = 0.7 at an angle of attack of 72 degrees. This coincided with the large decrease in normal force noted earlier.

d. Forebody Axial Force

The leeward, aft strut did not alter the axial force acting on the forebody. No figure is included.

e. Base Drag

A strut placed in this position can affect the base pressure through two effects: (a) the thickness-distribution of the strut can produce a change in static pressure in its wake and thus alter the base pressure, and (b) the strut can alter the strength of vortices passing near it by introducing the reaction vortices

induced by the lift distribution arising from the incident body vortices. The new resulting vortices will tend to oppose the initial set. In view of the large variation of base drag with side-force acting on the baseline configuration, it is felt that the vortex influence is very strong and that the strut, in fact, suppressed the vortex strength near the model base. At the highest angle of attack at M = 0.7, the leeward aft strut yielded a 17-percent reduction in base drag even though it was immersed in the wake of both model and sting. This result [Figure 20(b)] suggests that the sting itself may be very important. The results for M = 0.9 are not plotted because the reduction in base drag was about equal to the resolution in the data.

4. EFFECT OF WINDWARD STRUT AT MODEL BASE

The changes in aerodynamic forces acting on the model resulting from adding the windward strut at the model base (45 degree sweep) were generally less than, or comparable to, the expected uncertaintites in the respective quantities. The results are detailed below.

a. Normal Force

The variation of normal force with observed side force is shown in Figure 21 for several angles of attack and Mach numbers for the model with and without the dummy strut in the windward base position. A minute loss in normal force is suggested. There is no evidence of alteration of the systematic variation normal force with side force and none to indicate alteration of the tendency to generate side forces. At the lower angles of attack only modest scatter remains in the plots of normal force versus side force, and these plots show little effect from the strut. Similarly, the 15-percent range of normal force at α = 60.8 degrees, M = 0.5 persists. Underlying this apparent residual scatter in results is excellent point-for-point correspondence at the eight roll positions between the baseline model results and those for the windward strut. The pairings of tests at the same roll position can be recognized easily. It is therefore concluded that the strut did not alter the flow noticeably except to shield the rear portion of the model slightly.

b. Side Force

The data in Figure 21 indicate the minimal effect of the windward strut on the side forces exerted on the baseline model.

c. Normal-Force Center-of-Pressure Position

Comparison of the center-of-pressure data for the baseline and windward-strut configurations (Figure 22) reveals a small forward shift and no change in the systematic variation of the center-of-pressure with side force. The small forward shift is consistent with the modest reduction in normal force acting on the aft portion of the model, as noted above.

d. Forebody Axial Force

Study of the data reveals no significant influence of the strut on forebody axial force. Therefore, no data plot is included.

e. Base Pressure

The windward strut appears to have had no significant effect on base pressure regardless of the side force acting on the body. This finding reinforces the earlier finding that interference with nearby vortices (and not thickness effects) is the basic mechanism for reducing base drag.

5. LEEWARD STRUT MOUNTED AT MID-CYLINDER POSITION

This configuration is different from the others principally in that the strut's effects on the wake of the model can be felt for a substantial distance aft of the strut itself.

a. Normal Force

At angles of attack up to 61 degrees, the normal force acting on the model was only slightly reduced as a result of installing the dummy strut for those cases in which the side force remained small (see Figure 23). With increasing side force the normal force is seen to increase as before, but the reduction of maximum side force observed at the two lower angles of attack resulted in a reduced range of normal force coefficients. At 50.7 degrees, on the other hand, the strut suppresses, to a small degree, the normal-force increase even at large side force.

At the highest angle of attack at M = 0.7, the normal force was reduced by about 11 percent with the strut installed at mid-cylinder. This loss of normal force is believed to be analogous to the reduction of drag acting on a right circular cylinder in two-dimensional flow resulting from installation of a splitter plate in the wake (References 6 and 7). The oil-flow pictures in Figure 8 of Reference 8 show that the surface streamlines on the lee part of an ogive-cylinder model at 90-degree angle of

attack are drastically rearranged by introduction of the dummy strut. A similarly drastic reduction of normal force accompanies this change in configuration. Since the present strut can affect the body's wake flow both forward and aft of its own position, it is potentially more influential than it would be if placed near the model base. In the latter case the reduction in normal force was only about 5 percent [see Figure 18(b)]. The influence is seen to be much weaker at smaller incidence and at $M = 0.5$ even at the highest angle of attack. Operation of this configuration at $M = 0.9$ resulted in violent vibration of the strut, so no data were obtained at incidence above 42 degrees.

b. Normal-Force Center-of-Pressure Position

The plots of Figure 24 show that this placement of the leeward strut appears to introduce systematic forward and aft shifts of center of pressure depending on angle of attack.

c. Side-Force Center-of-Pressure Position

The mid-cylinder strut yielded forward movements in side-force center of pressure position of about 1.0 to 1.6 diameters even when the side force was substantial. For example, at $M = 0.5$ and $\alpha = 50.7$ degrees, introducing the strut moved the side-force center of pressure forward by about one diameter even at a side force coefficient of 2.5. At the two highest angles of attack, the mid-cylinder strut had no important systematic effect on side force.

At $M = 0.70$ and 41.1 degrees angle of attack, the strut interference moves the side force center of pressure forward by about two diameters while reducing the force itself to one-third the value recorded with only the leeward support blade in place. While these large effects are of considerably importance, the data are insufficient to establish trends; no figures are included.

d. Base Pressure

At $M = 0.5$, Figure 25 shows that introduction of the strut at the leeward mid-cylinder position appeared to result in a small reduction in base drag except at $\alpha = 50.7$ degrees, where the base drag was reduced by 20 percent regardless of side force. At 40.5 degrees angle of attack, the range of base pressure was greatly reduced as was the range of side force in the strut-present tests. At $M = 0.7$, a similar, but smaller effect on base drag (10-percent reduction) was noted at 41.1 degrees angle of attack. At $\alpha = 72.0$ degrees, a large reduction in base drag resulted from the presence of the leeward mid-cylinder strut.

SECTION VI

CONCLUSIONS

The present study of support interference on an ogive cylinder at angles of attack has led to the conclusion that a conventional sting entering the body at its base causes the least, and most easily estimated, interference with aerodynamic loads. If a strut support must be used, it should enter the body along the body's windward meridian. Use of an airfoil, or flat-sided strut located in the frequently unsymmetrical and/or unsteady wake of the model results in major and unpredictable changes in the loads and base pressure acting on the model.

Two results of this study may be of assistance in understanding the complexities of the asymmetric flow. The first of these is that various aerodynamic properties of the model correlated well with side force for those combinations of angle of attack and Mach number associated with flow-field asymmetry. The second is that the flow asymmetry may be directed left or right by a small asymmetric trigger. The cases analyzed suggest that a small bump near the nose is very effective if placed near the leeward meridian and very ineffective when near the windward meridian.

Finally, it is concluded that until the occurrence and degree of asymmetry can be controlled in test and flight, it will be necessary to utilize triggers in all relevant tests to avoid missing the natural extremes of asymmetry.

REFERENCES

1. Dietz, W. E., Jr. and Altstatt, M. C.: Experimental Investigation of Support Interference on an Ogive Cylinder at High Incidence. AIAA Paper No. 78-165, 16th Aerospace Sciences Meeting, January 1978.

2. Nelson, R. E. and Mouch, T. N.: The Influence of Aerodynamic Interference on High Angle of Attack Wind Tunnel Testing. AIAA Paper No. 78-827, 16th Aerospace Sciences Meeting, January 1978.

3. Thomson, K. D. and Morrison, D. F.: The Spacing, Position and Strength of Vortices in the Wake of Slender Cylindrical Bodies at Large Incidence. Australian Paper, HSA, 25, 1969.

4. Nielsen, J. N., Hemsch, M. J., and Smith, C. A.: A Preliminary Method for Calculating the Aerodynamic Characteristics of Cruciform Missiles to High Angles of Attack Including Effects of Roll Angle and Control Deflection. NEAR TR 152, November 1977.

5. Baker, W. B., Jr.: Static Aerodynamic Characteristics of a Series of Generalized Bodies With and Without Fins at Mach Numbers from 0.6 to 3.0 and Angles of Attack from 0 to 180 Deg. AEDC-TR-75-124, Vol. 1 (Revised), 1975.

6. Roshko, A.: Experiments on the Flow Past a Circular Cylinder at Very High Reynolds Numbers. J. of Fluid Mechanics, Vol. 10, Pt. 3, 1961.

7. Nelson, R. C.: The Influence of a Wake Splitter Plate on the Pressure Drag Coefficient of a Right Circular Cylinder. Presented at the 11th Navy Aeroballistics Symposium, August 1978.

8. Altstatt, M. C. and Dietz, W. E., Jr.: Support Interference on an Ogive-Cylinder Model at High Angle of Attack in Transonic Flow. AEDC-TR-78-8, March 1978.

TABLE 1. CONFIGURATION KEY

All Configurations Employ Model with Epoxy Trigger

Number	$\frac{\text{Sting Diameter}}{\text{Model Diameter}}$	Lee Support Blade	Strut Position	Strut Sweep Angle
3	0.93	No	NA	NA
4	0.43	Yes	NA	NA
5	0.43	Yes	Lee Aft	45°
6	0.43	Yes	Lee Mid	45°
7	0.43	Yes	Lee Mid	15°
8	0.43	Yes	Lee Aft	15°
9	0.43	No	Wind Aft	45°
10	0.43	No	NA	NA
11	0.64	No	NA	NA
12	0.78	No	NA	NA

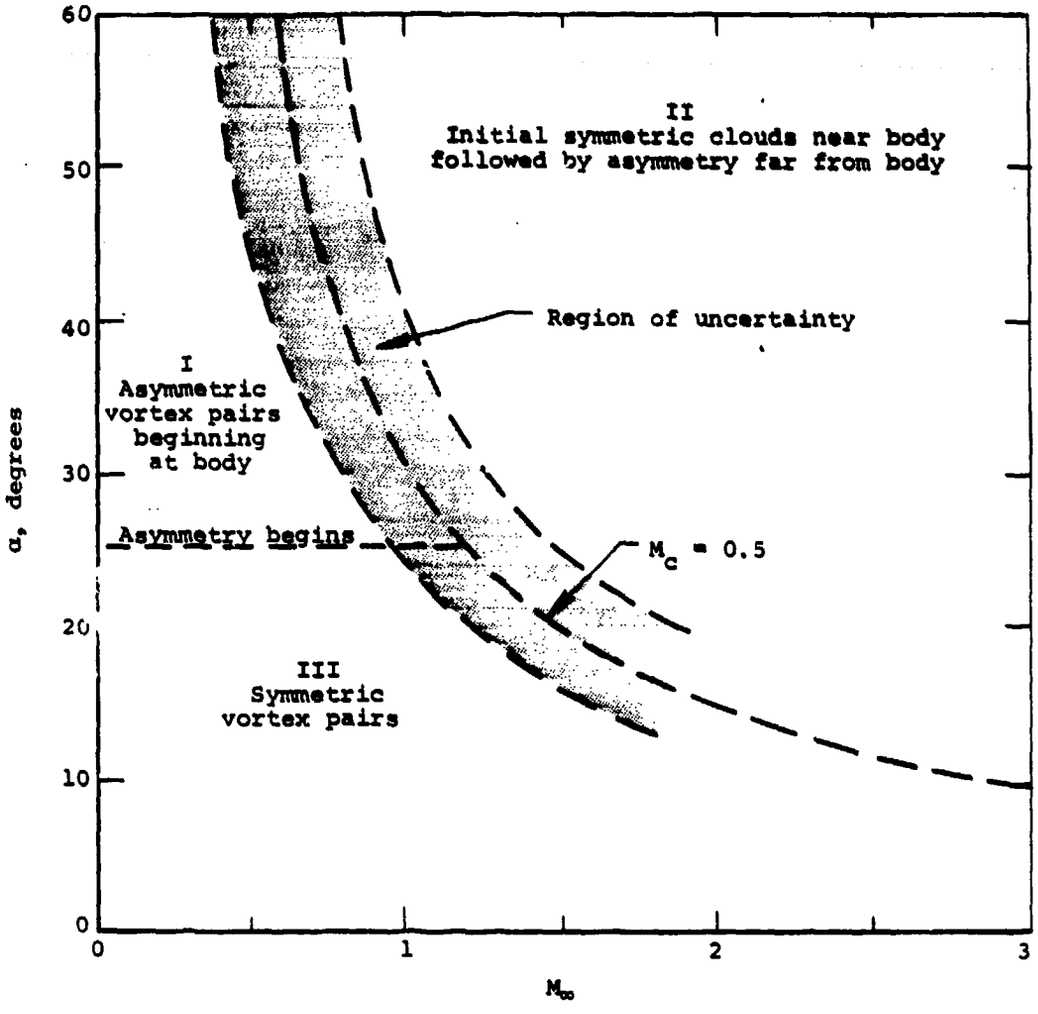

Figure 1. Regions of Symmetric and Asymmetric Vortex Patterns

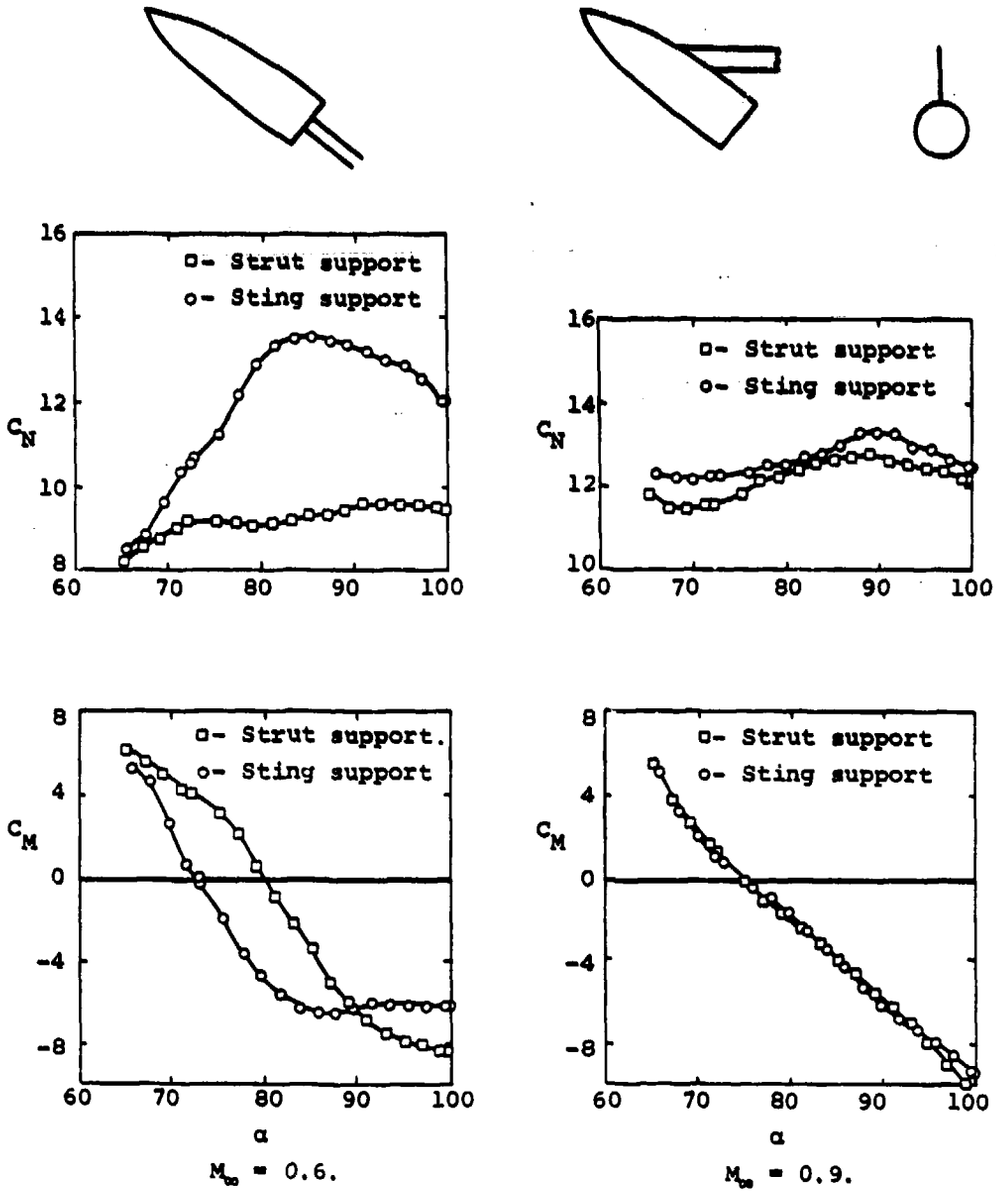

Figure 2. Effect of Support Type on Normal Force and Pitching Moments (Adapted from Reference 1)

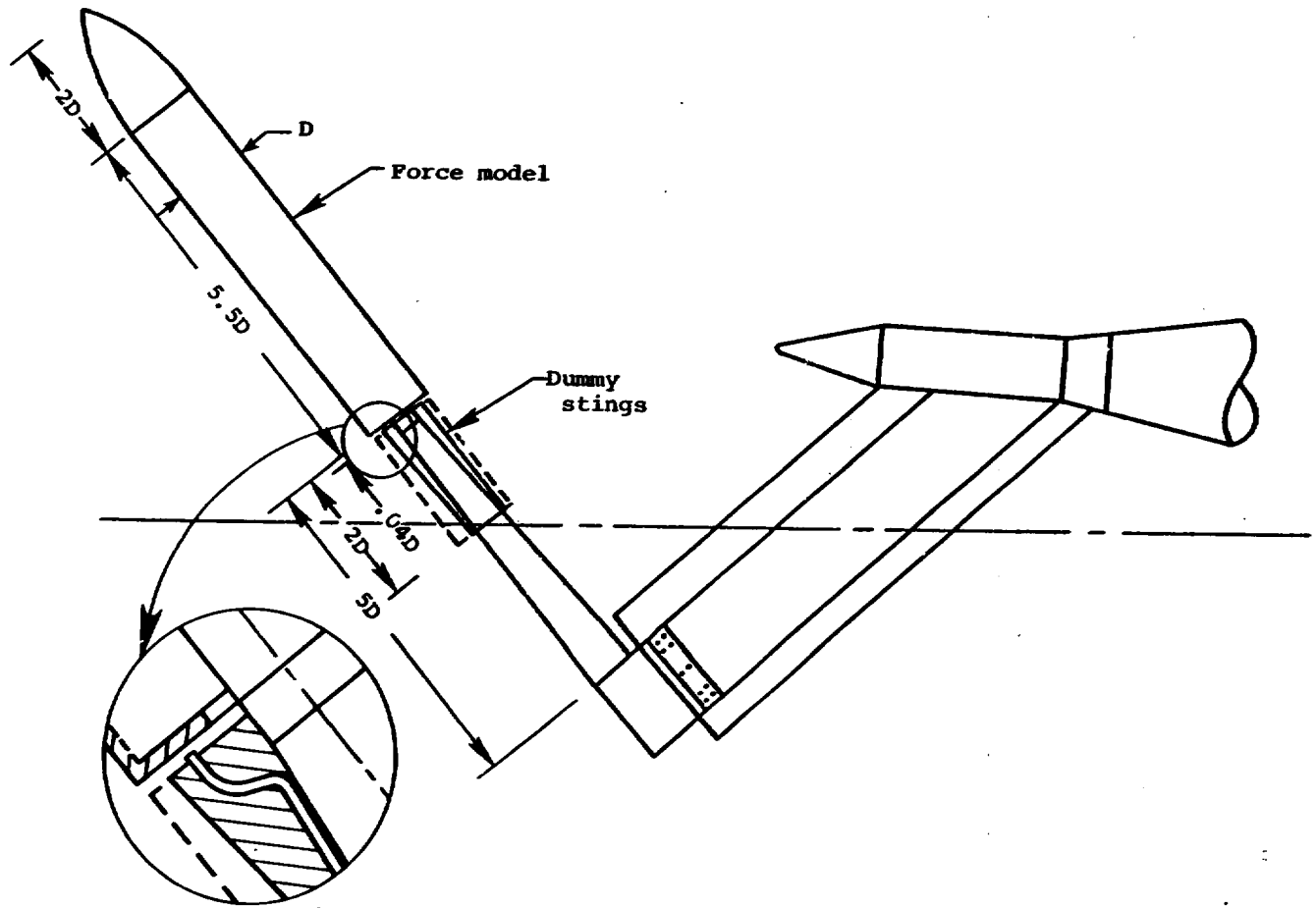

Figure 3a. Model and Baseline Support: Dummy Stings Shown

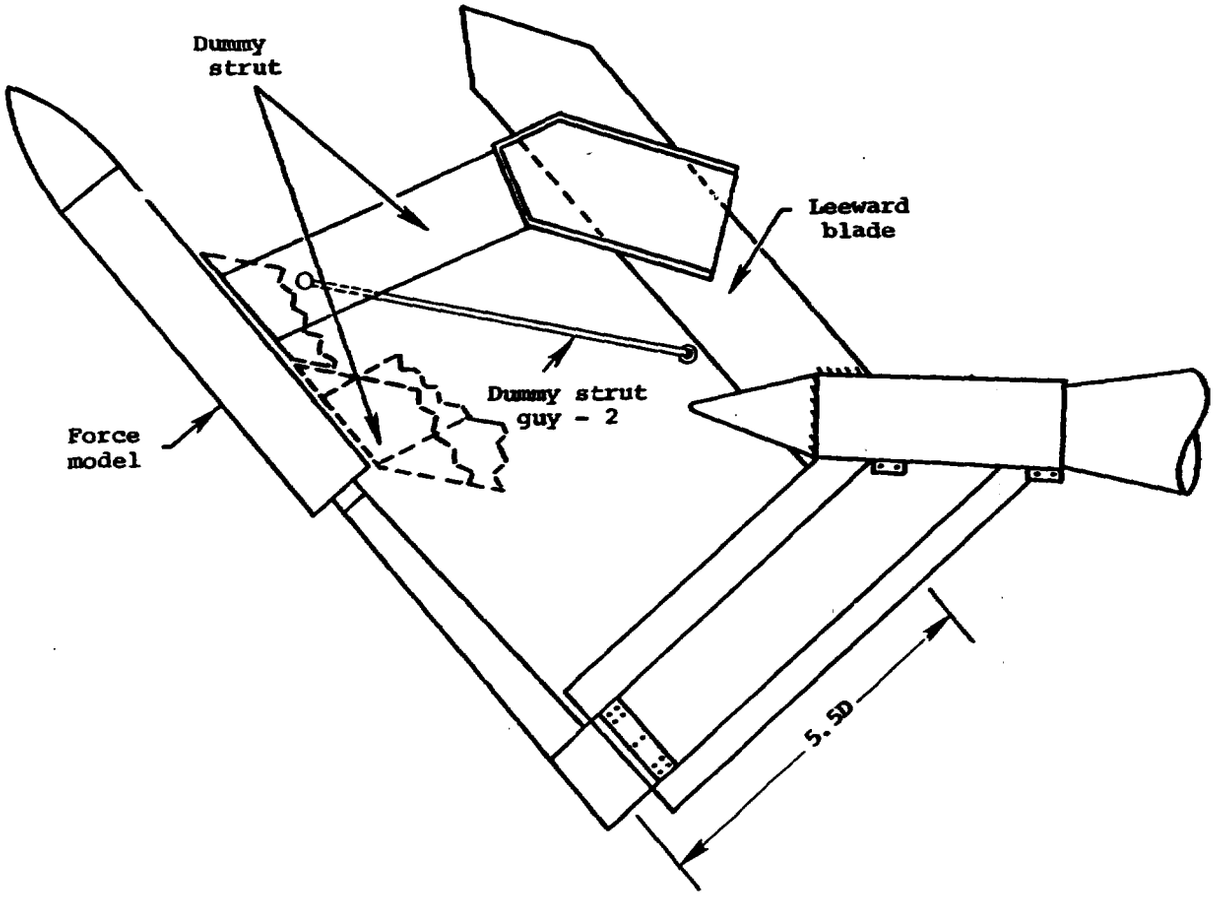

Figure 3b. Model and Leeward Dummy Strut Positions

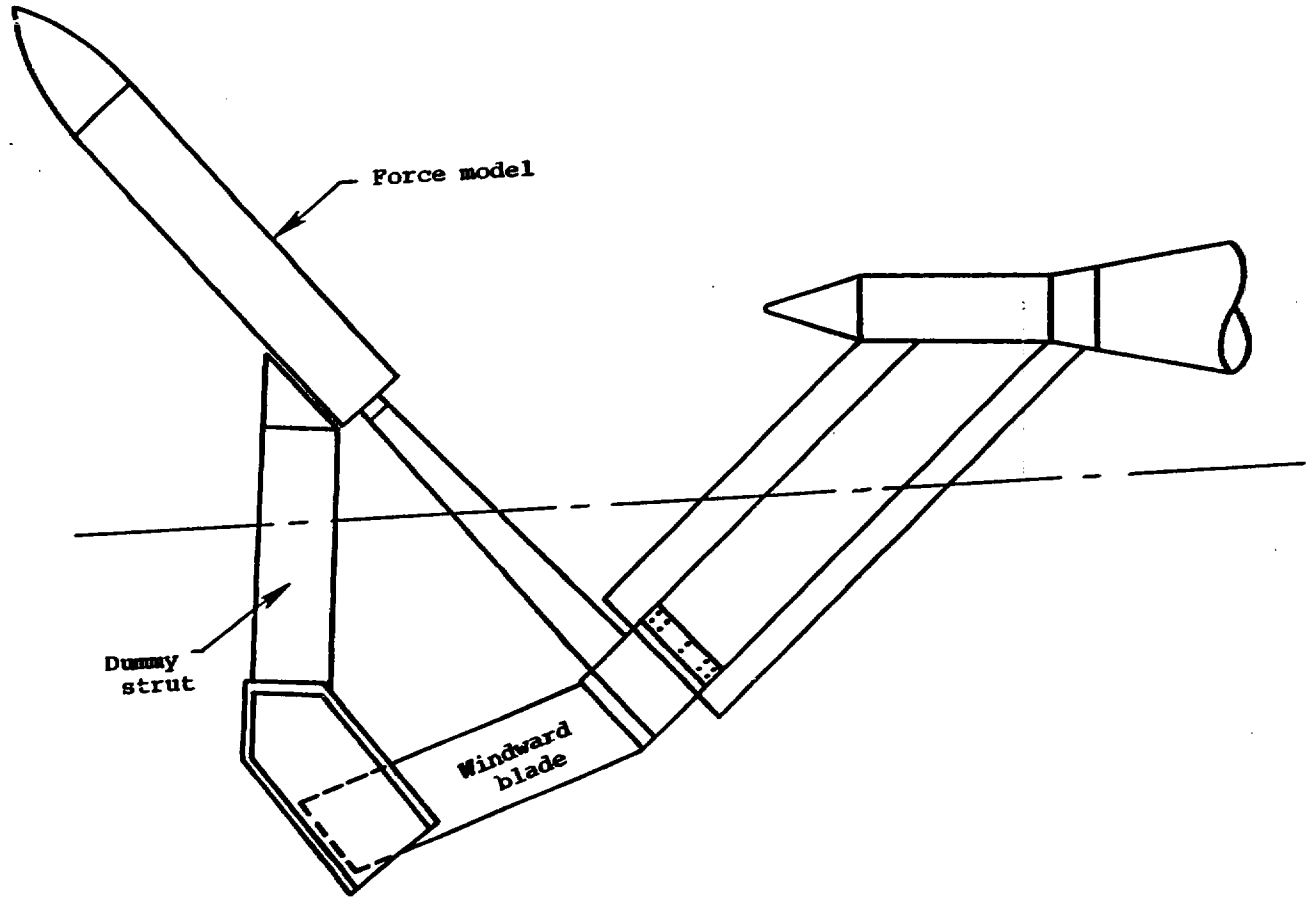

Figure 3c. Model with Windward Dummy Strut

Figure 4a. Photograph of Model and Windward Dummy Strut Mounted in NASA/Ames 14-Ft. Transonic Wind Tunnel

Figure 4b. Model with Leeward Dummy Strut

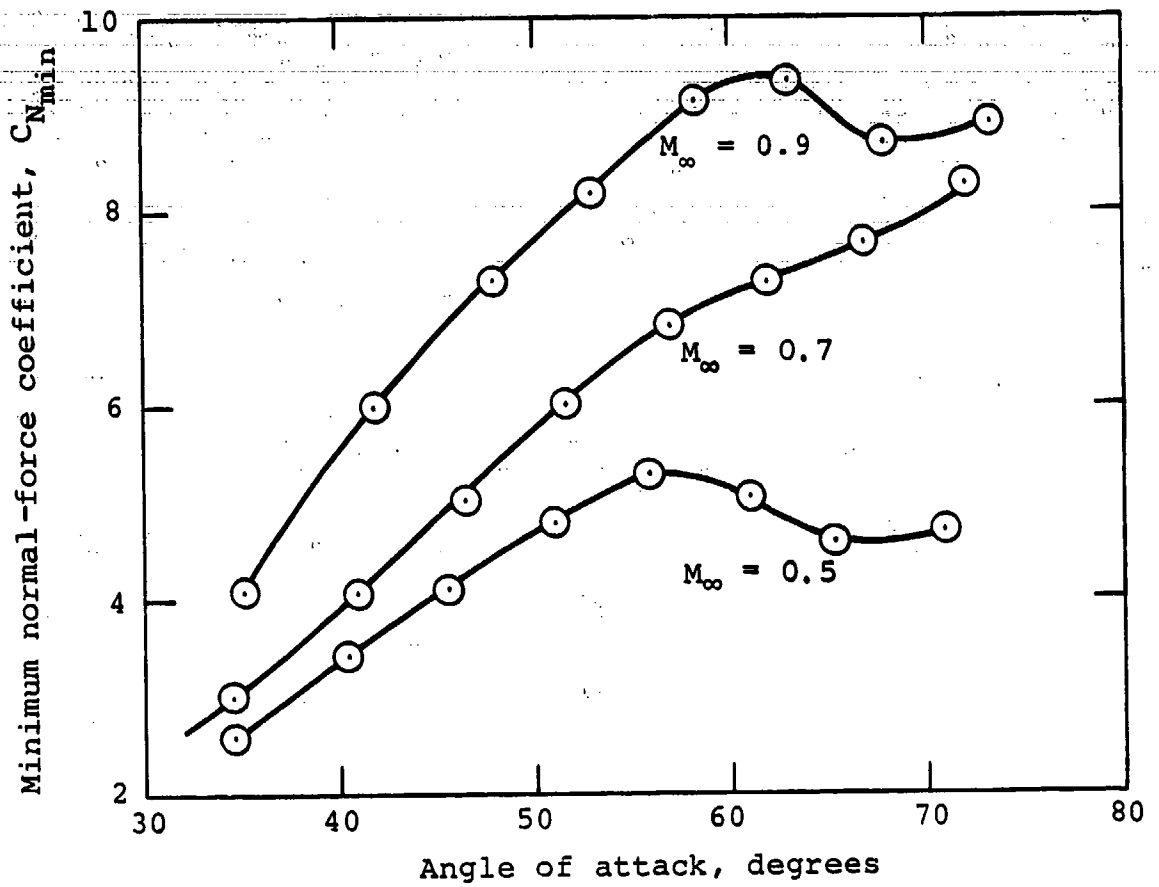

Figure 5. Variation of Minimum Observed Normal Force with Angle of Attack (Sting Diameter = 0.43 × Body Diameter)

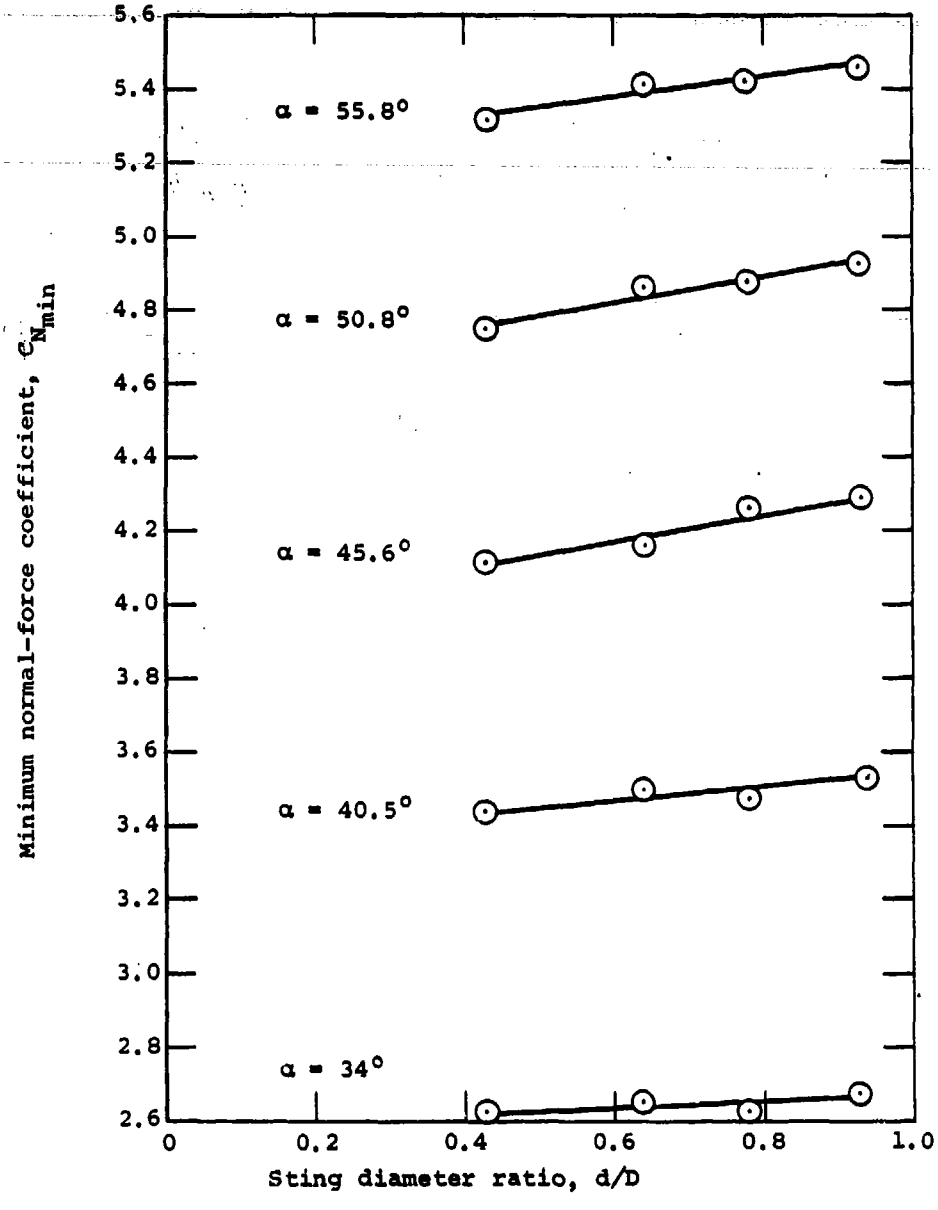

(a) M = 0.5

Figure 6. Effect of Sting Diameter on Minimum Normal Force

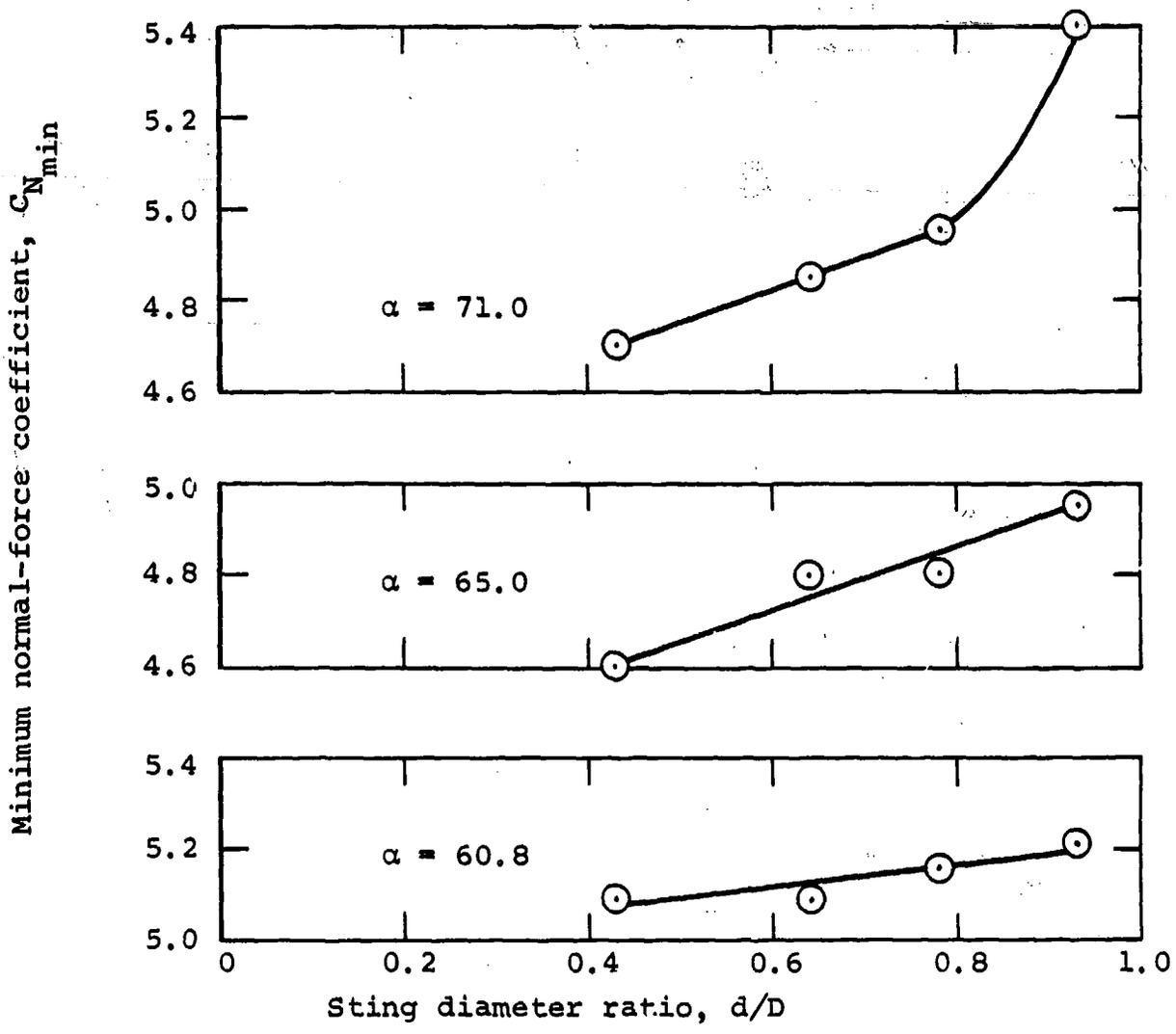

(b) M = 0.5

Figure 6. Effect of Sting Diameter on Minimum Normal Force (Continued)

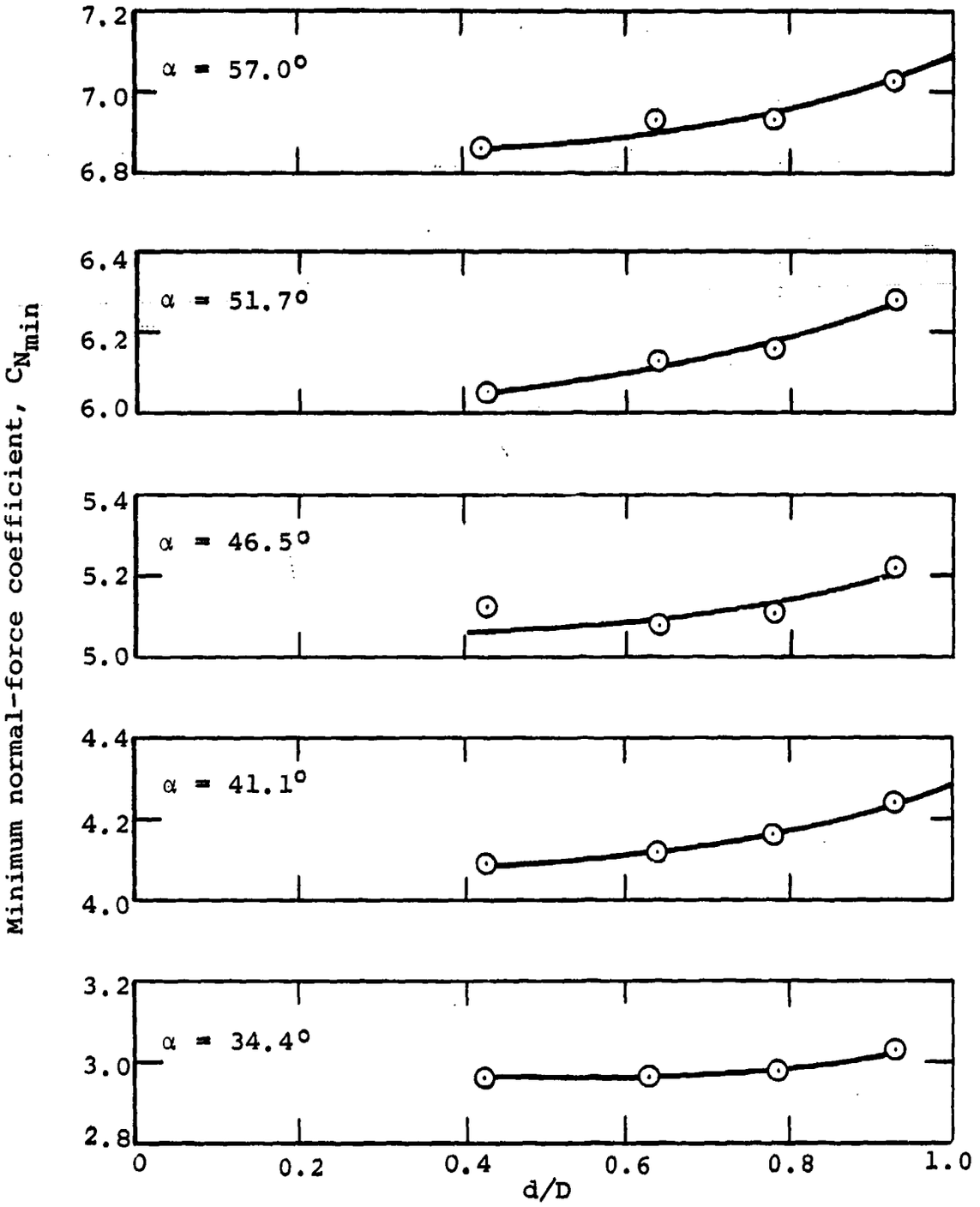

(c) M = 0.7

Figure 6. Effect of Sting Diameter on Minimum Normal Force (Continued)

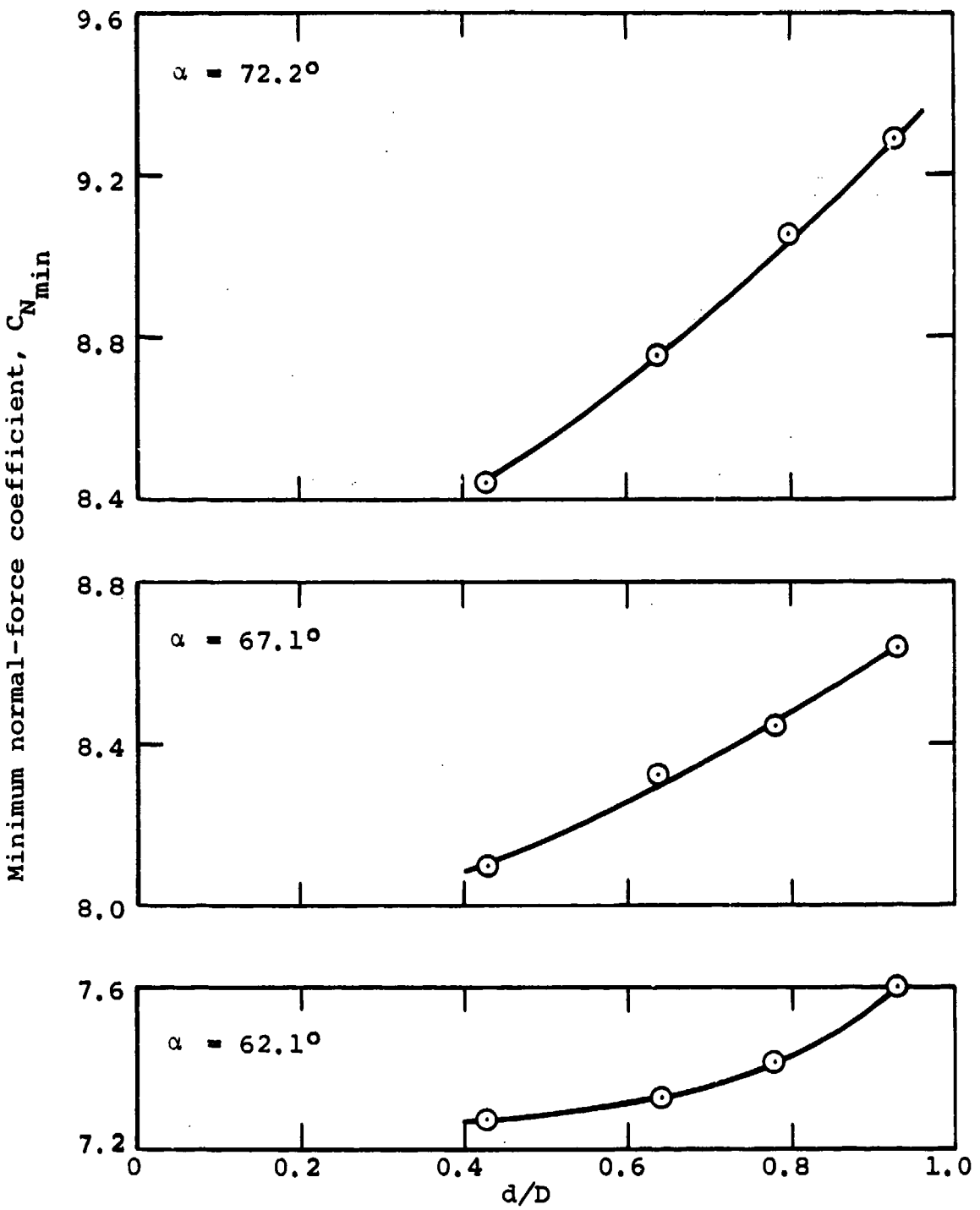

(d) M = 0.7

Figure 6. Effect of Sting Diameter on Minimum Normal Force (Continued)

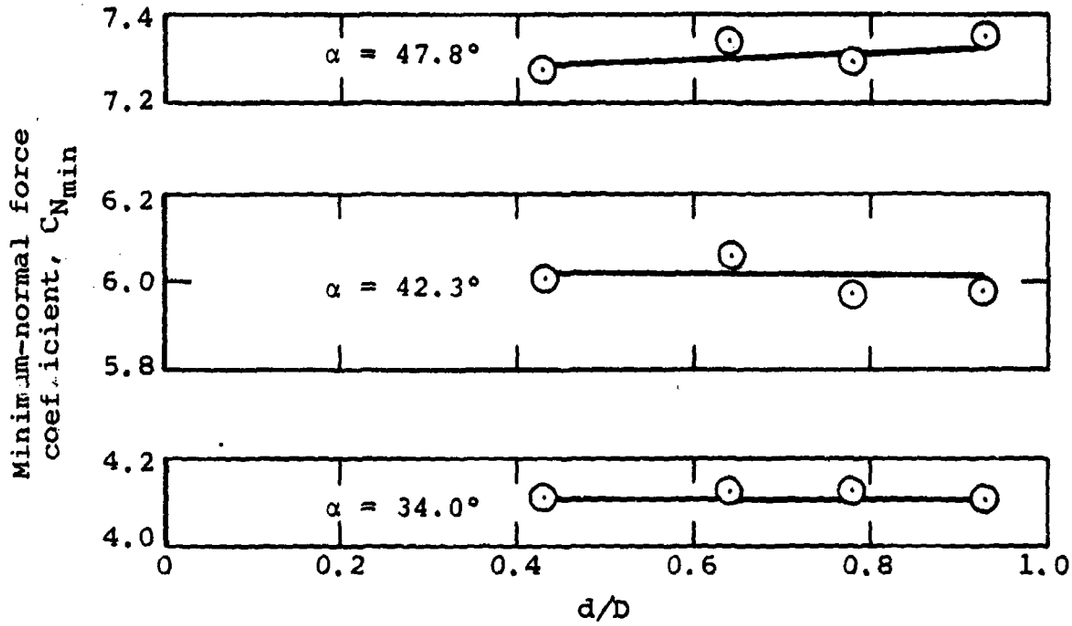

(e) M = 0.9

Figure 6. Effect of Sting Diameter on Minimum Normal Force (Continued)

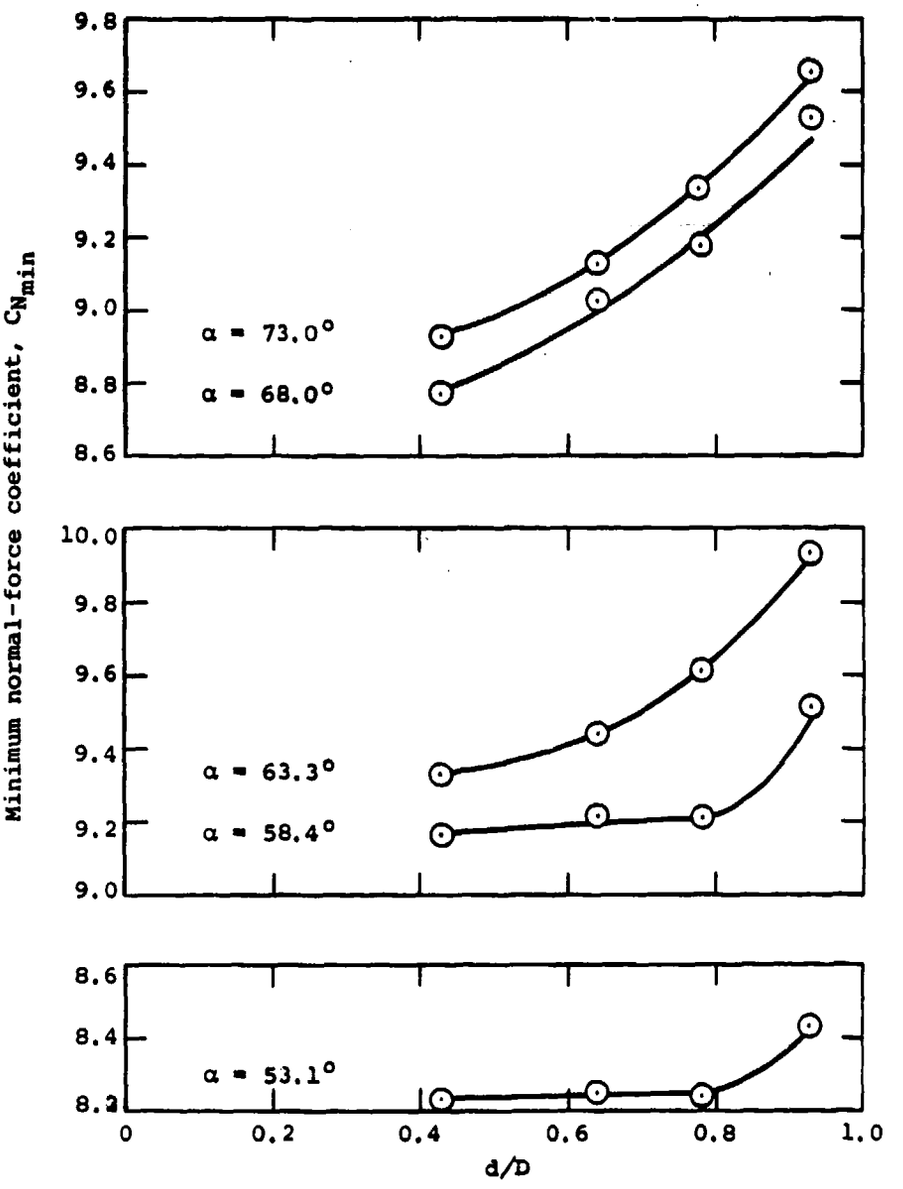

(f) M = 0.9

Figure 6. Effect of Sting Diameter on Minimum Normal Force (Concluded)

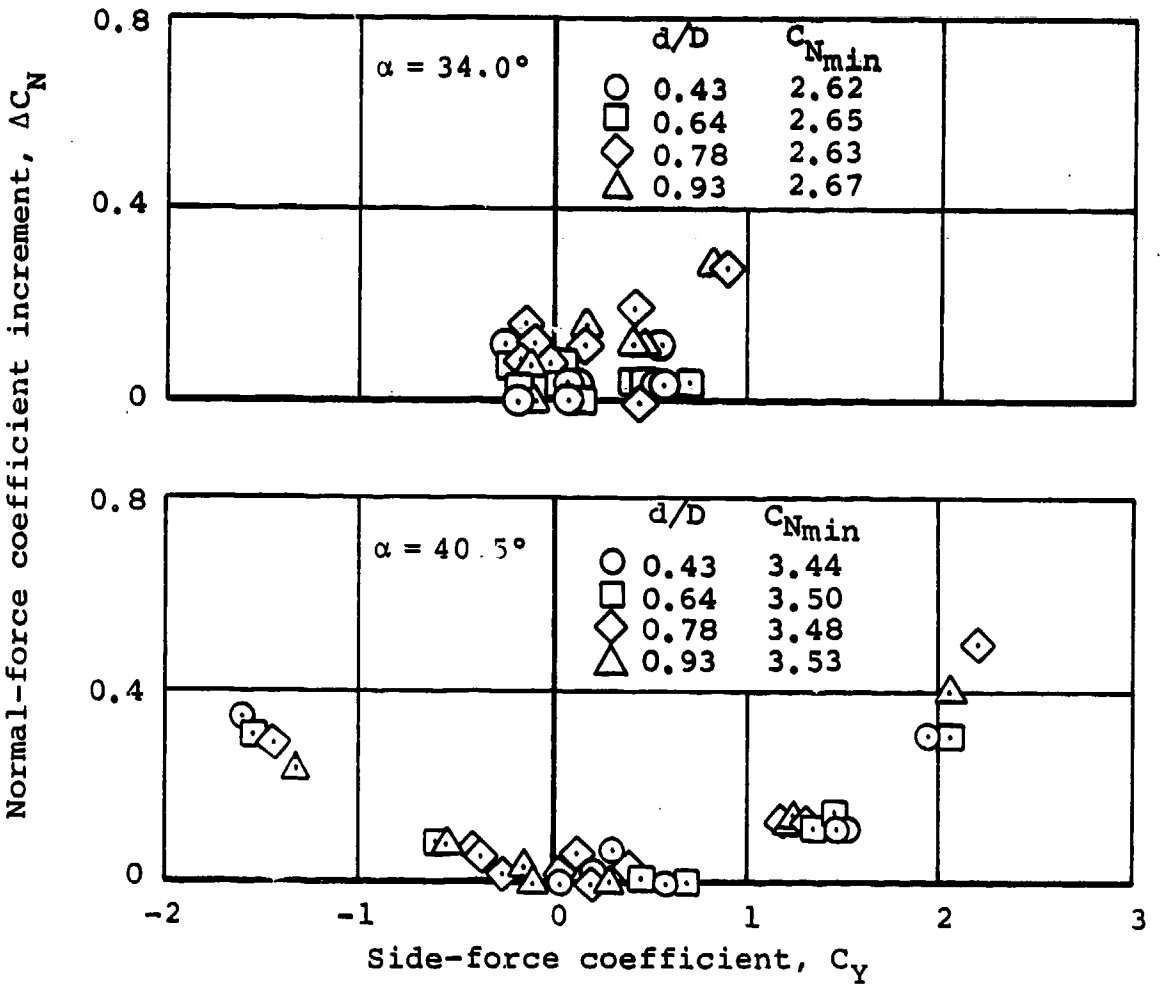

(a) α = 34.0° and 40.5°

Figure 7. Normal-force Relationship to Side Force for Four Sting Diameters at M_∞ = 0.5

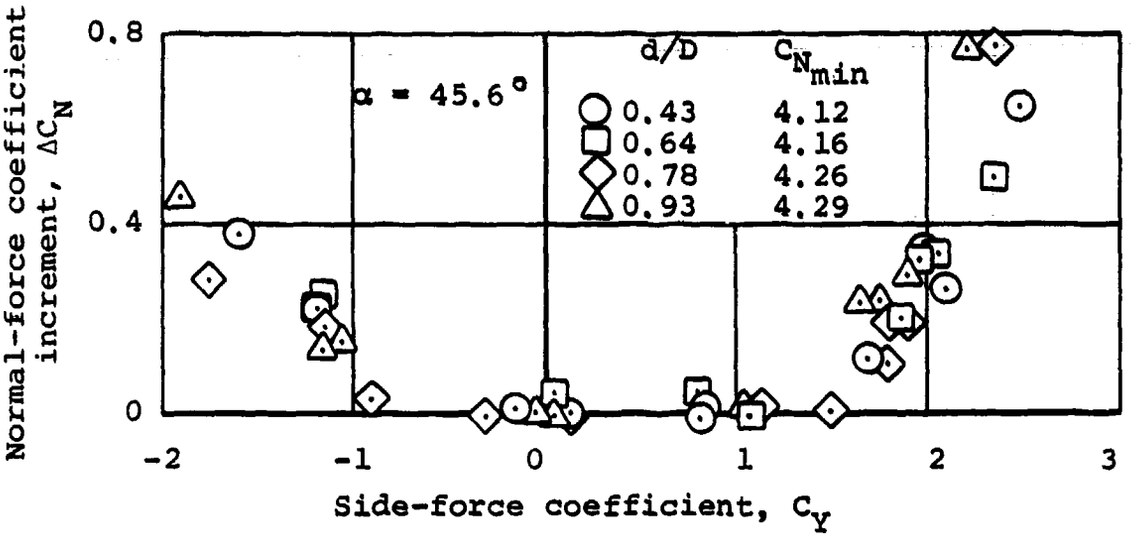

(b) α = 45.6°

Figure 7. Normal-Force Relationship to Side Force for Four Sting Diameters at M_∞ = 0.5 (Continued)

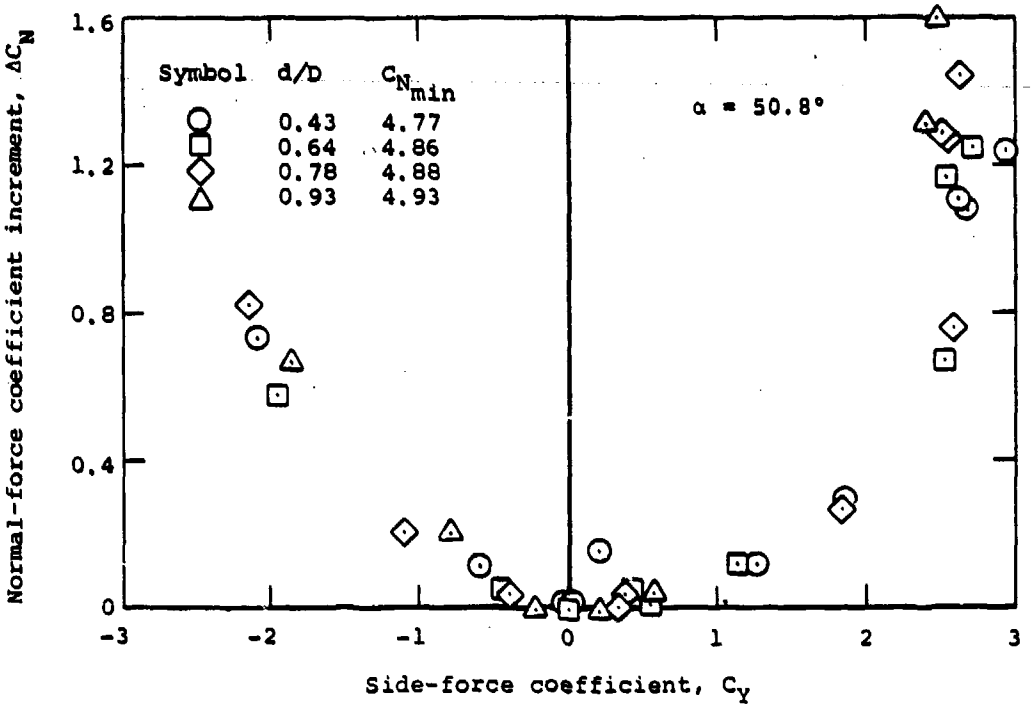

(c) $\alpha = 50.8°$

Figure 7. Normal-Force Relationship to Side Force for Four Sting Diameters at $M_\infty = 0.5$ (Continued)

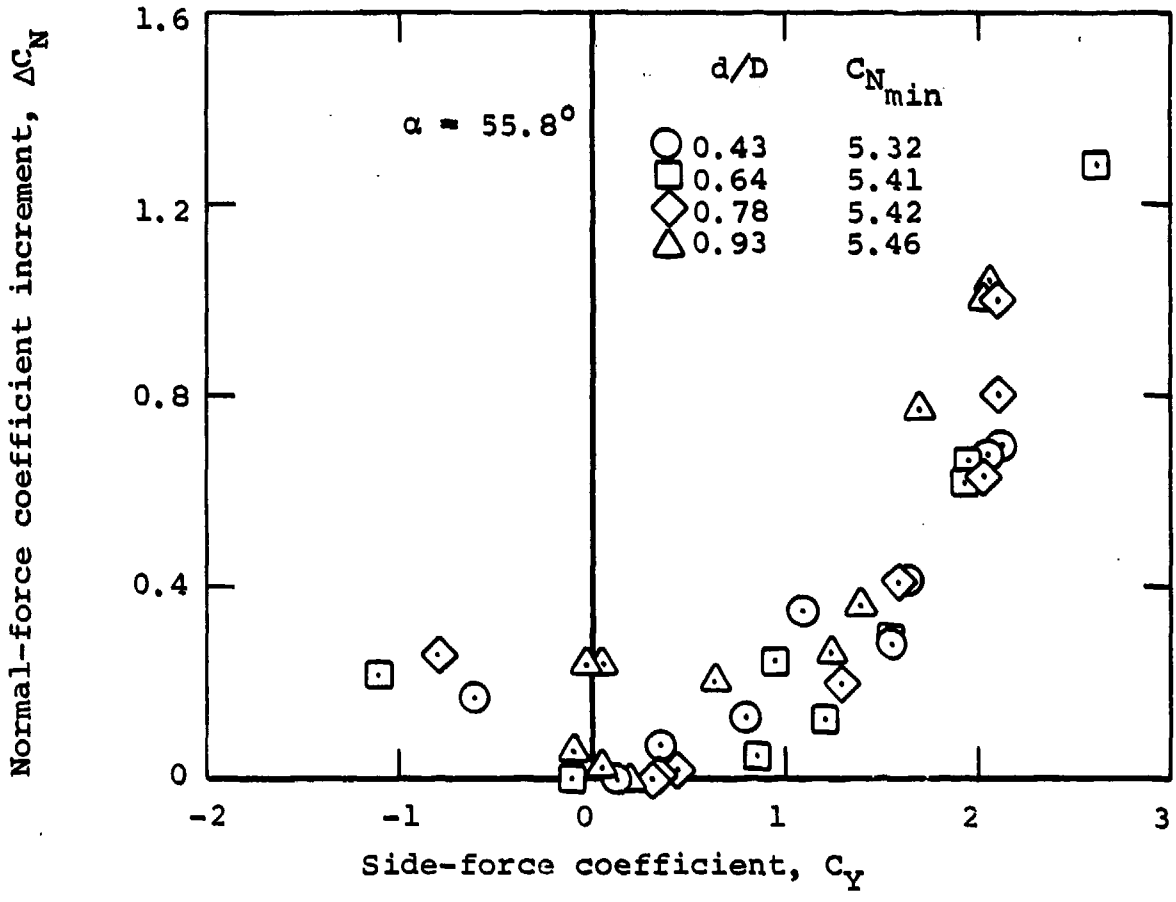

(d) α = 55.8°

Figure 7. Normal-Force Relationship to Side Force for Four Sting Diameters at M_∞ = 0.5 (Continued)

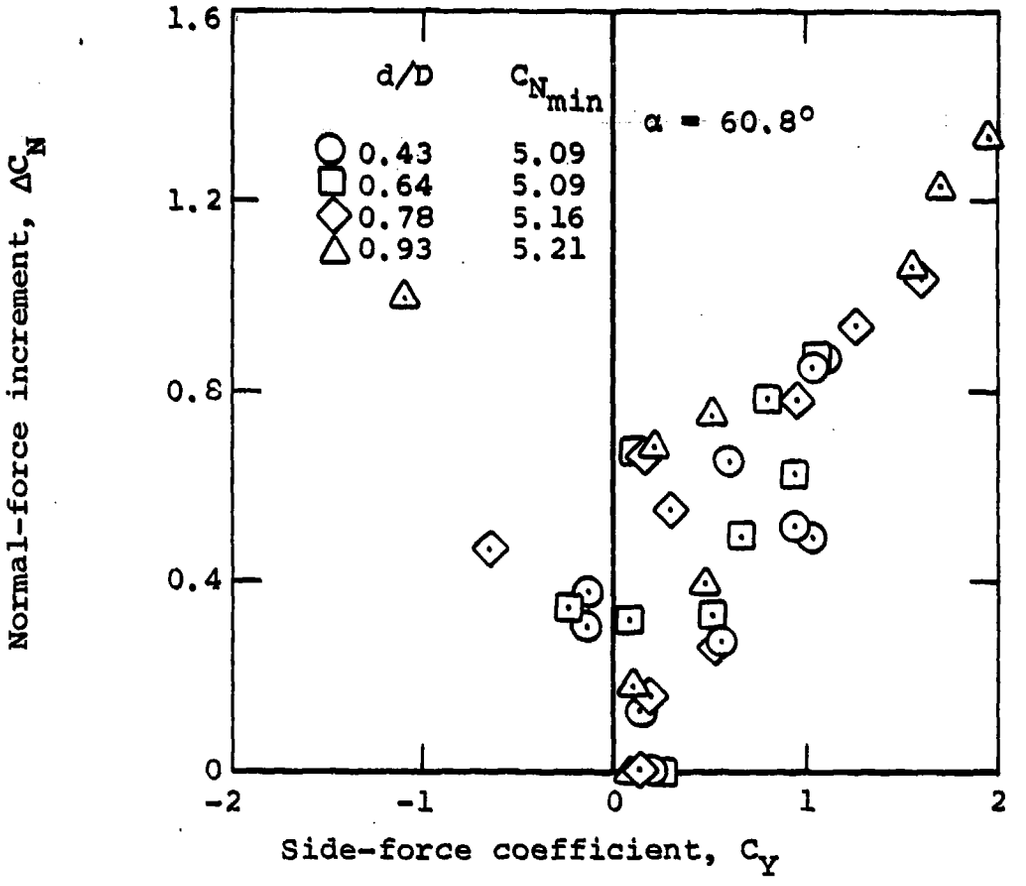

(e) $\alpha = 60.8°$

Figure 7. Normal-Force Relationship to Side Force for Four Sting Diameters at $M_\infty = 0.5$ (Continued)

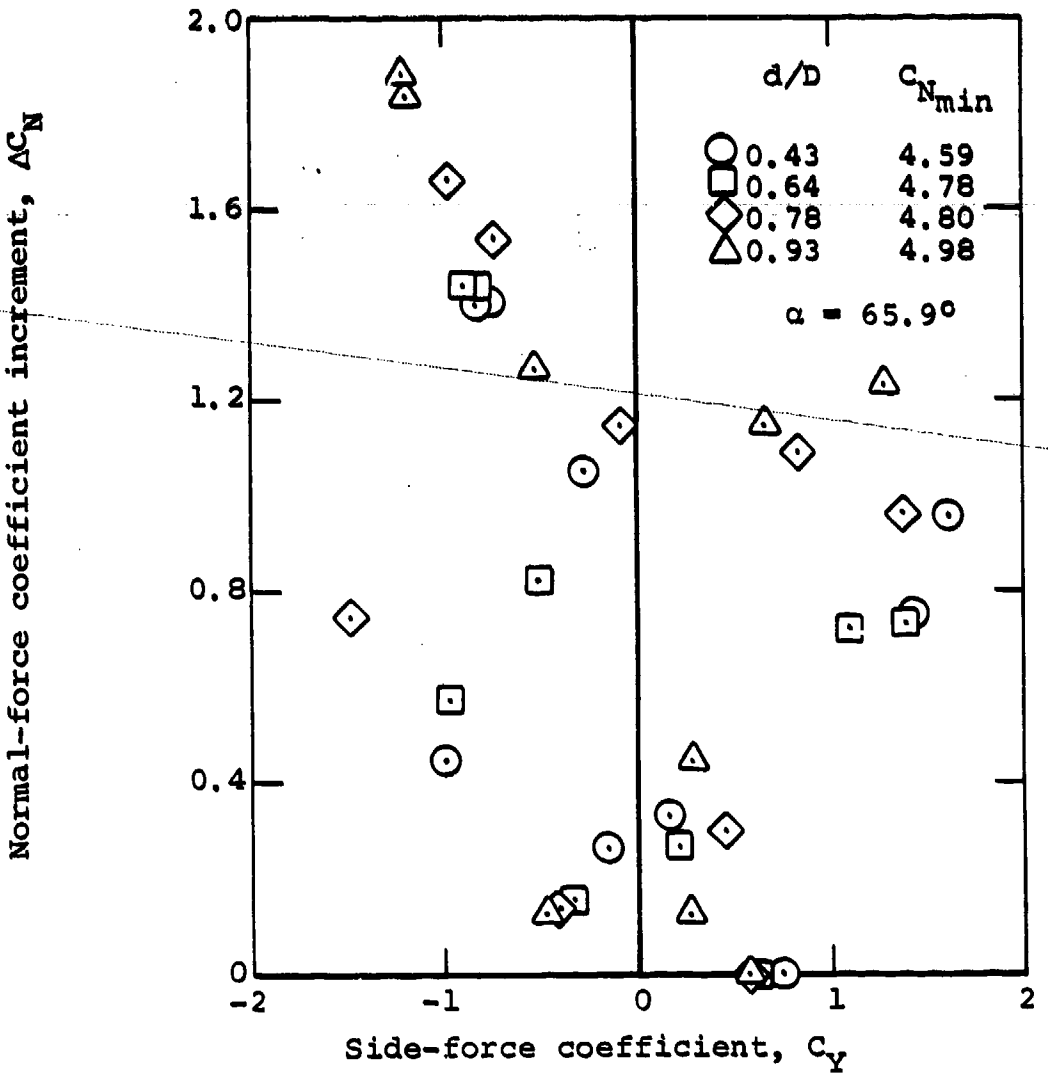

(f) $\alpha = 65.9°$

Figure 7. Normal-Force Relationship to Side Force for Four Sting Diameters at $M_\infty = 0.5$ (Continued)

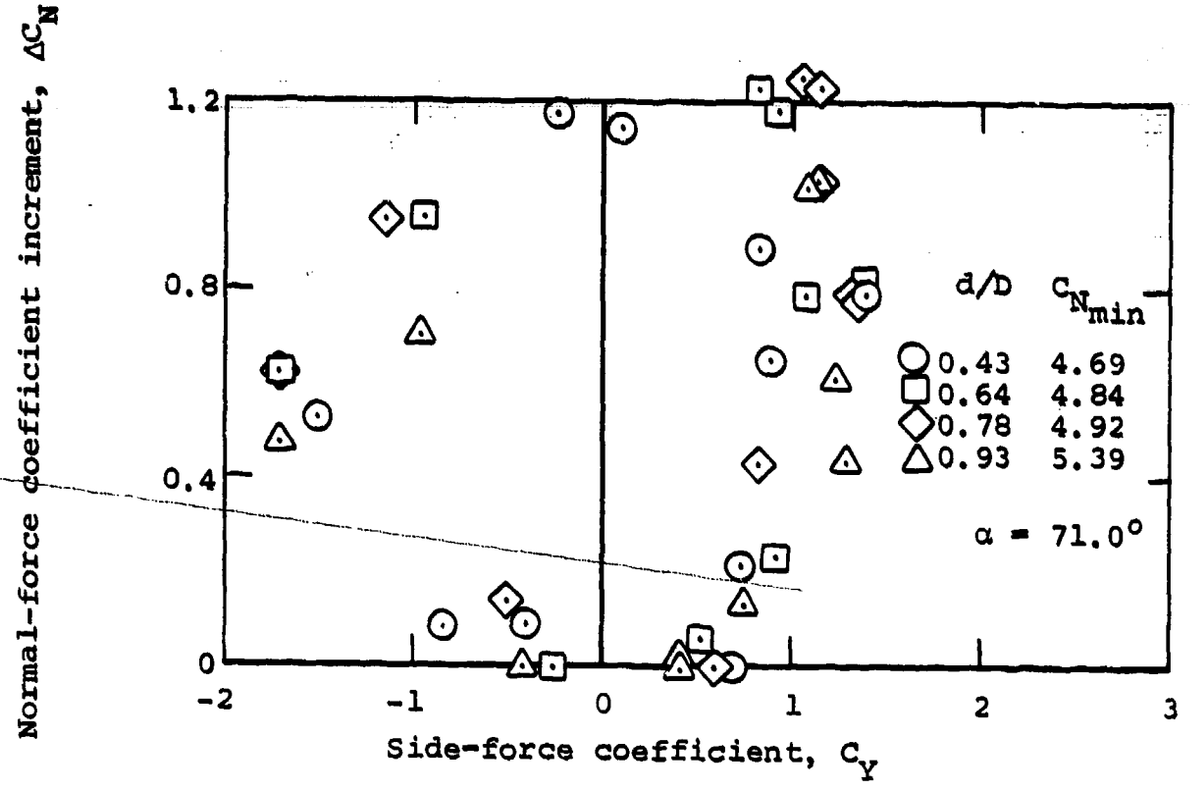

(g) $\alpha = 71.0°$

Figure 7. Normal-Force Relationship to Side Force for Four Sting Diameters at $M_\infty = 0.5$ (Concluded)

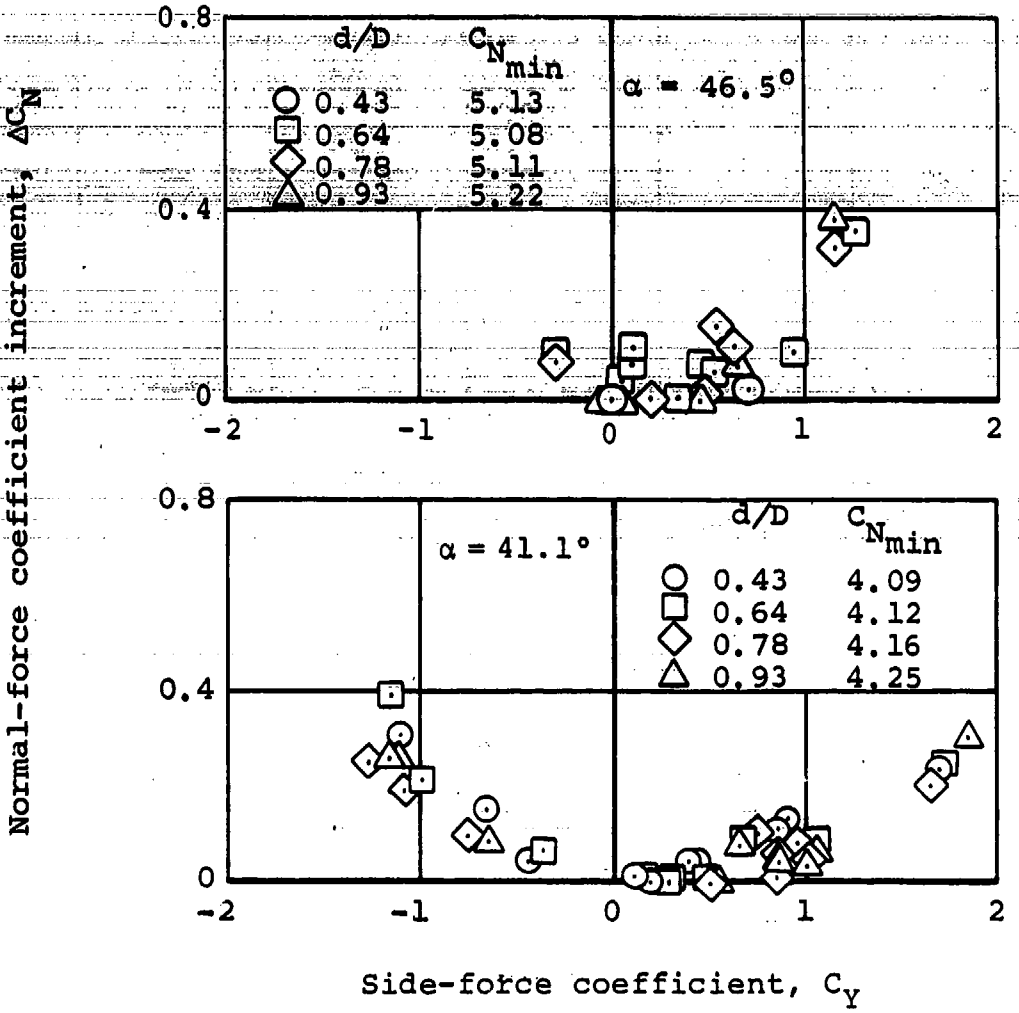

Figure 8. Normal Force Relationship to Side Force for Four Sting Diameters at M_∞ = 0.70 and α = 41.1 and 46.5 Degrees

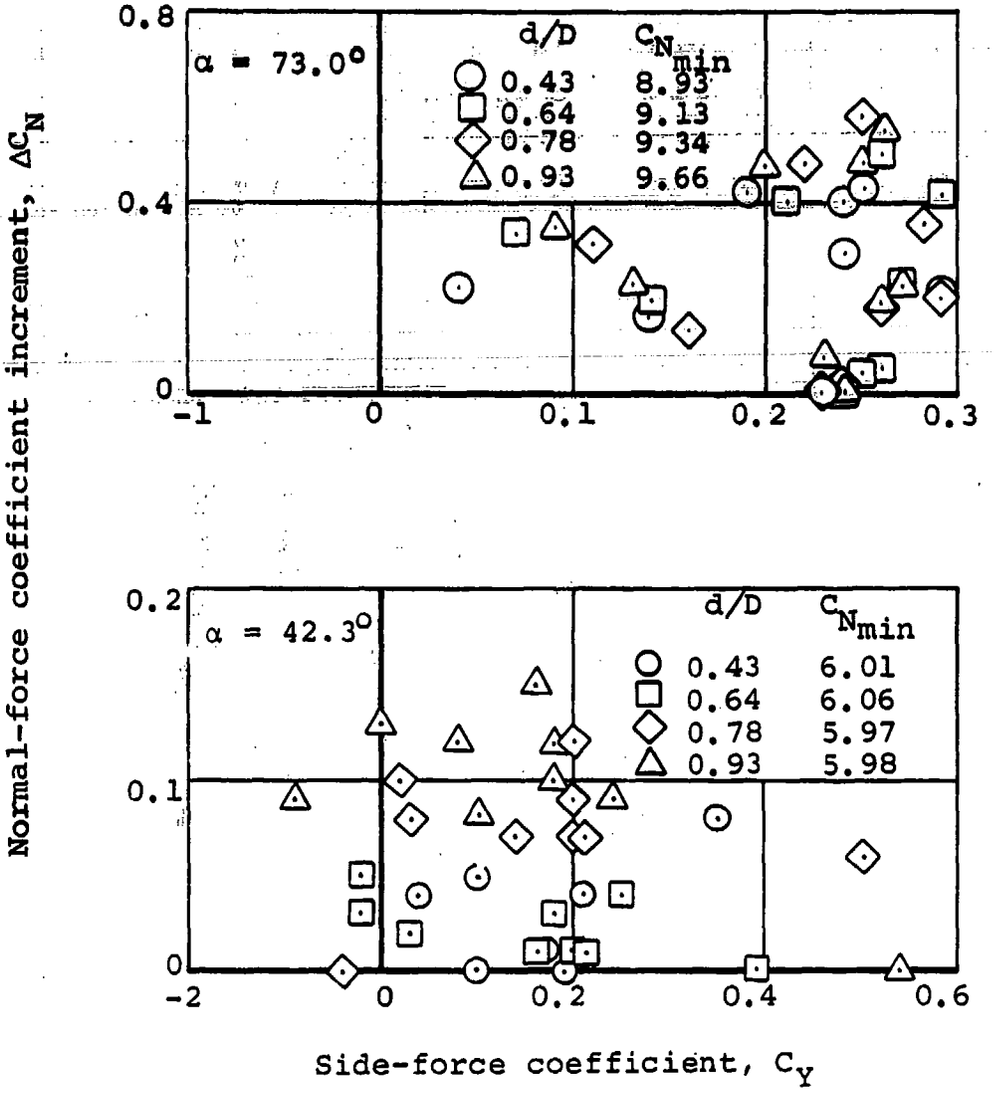

Figure 9. Normal-Force and Side-Force Results for Four Sting Diameters at M_∞ = 0.9 and α = 42.3 and 73.0 Degrees

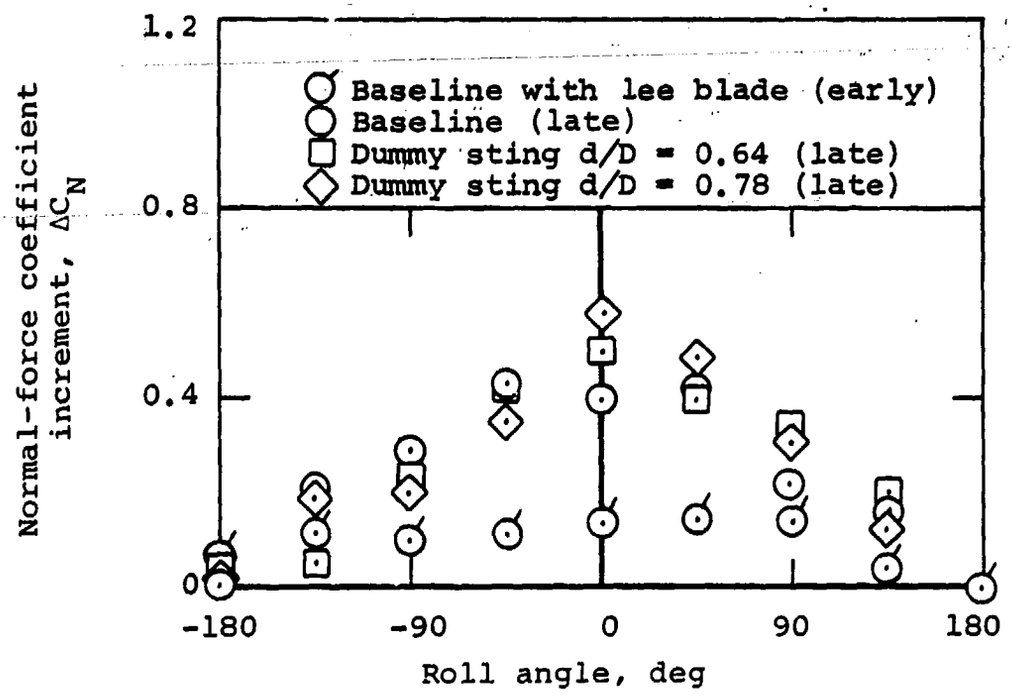

Figure 10. Effect of Elapsed Testing Time on Incremental Changes in Normal Force with Roll Position: M = 0.9, α = 73 Degrees

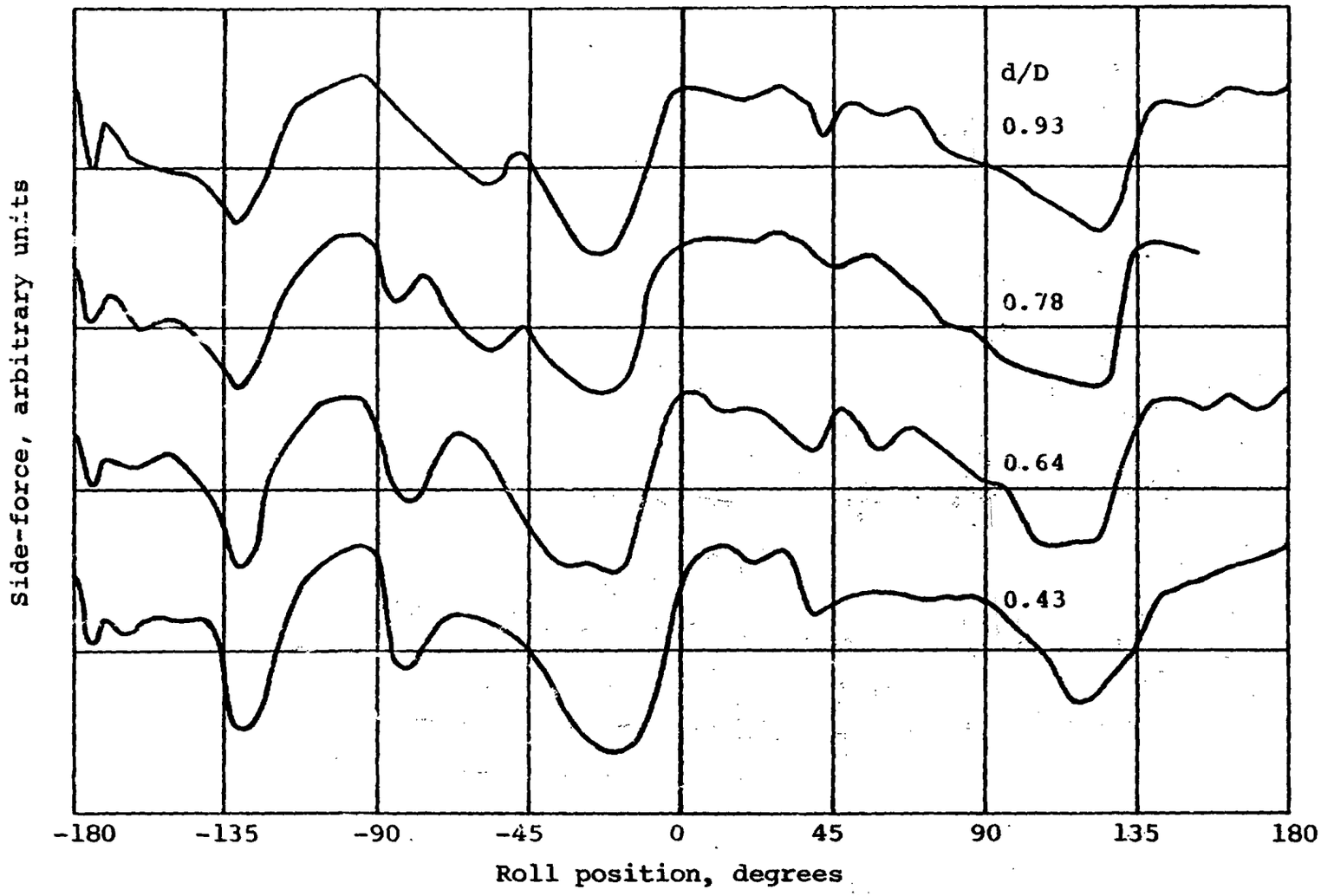

Figure 11. Side-Force Signatures with Four Sting Diameters: $M_\infty = 0.5$, $\alpha = 52$ Degrees

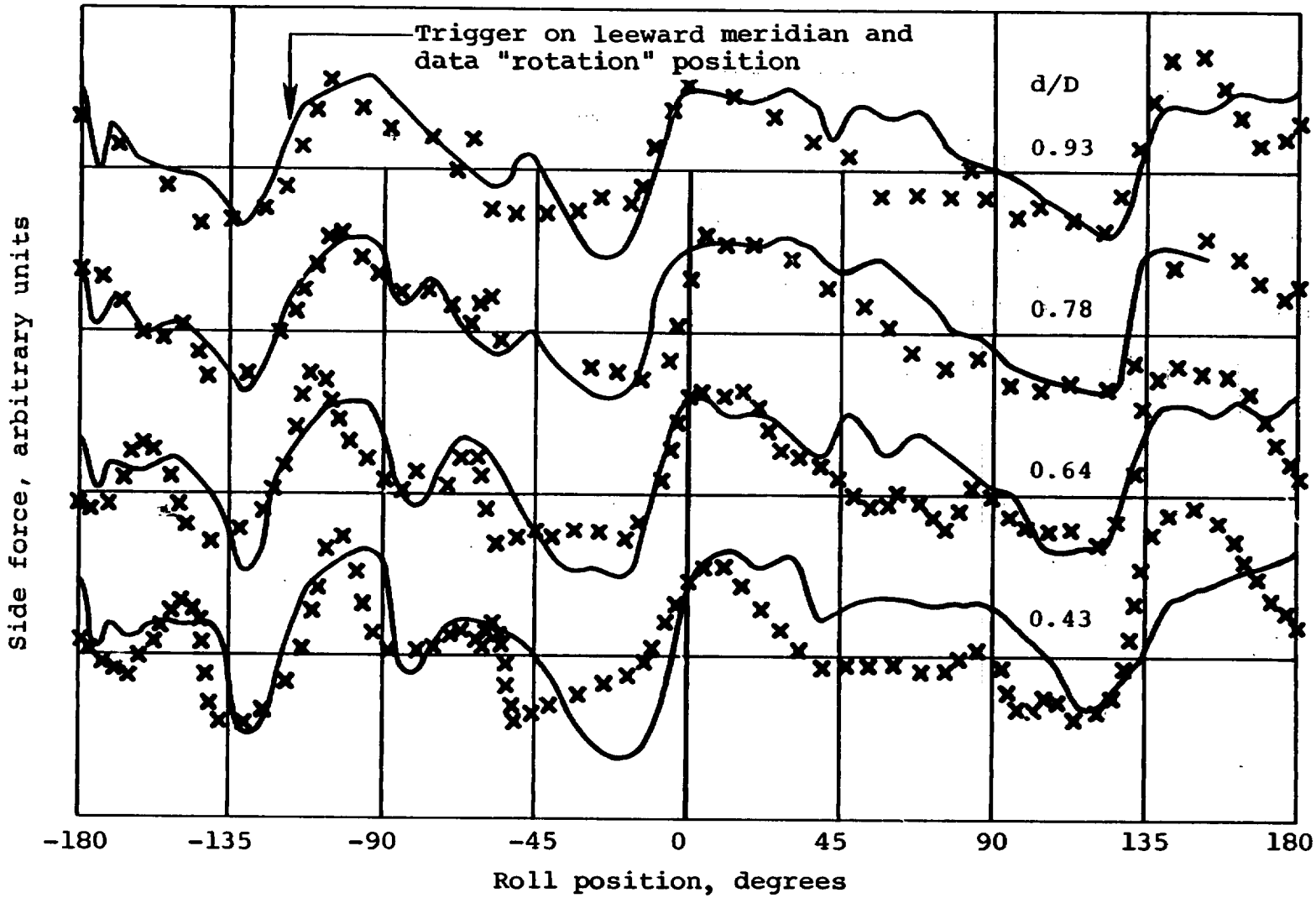

Figure 12. Symmetry of Side-Force Signatures with Four Sting Diameters: $M_\infty = 0.5$, $\alpha = 50$ Degrees

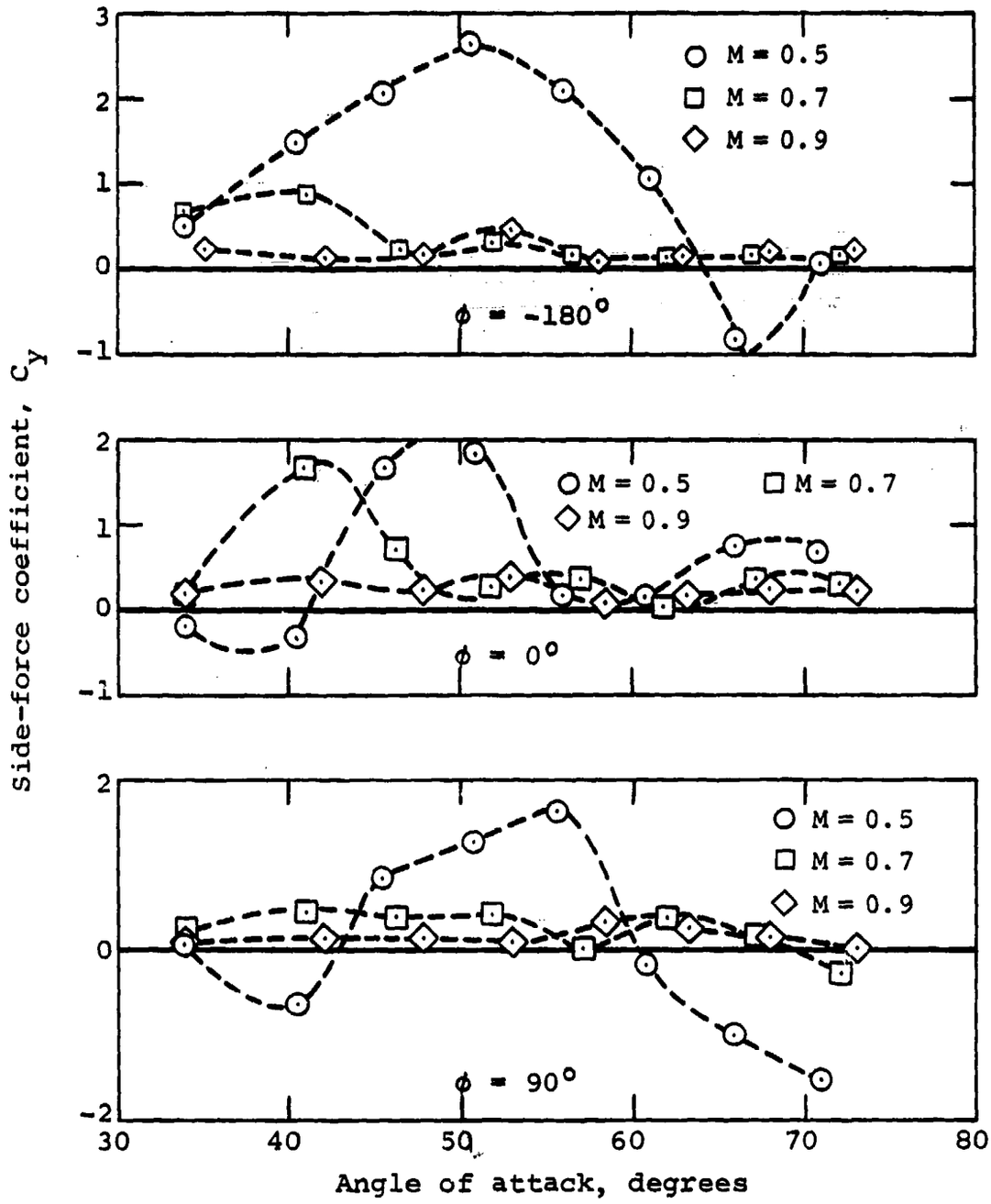

Figure 13. Variation of Side Force with Angle of Attack for Three Selected Roll Positions at Three Mach Numbers

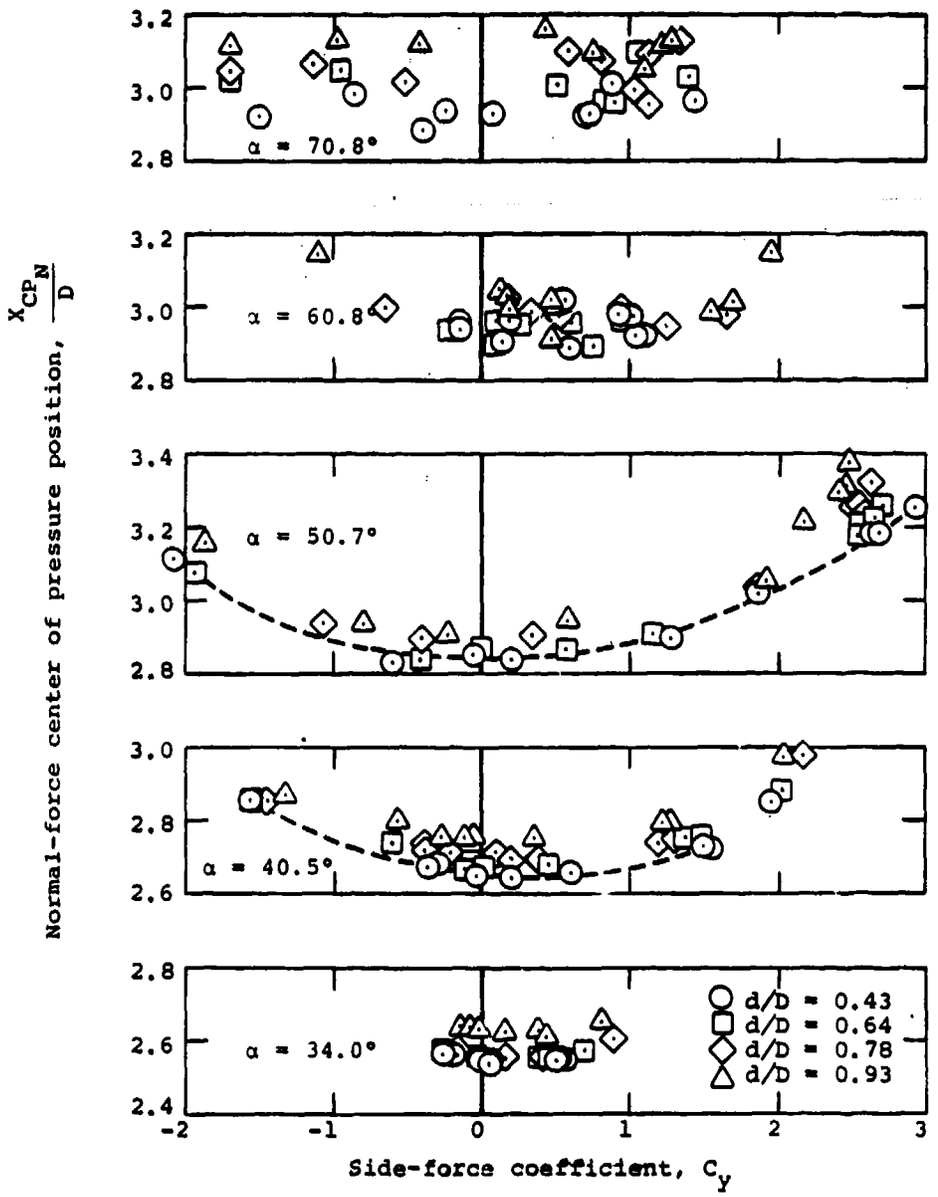

(a) M = 0.5

Figure 14. Effect of Sting Diameter on Position of Center of Pressure of Normal Force

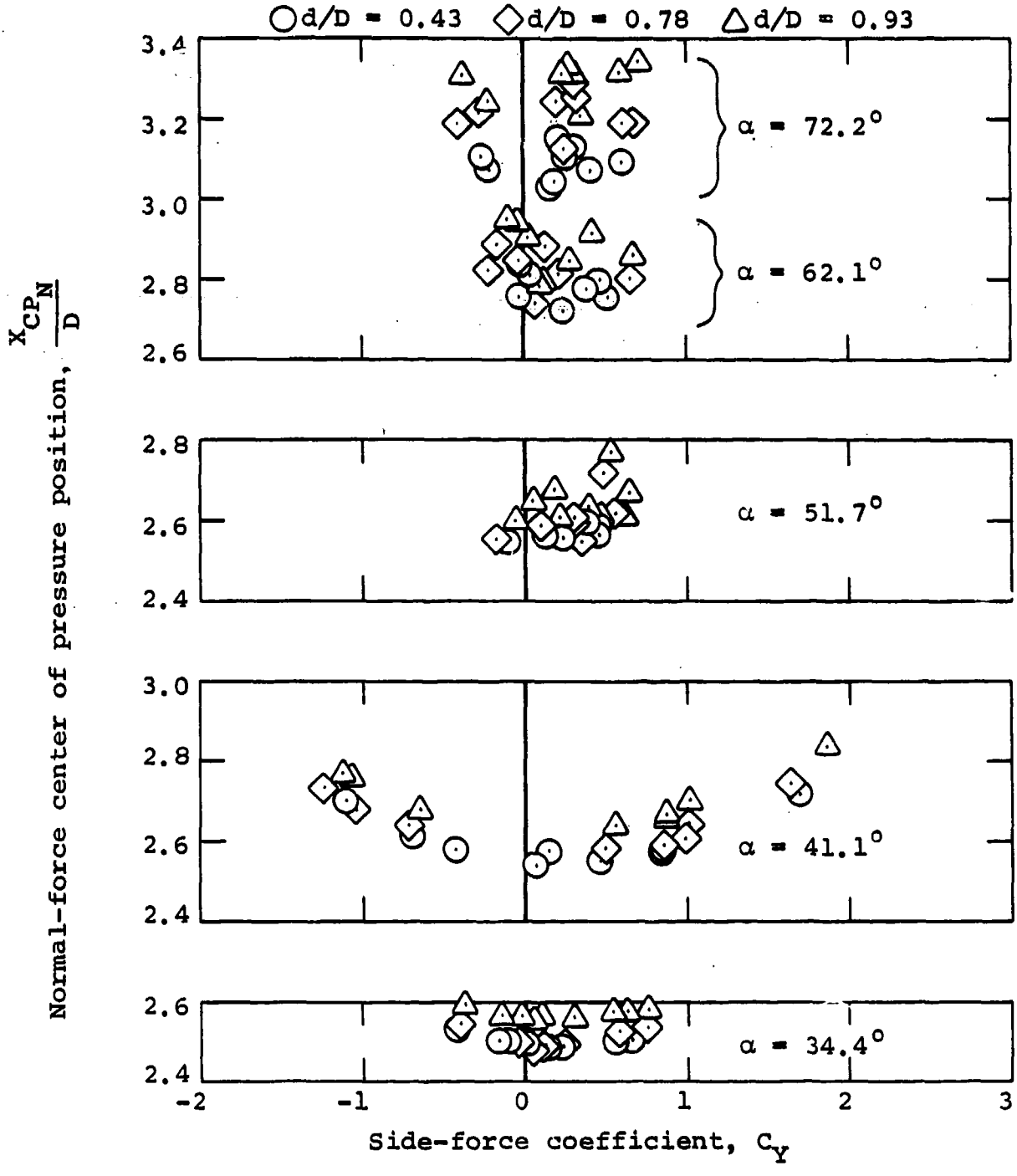

(b) M = 0.7

Figure 14. Effect of Sting Diameter on Position of Center of Pressure of Normal Force (Continued)

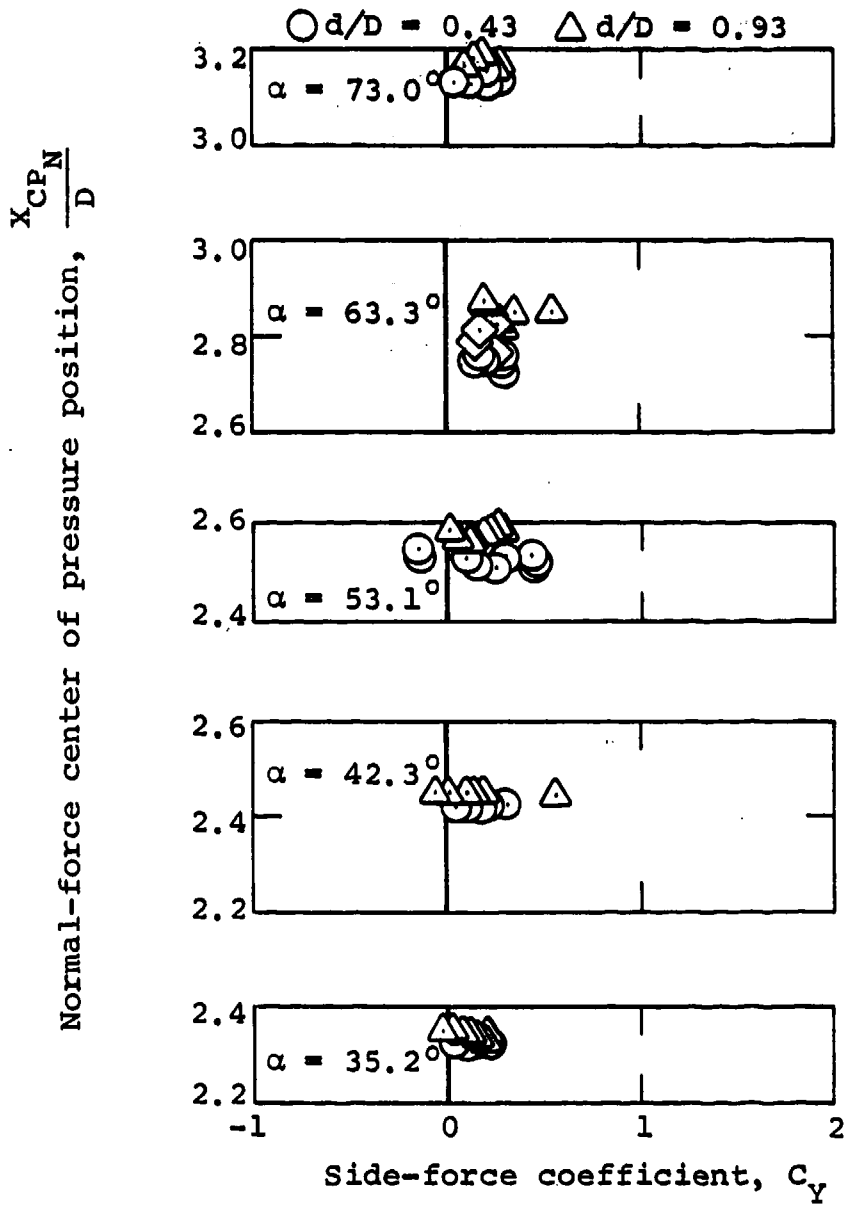

(c) M = 0.9

Figure 14. Effect of Sting Diameter on Position of Center of Pressure of Normal Force (Concluded)

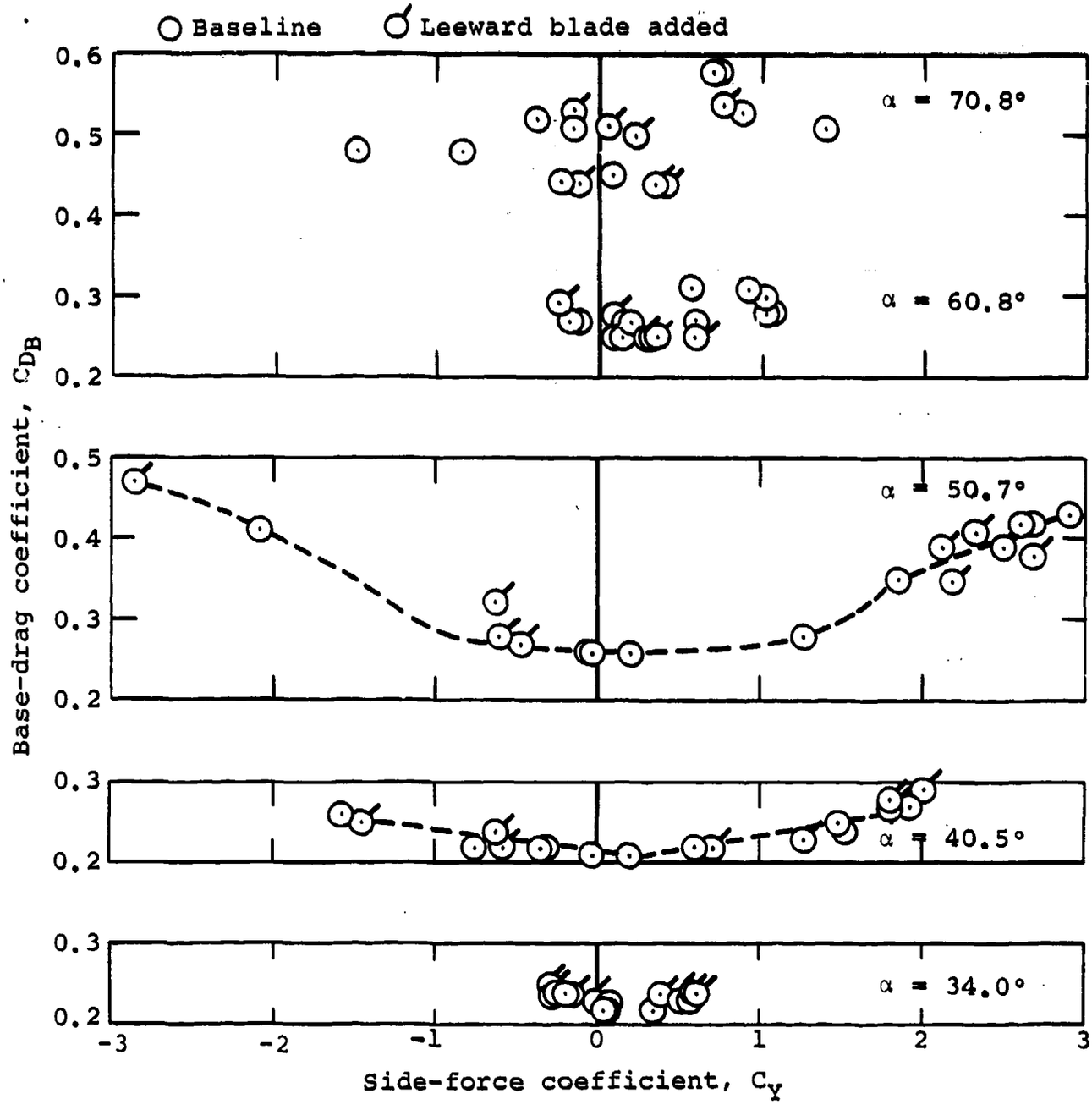

(a) M = 0.5

Figure 15. Relationship Between Base Drag and Side Force

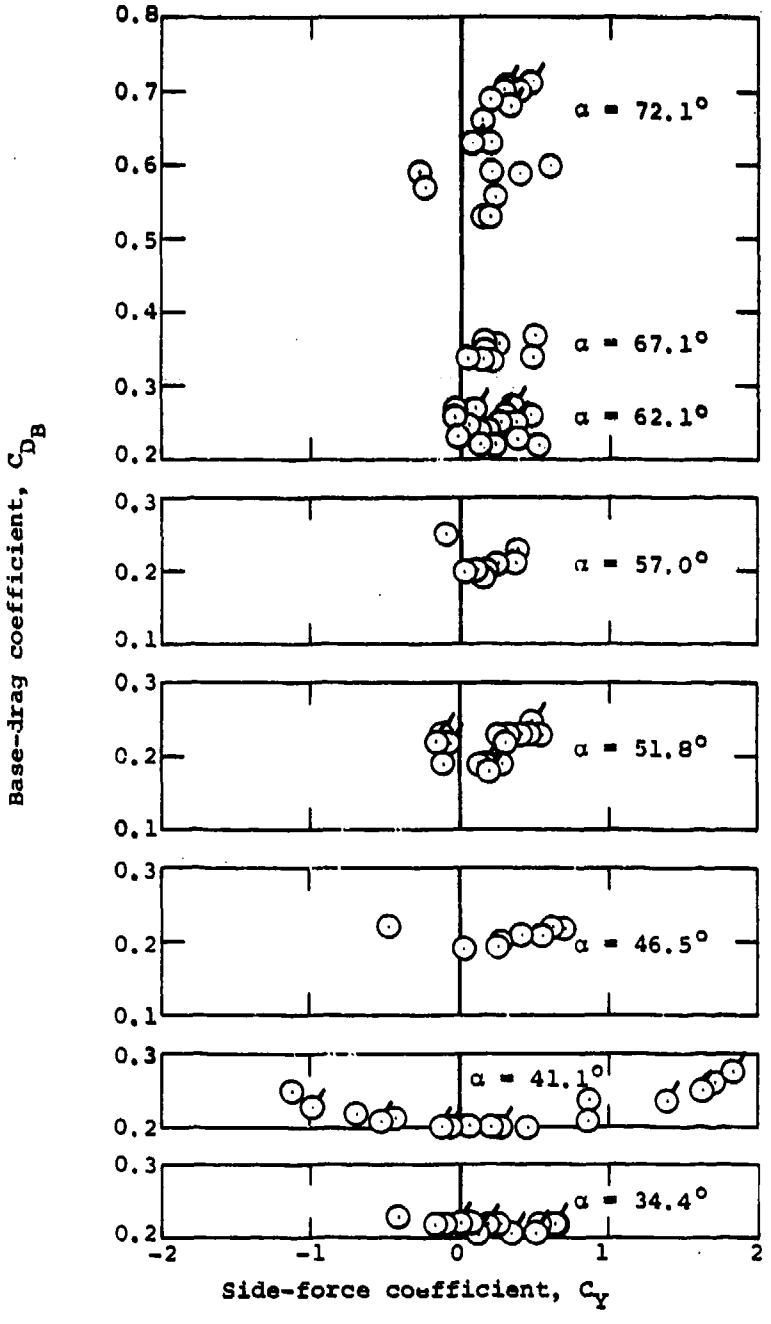

(b) M = 0.7

Figure 15. Relationship Between Base Drag and Side Force (Concluded)

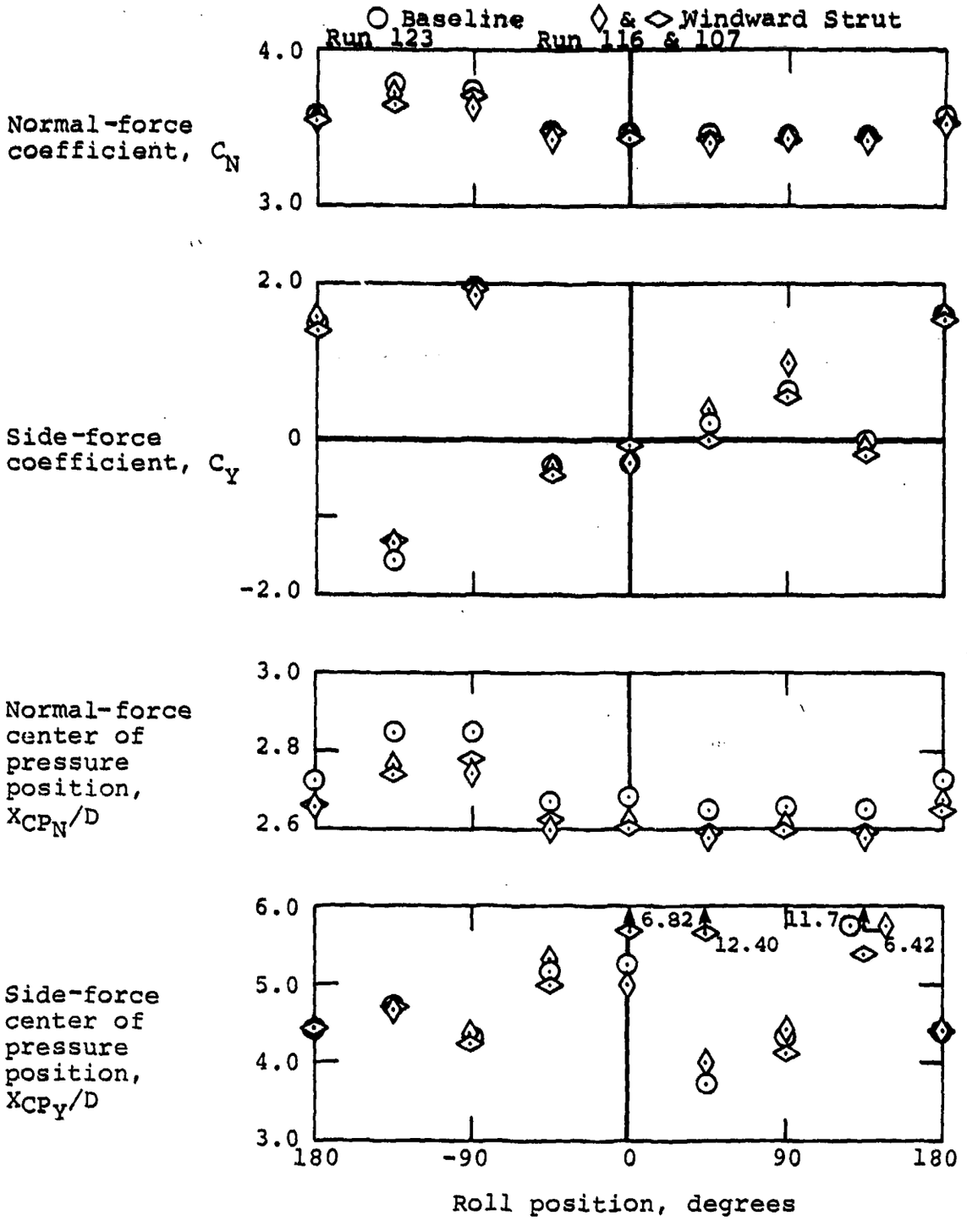

Figure 16. Short-Term Repeatability of Results and Effect of Windward Strut: $M_\infty = 0.5$, $\alpha = 40.5$ Degrees

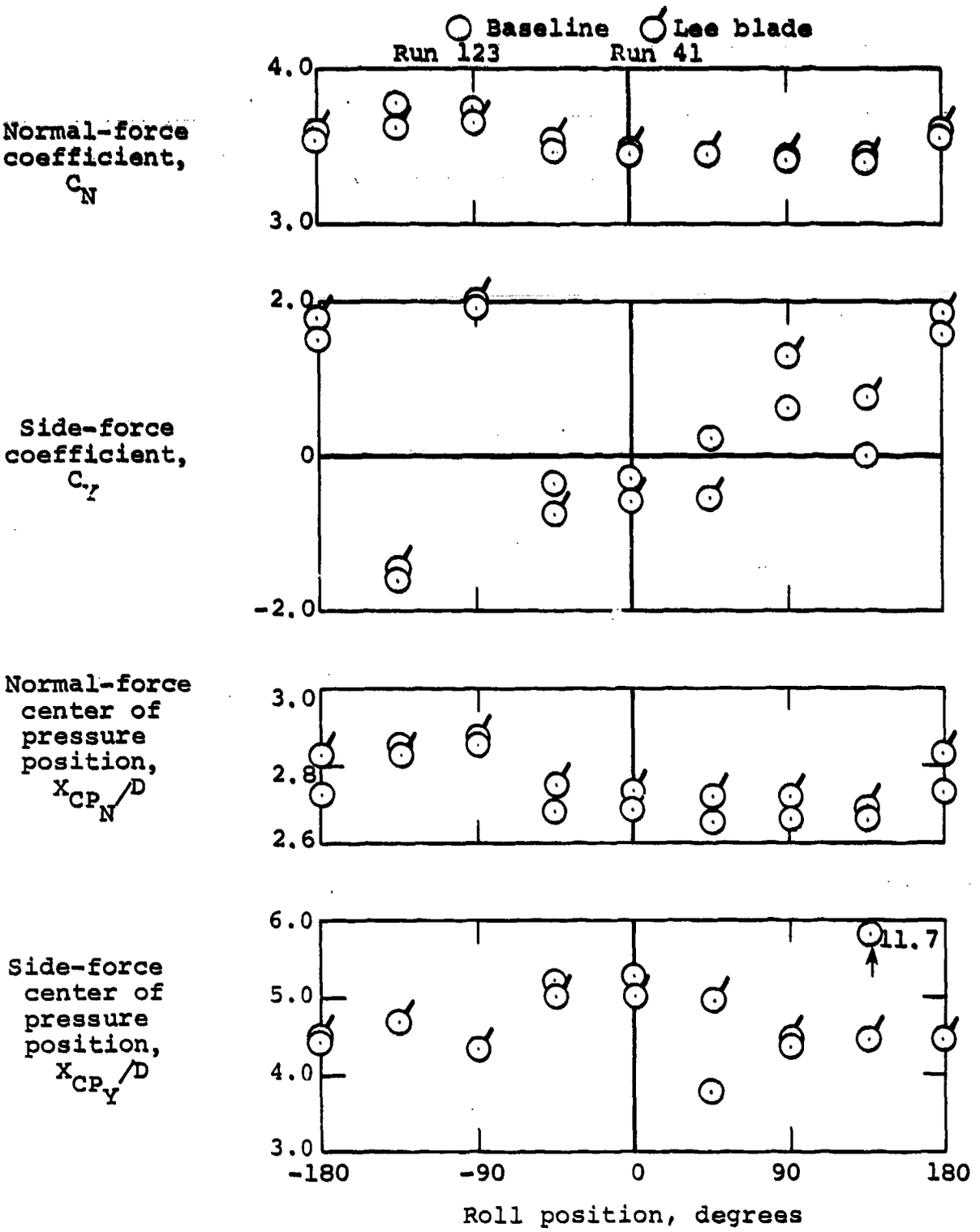

Figure 17. Long-Term Repeatability of Results and Effect of Leeward Support Blade: $M_\infty = 0.5$, $\alpha = 40.5$ Degrees

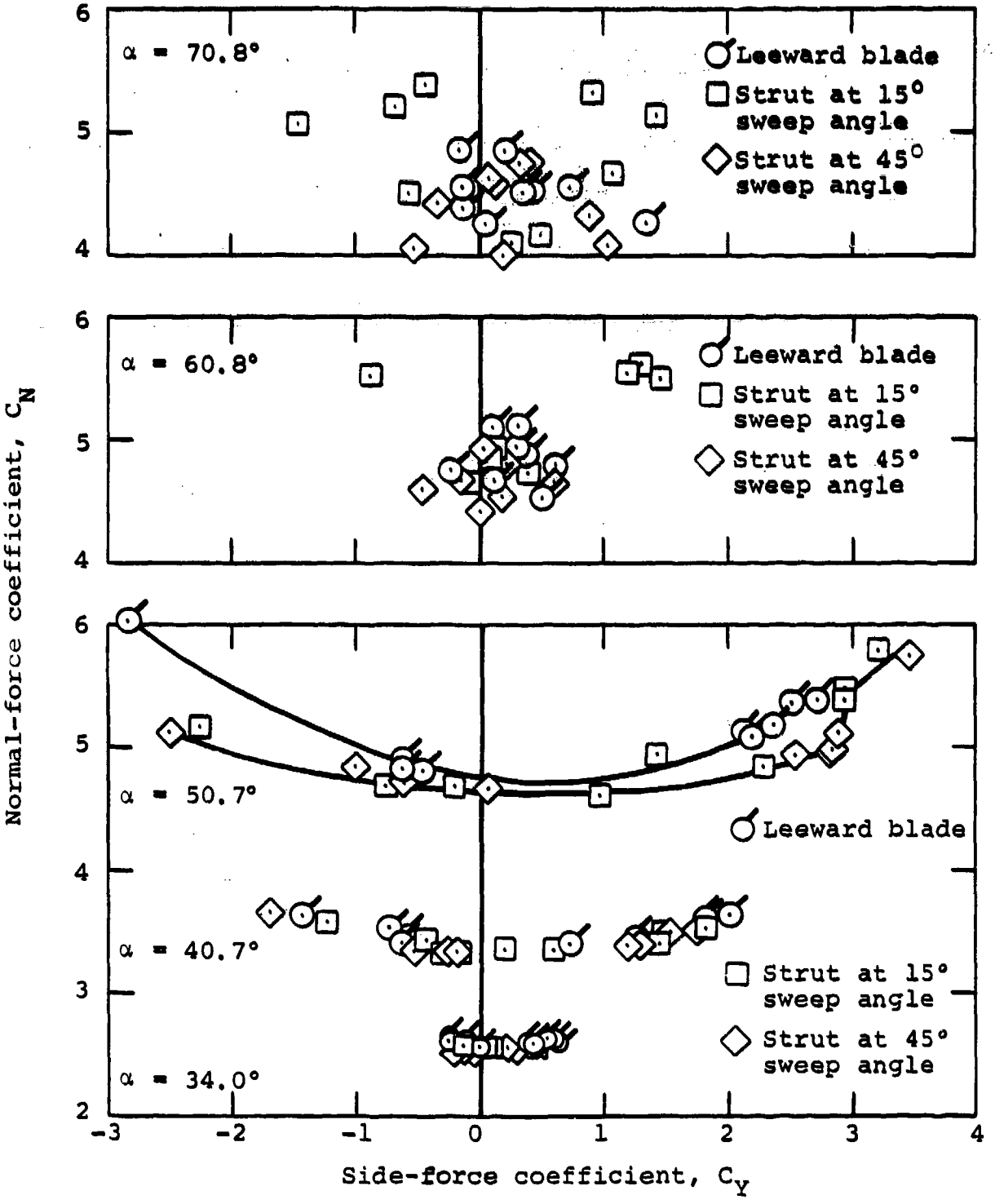

(a) M = 0.5

Figure 18. Effect of Leeward Aft Strut on Normal Force

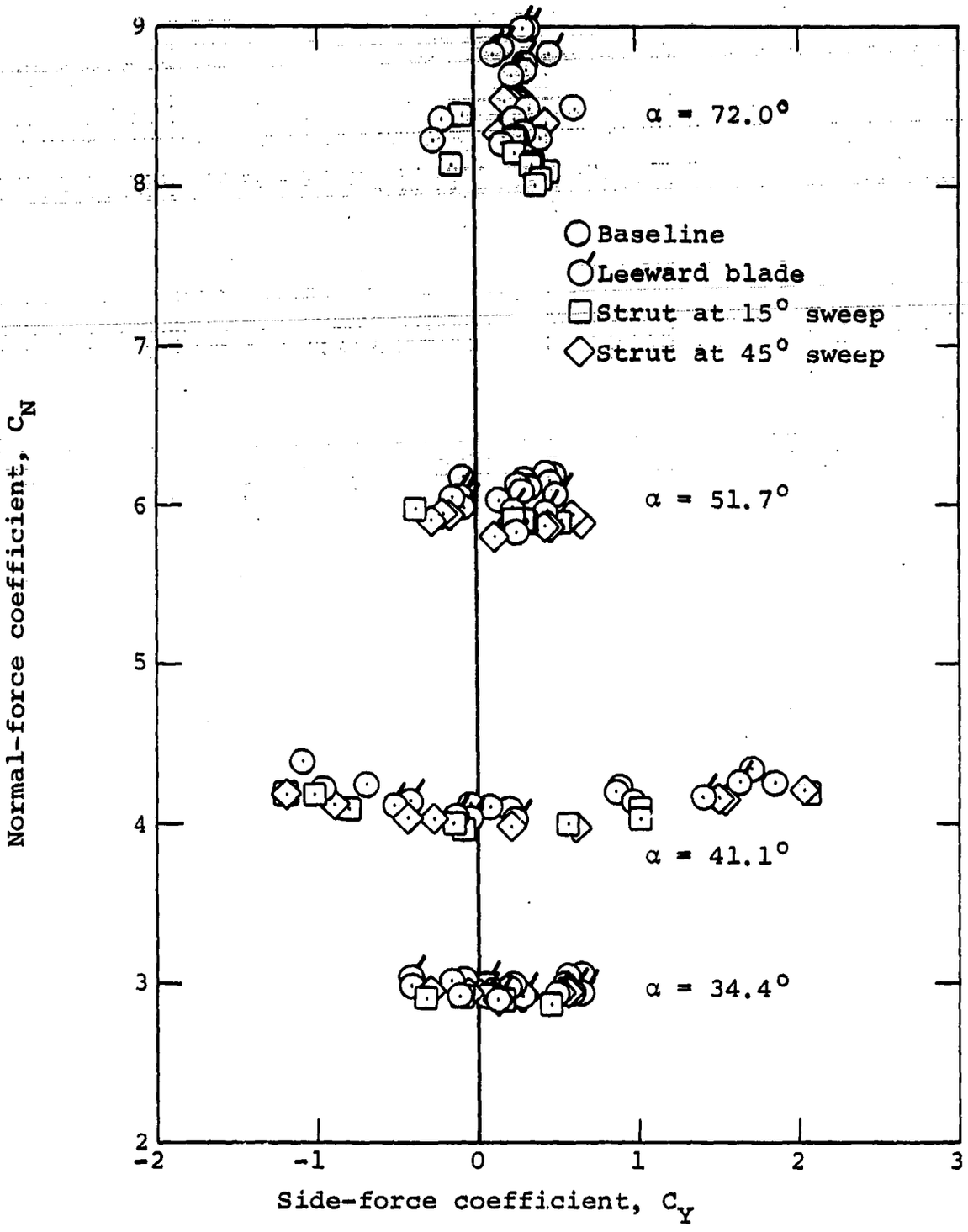

(b) M = 0.7

Figure 18. Effect of Leeward Aft Strut on Normal Force (Continued)

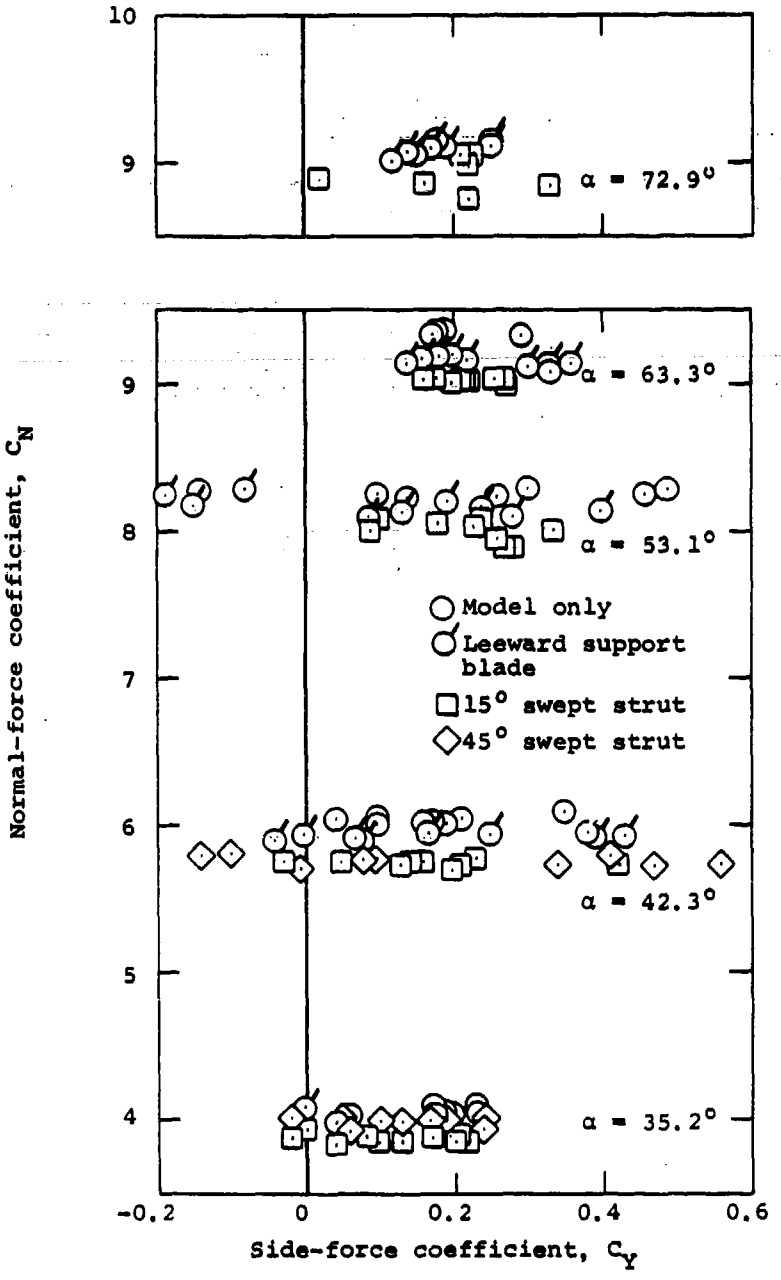

(c) M = 0.9

Figure 18. Effect of Leeward Aft Strut on Normal Force (Concluded)

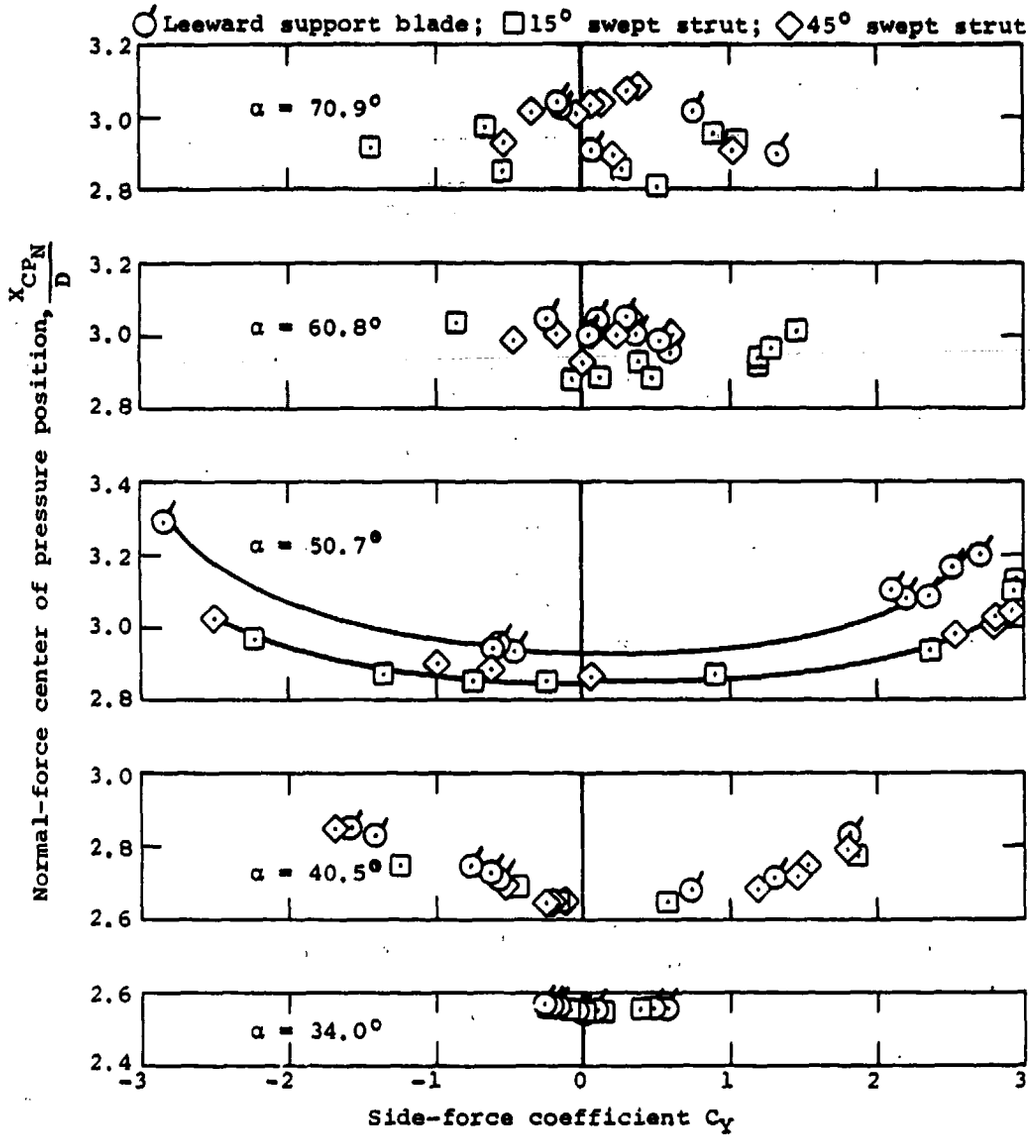

(a) M = 0.5

Figure 19. Effect of Lee, Aft Strut on Center of Pressure of Normal Force

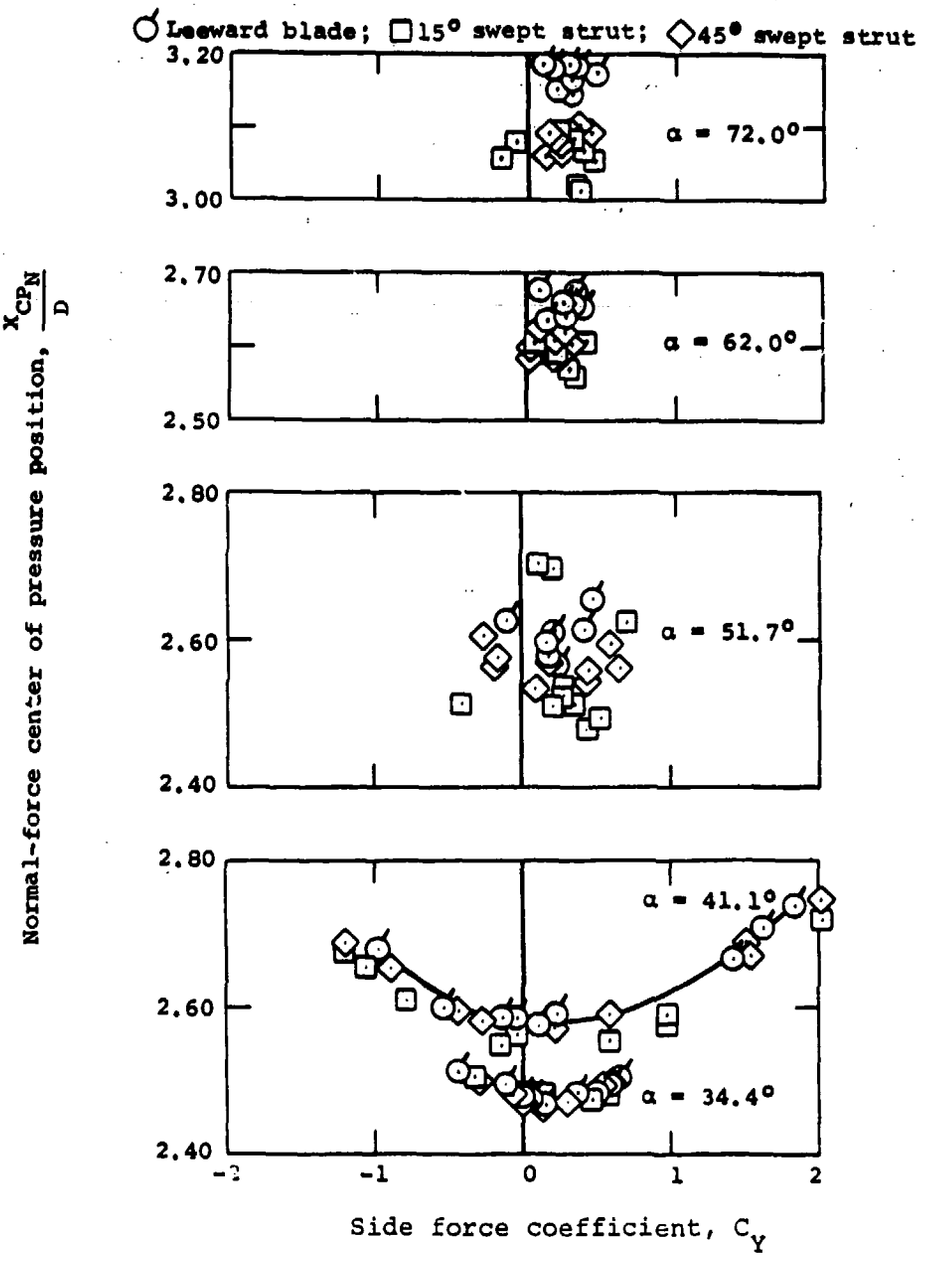

(b) M = 0.7

Figure 19. Effect of Lee, Aft Strut on Center of Pressure of Normal Force (Continued)

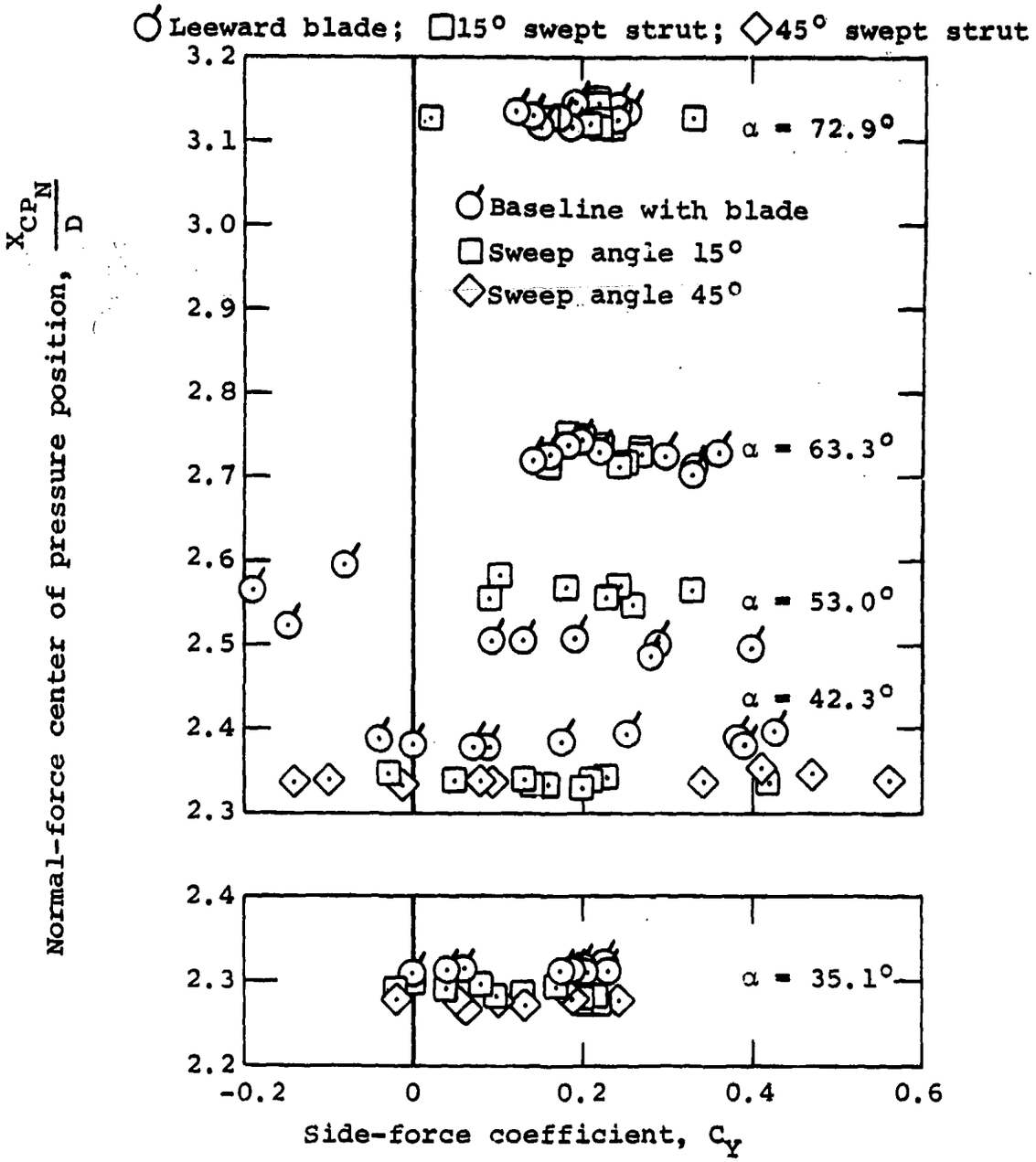

(c) M = 0.9

Figure 19. Effect of Lee, Aft Strut on Center of Pressure of Normal Force (Concluded)

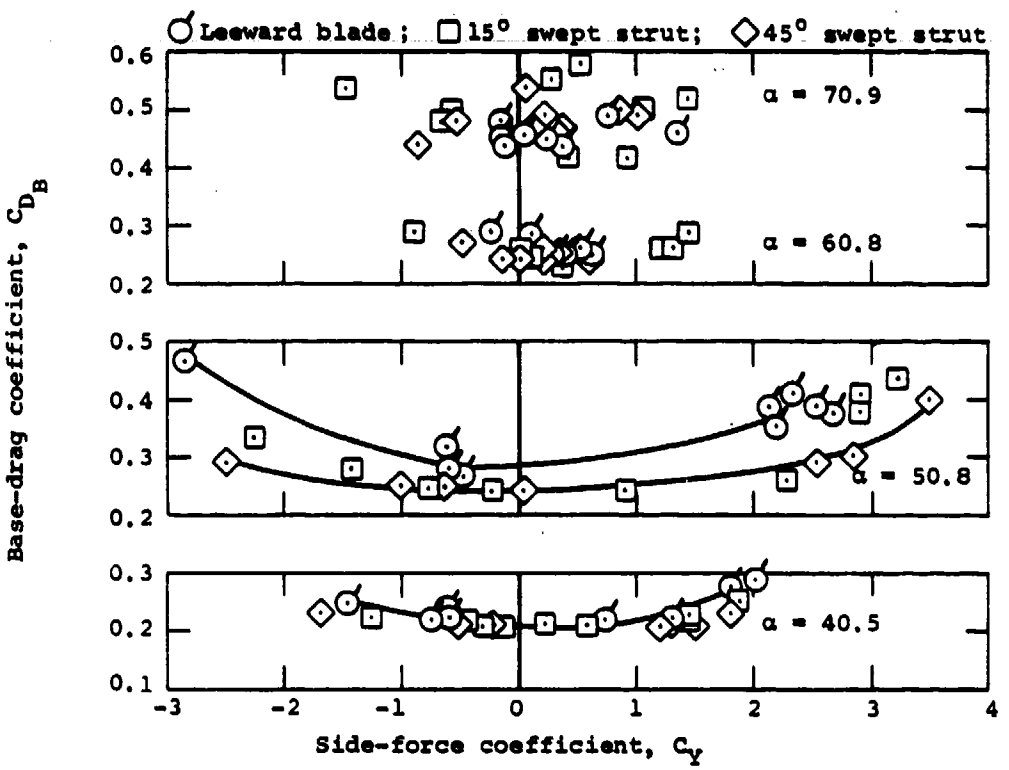

(a) $M_\infty = 0.5$

Figure 20. Effect of Leeward Aft Strut on Base Pressure

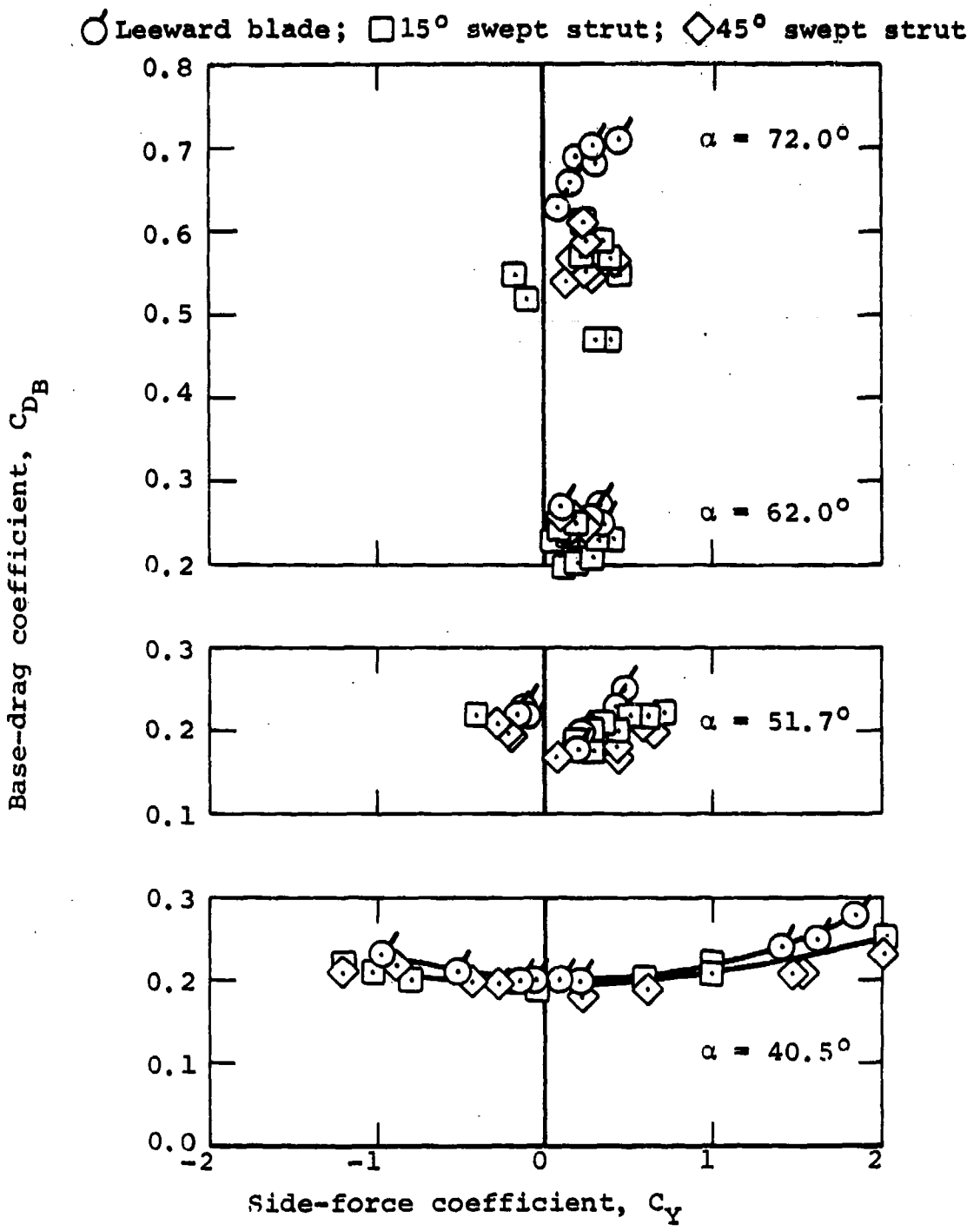

(b) $M_\infty = 0.7$

Figure 20. Effect of Leeward Aft Strut on Base Pressure (Concluded)

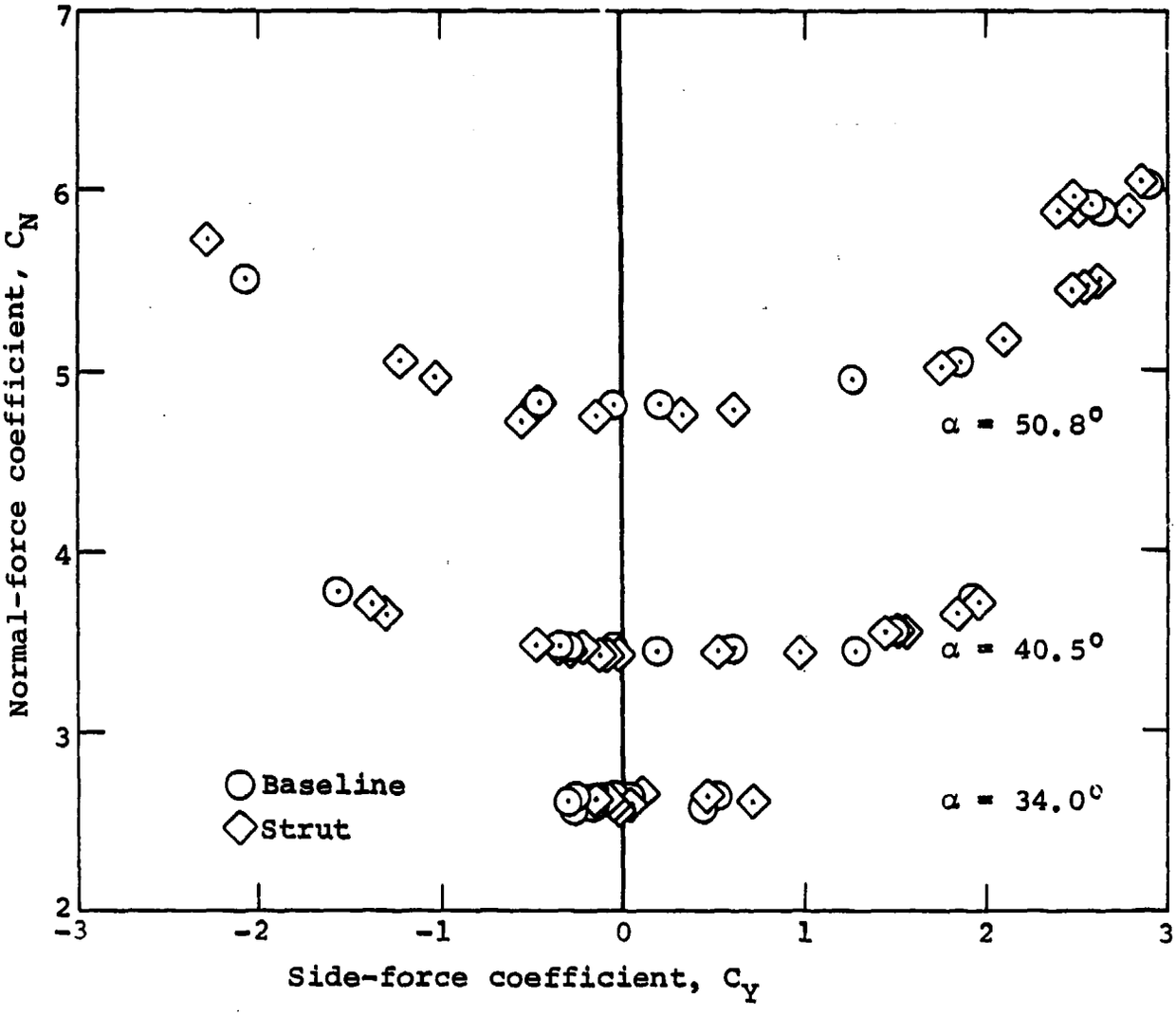

(a) M = 0.5

Figure 21. Effect of Windward Strut on Normal Force

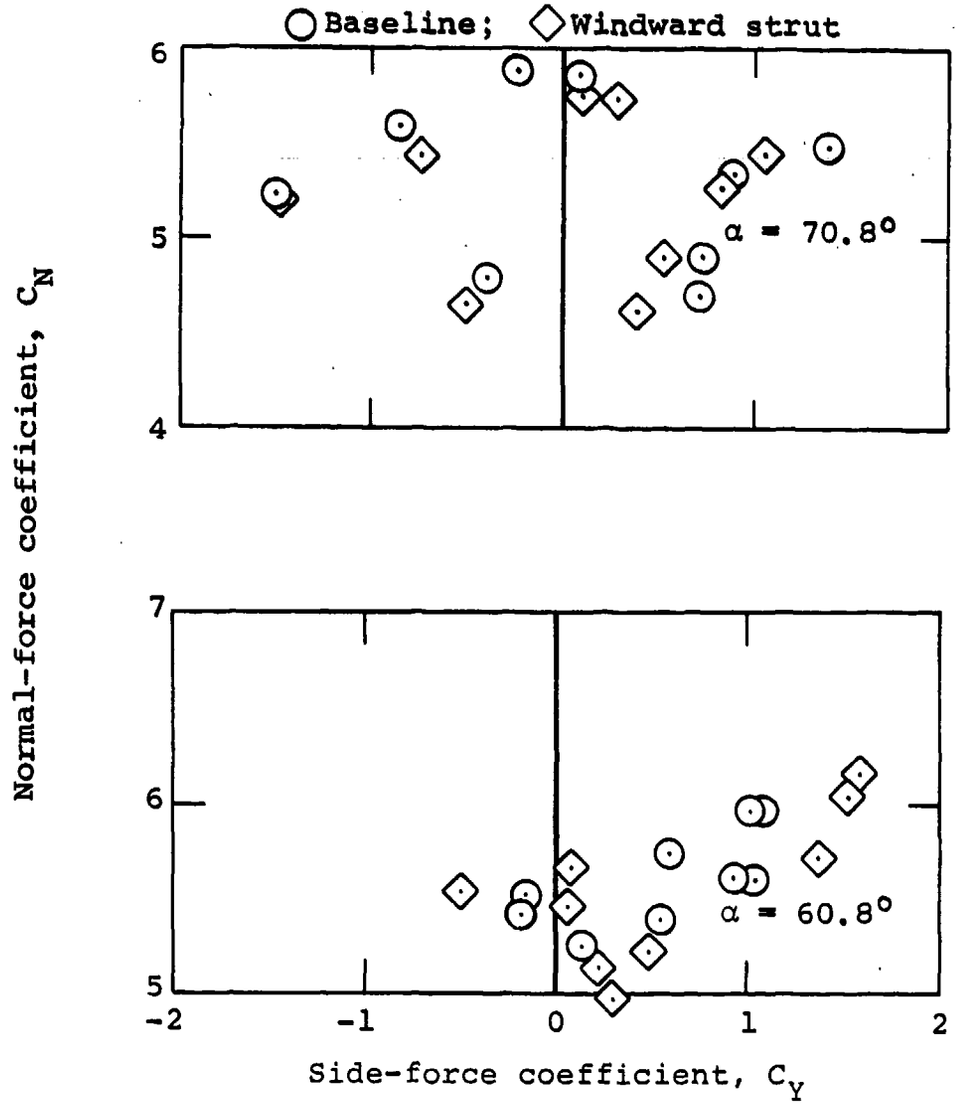

(b) M = 0.5

Figure 21. Effect of Windward Strut on Normal Force (Continued)

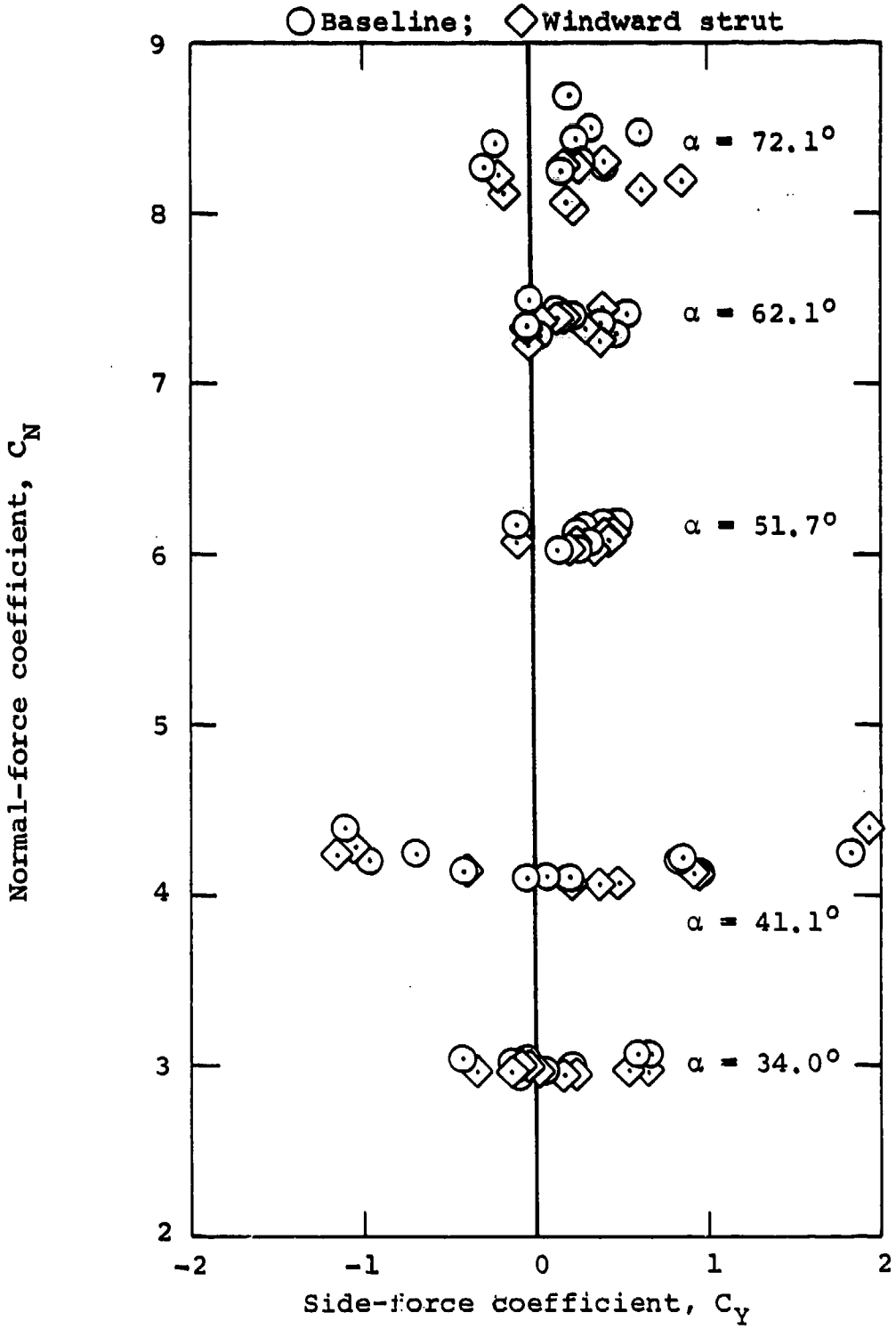

(c) M = 0.7

Figure 21. Effect of Windward Strut on Normal Force (Concluded)

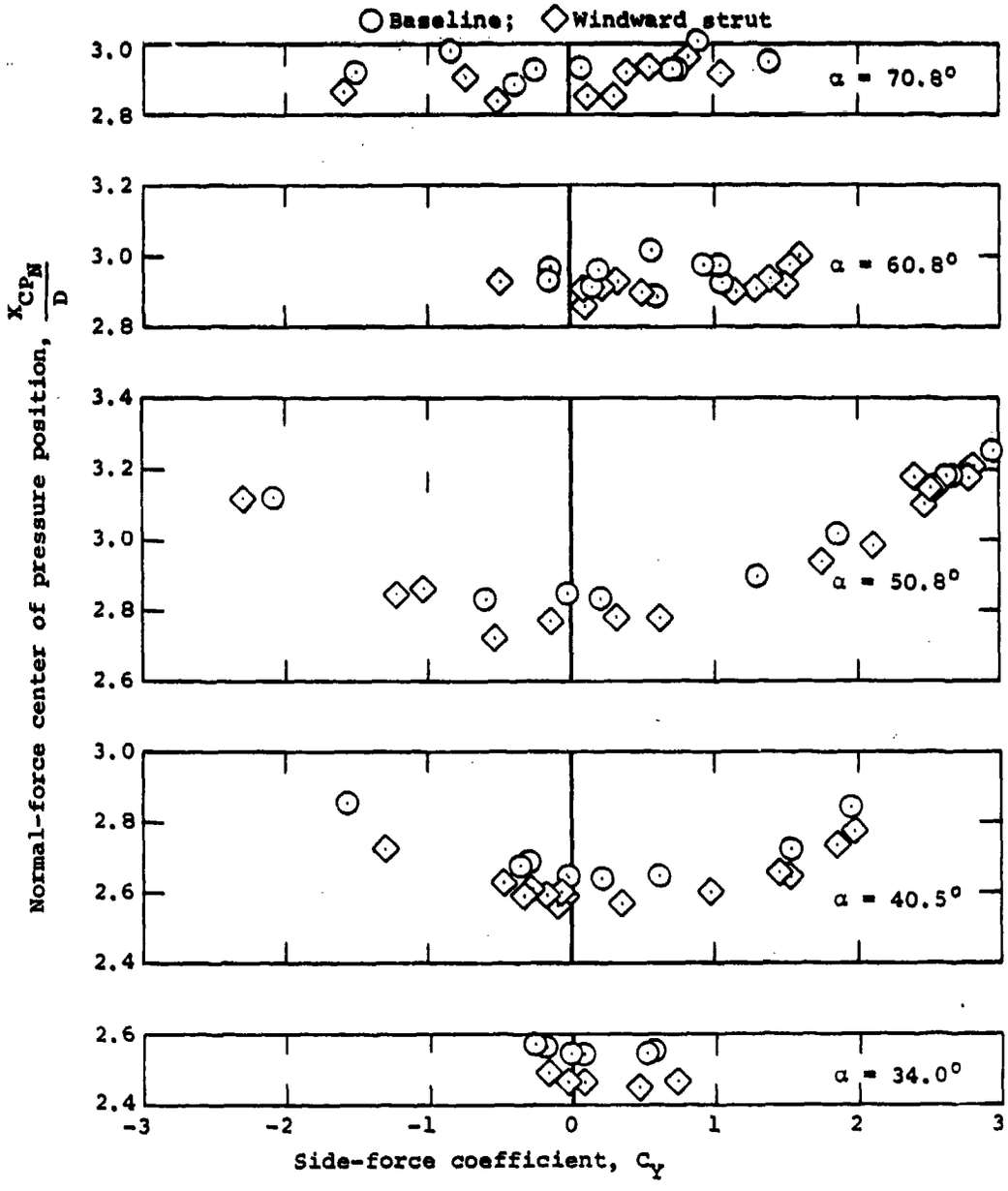

(a) $M_\infty = 0.5$

Figure 22. Effect of Windward Strut on Normal-Force Center of Pressure Position

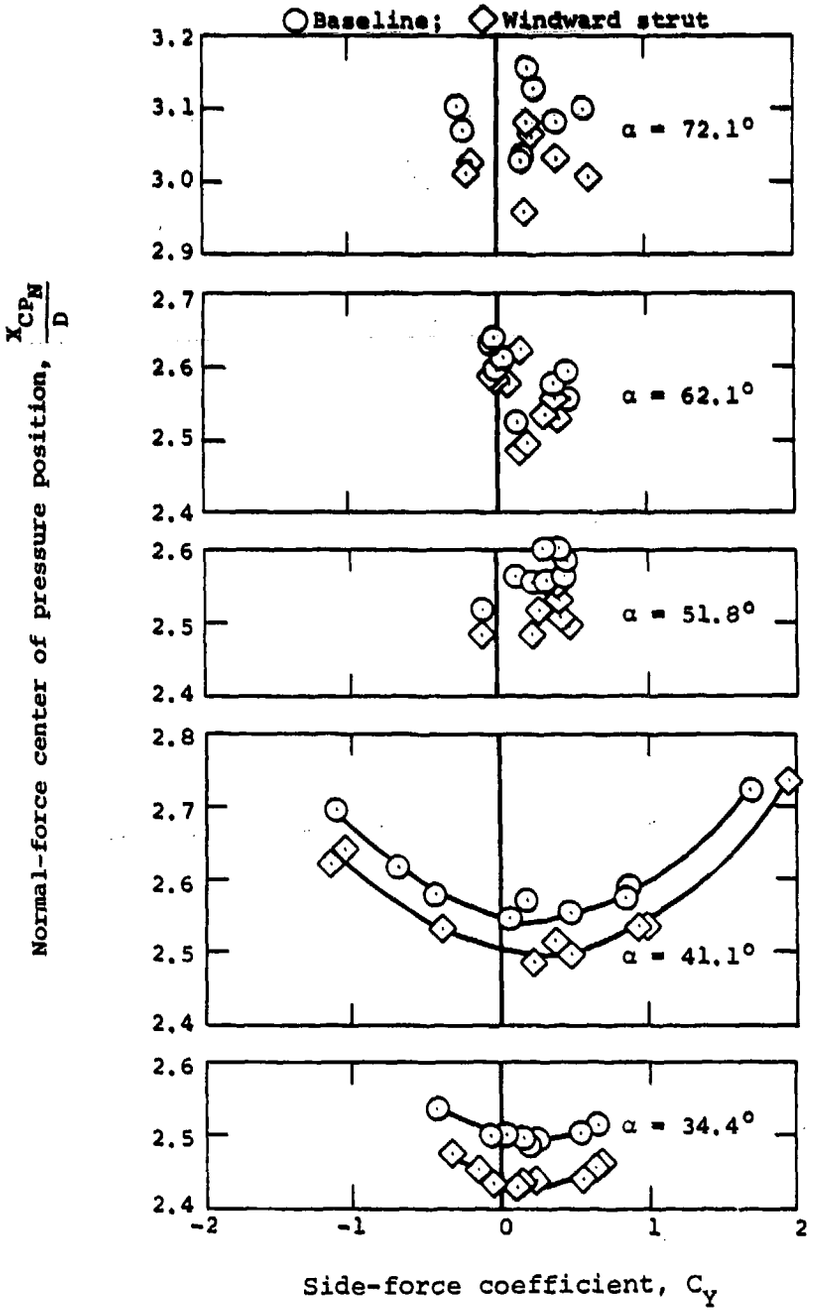

(b) $M_\infty = 0.7$

Figure 22. Effect of Windward Strut on Normal-Force Center of Pressure Position (Concluded)

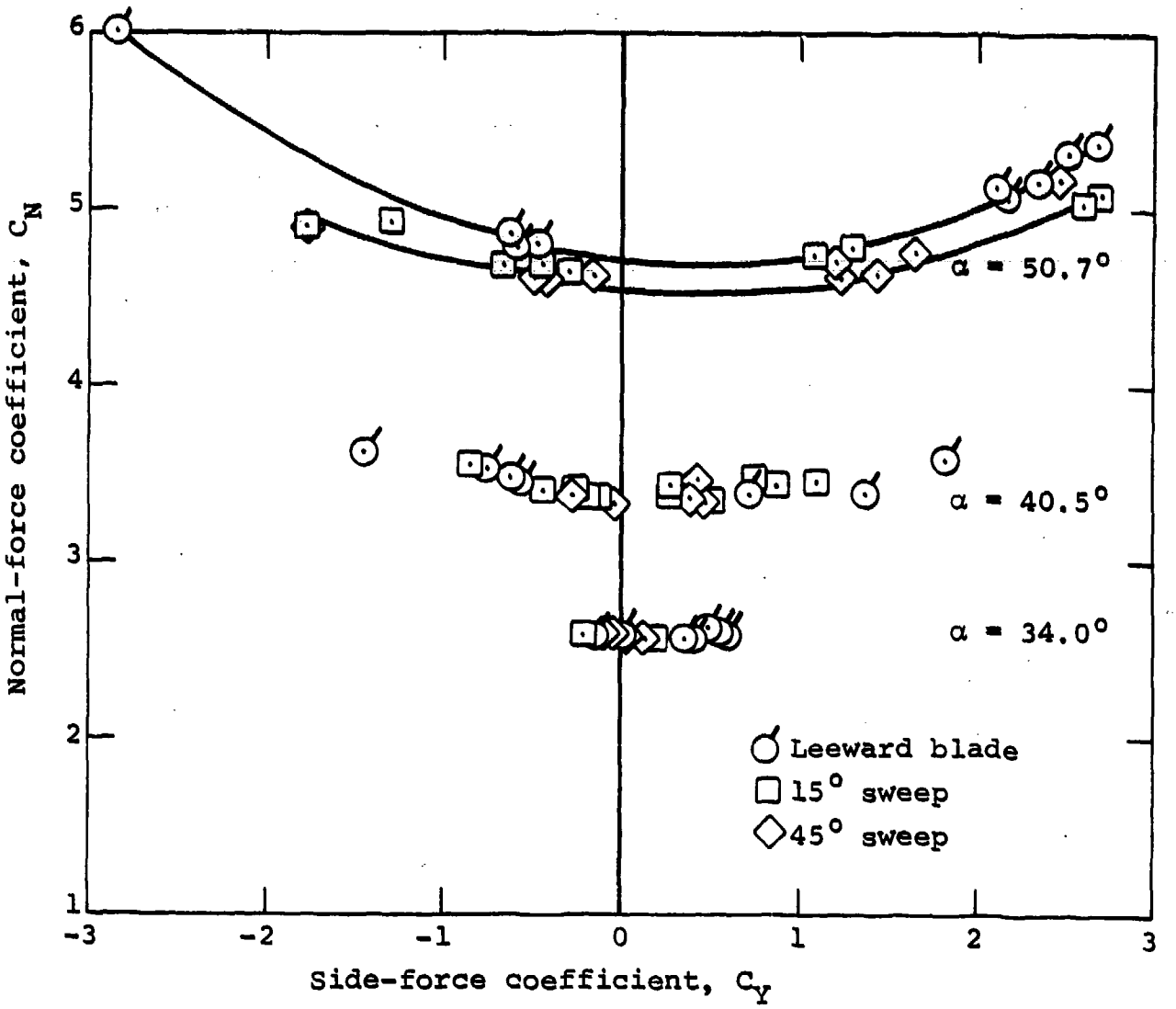

(a) M = 0.5

Figure 23. Effect of Leeward Strut at Mid-Cylinder on Normal and Side Forces

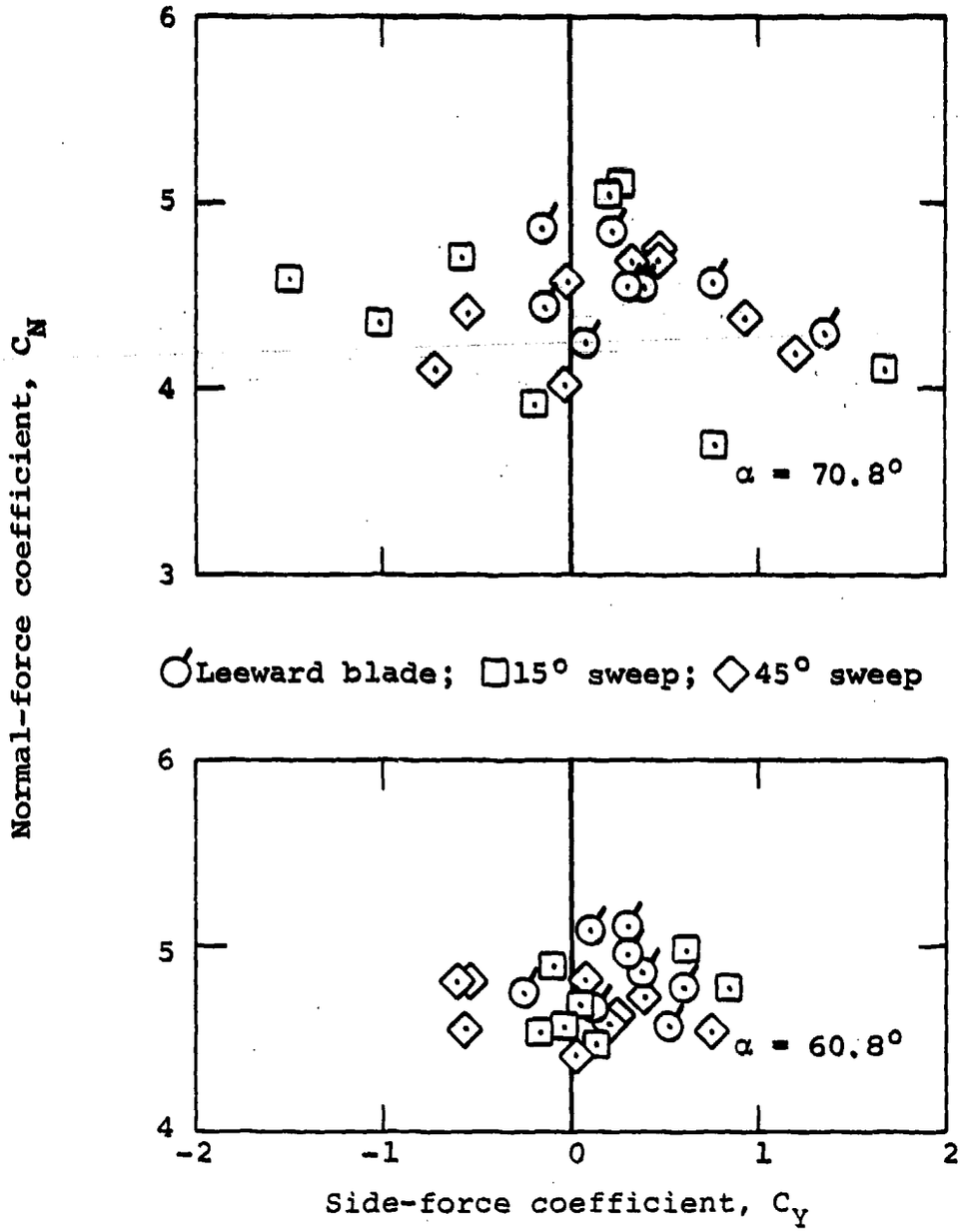

(b) M = 0.5

Figure 23. Effect of Leeward Strut at Mid-Cylinder on Normal and Side Forces (Continued)

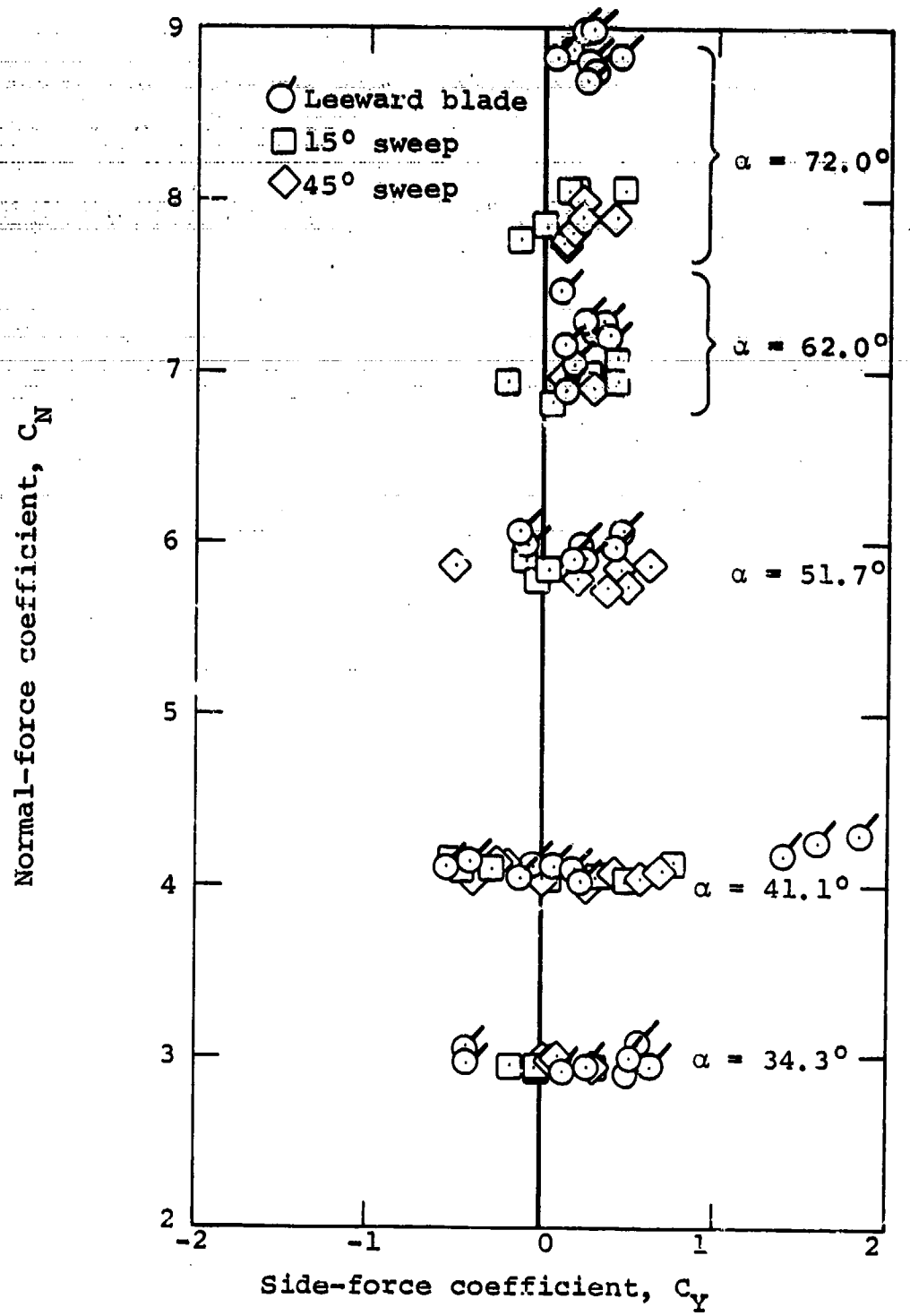

(c) M = 0.7

Figure 23. Effect of Leeward Strut at Mid-Cylinder on Normal and Side Forces (Continued)

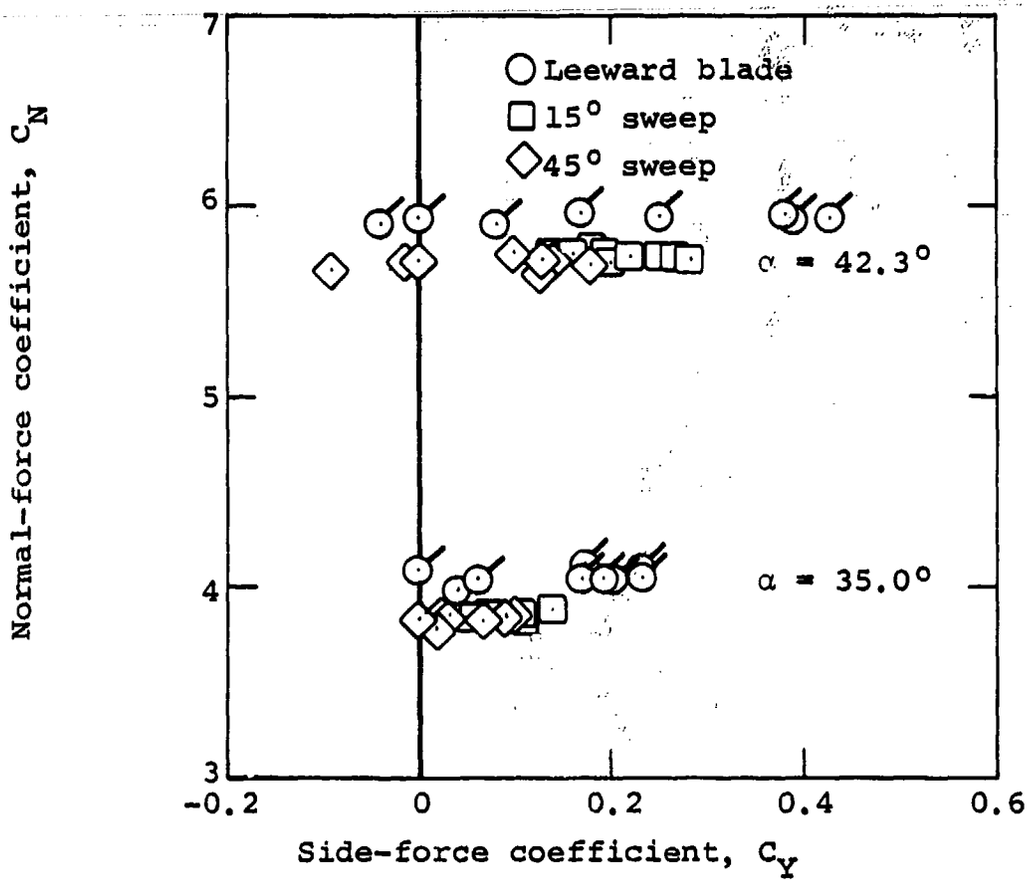

(d) M = 0.9

Figure 23. Effect of Leeward Strut at Mid-Cylinder on Normal and Side Forces (Concluded)

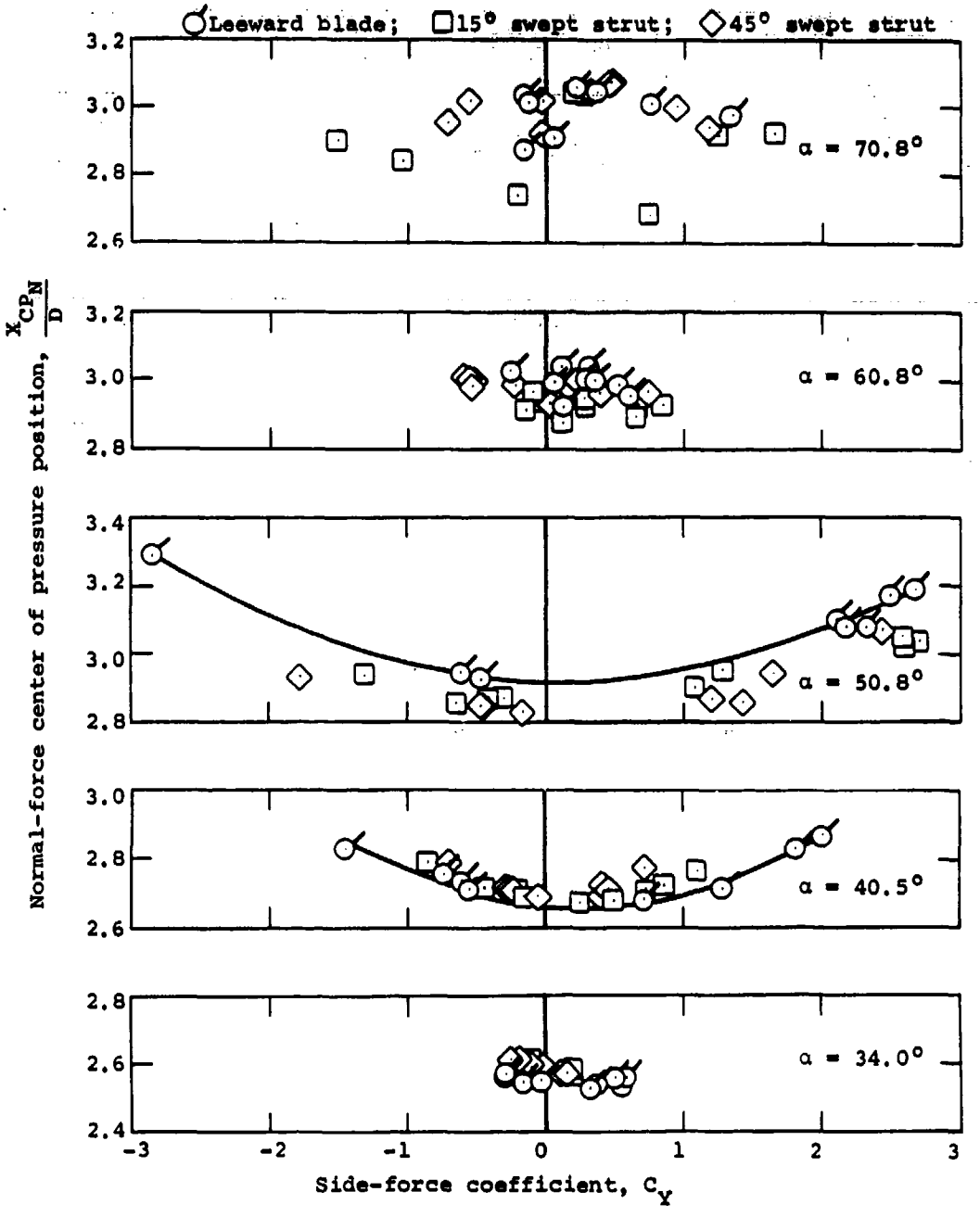

(a) $M_\infty = 0.5$

Figure 24. Effect of Leeward Mid-Cylinder Strut on Normal-Force Center of Pressure Position

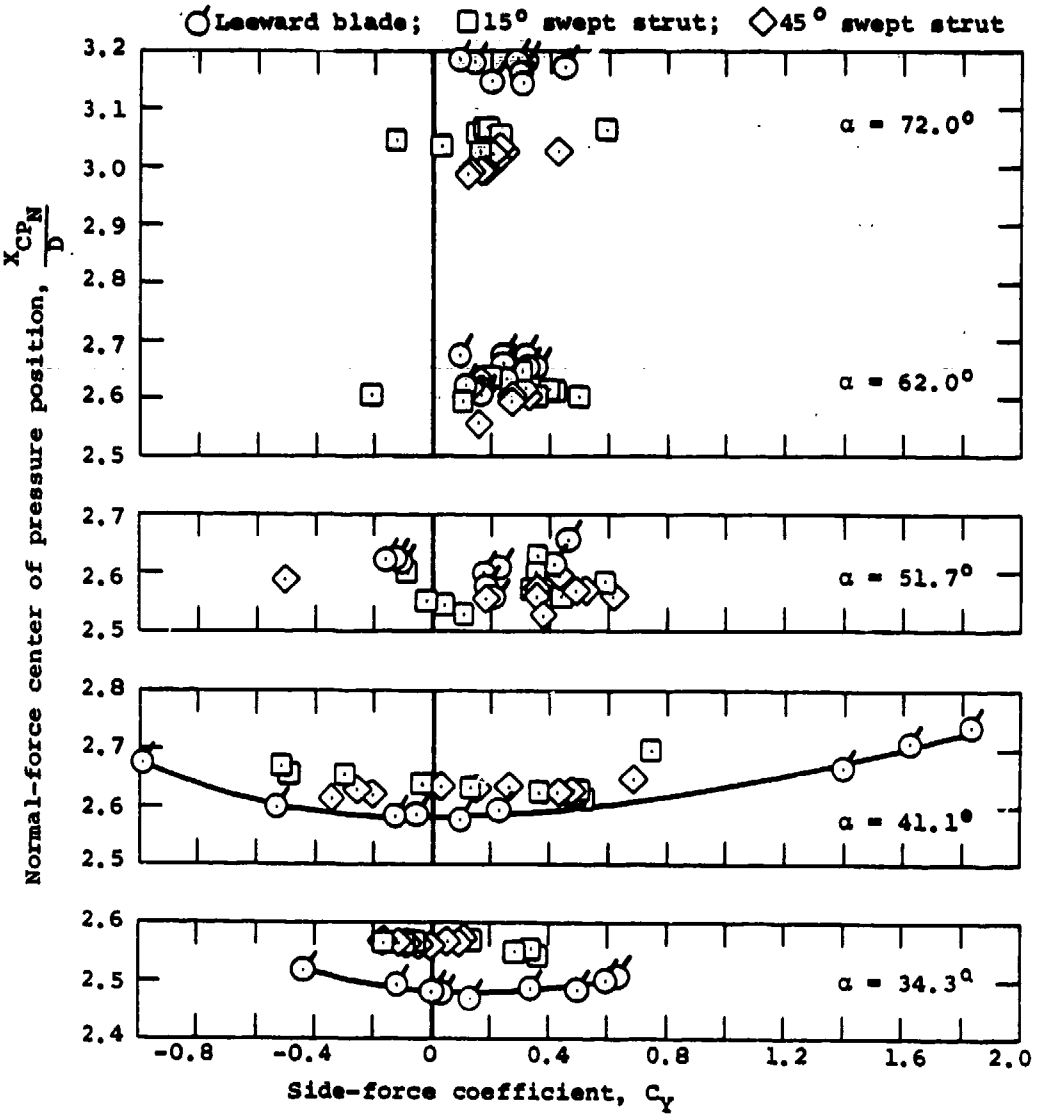

(b) $M_\infty = 0.7$

Figure 24. Effect of Leeward Mid-Cylinder Strut on Normal-Force Center of Pressure Position (Concluded)

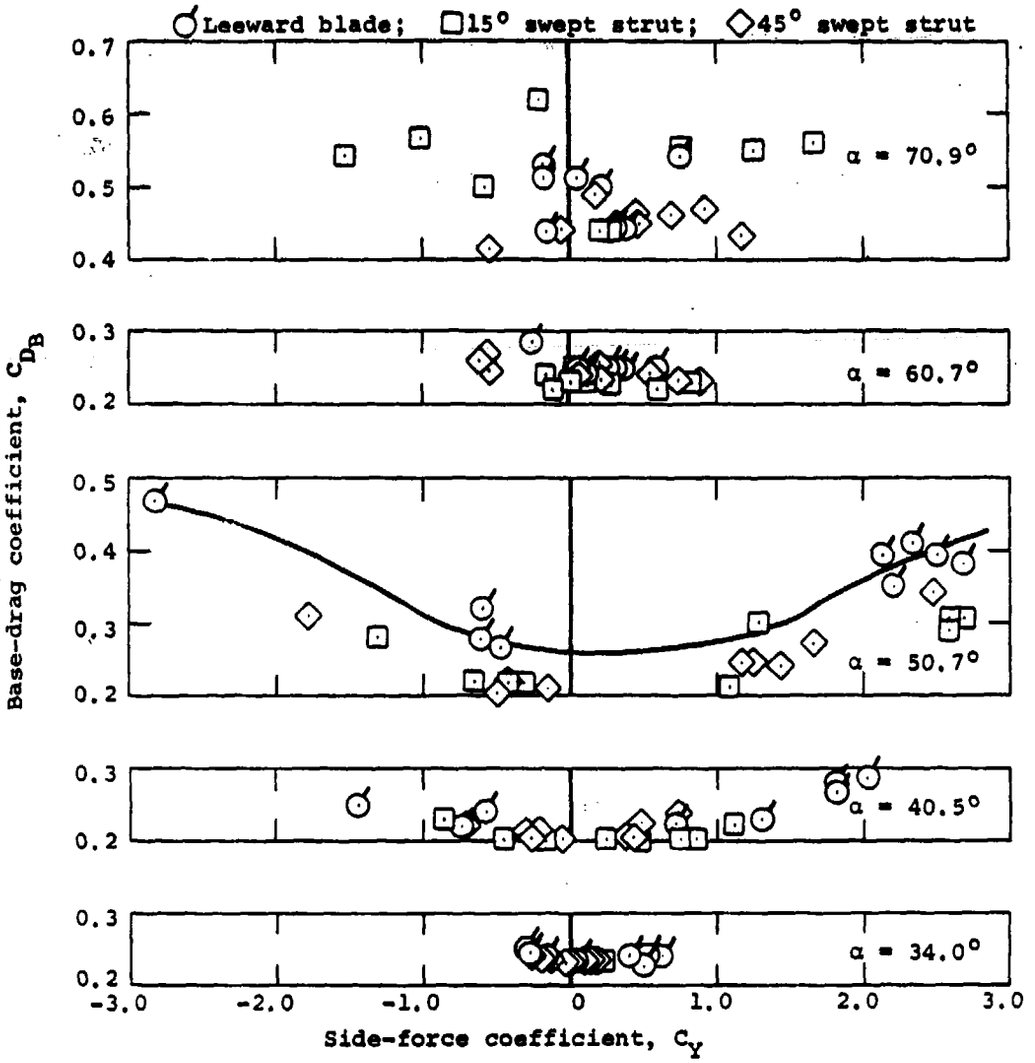

(a) M = 0.5

Figure 25. Effect of Leeward Mid-Cylinder Strut on Base Pressure

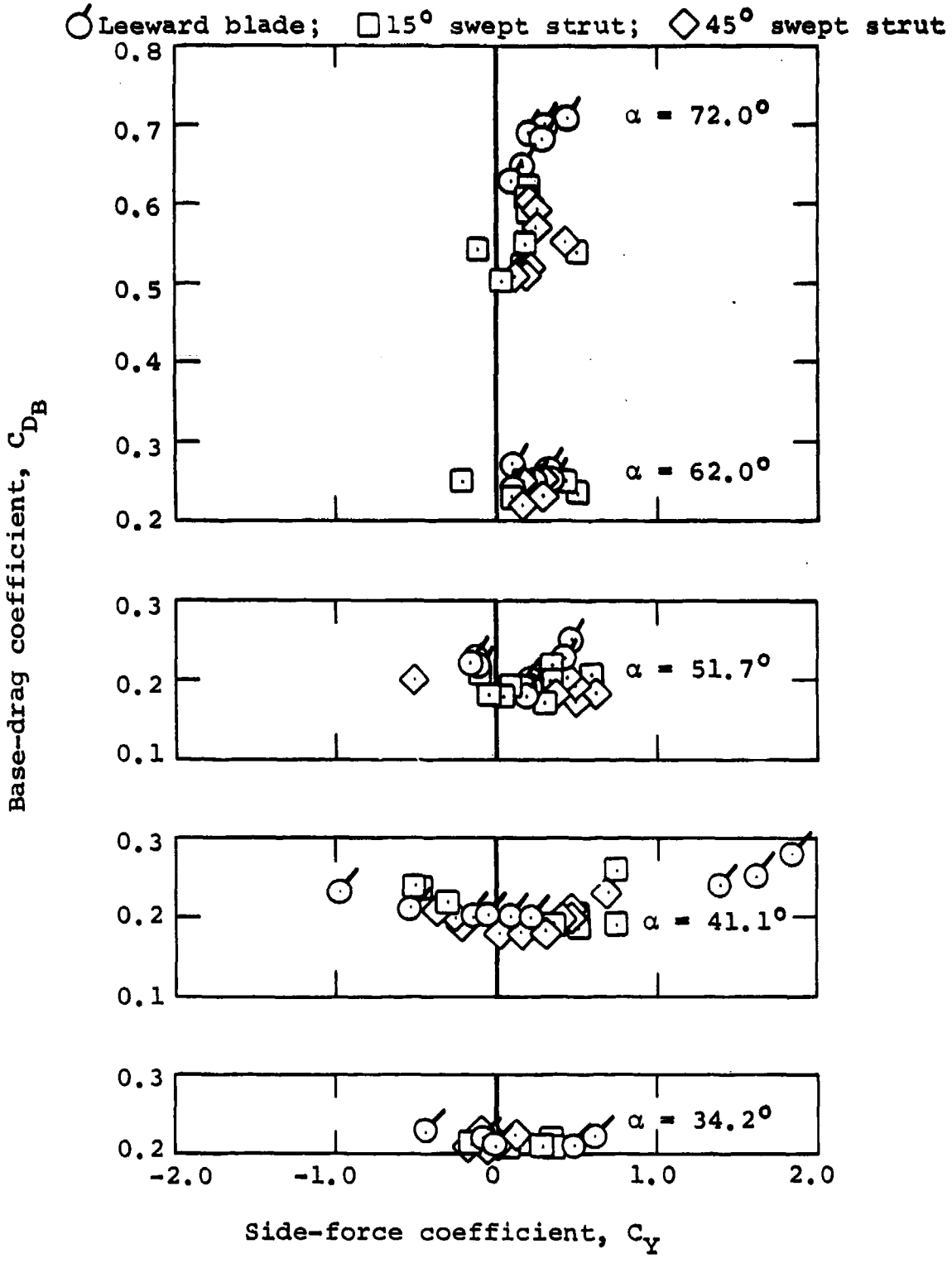

(b) M = 0.7

Figure 25. Effect of Leeward Mid-Cylinder Strut on Base Pressure (Concluded)